Smouldering Combustion of Organic Liquids in Porous Media for Remediating NAPL-contaminated Soils

Presented by

Paolo Pironi

For the degree of

Doctor of Philosophy

The University of Edinburgh

2009

For my parents

Declaration

This thesis and the work described within have been completed solely by Paolo Pironi at the BRE Centre for Fire Safety Engineering at the University of Edinburgh, under the supervision of Dr. Jason I. Gerhard and Prof. Jose L. Torero. Where others have contributed or other sources are quoted references are given.

Paolo Pironi
August 2009

Abstract

This research investigated the potential of smouldering combustion to be employed as a remediation approach for soil contaminated by non-aqueous phase liquids (NAPLs). Small-scale (~ 15 cm), proof-of-concept experiments were the first to demonstrate that organic liquids embedded within an inert soil matrix can be successfully smouldered. Intermediate-scale (~ 30 cm) column experiments examined in detail the behaviour of the combustion process including its relationship to mass and energy balance and the evolution of temperature profiles. In addition, detailed evaluations of environmental parameters (e.g., soil concentrations, gas emissions) were conducted.

For the first time, it was demonstrated that NAPL smouldering combustion can be self-sustaining (i.e., propagation of the smouldering front after termination of the igniter) and self-terminating (i.e., natural extinction of the reaction after all of the NAPL is destroyed). More than 30 column sensitivity experiments quantified the broad range of process parameters - including contaminant type, contaminant mass, soil type, and oxidizer flow rates - within which the process was self-sustaining and essentially complete remediation was achieved (i.e. contaminant mass removal in excess of 99.5%).

Maximum burning temperatures were observed in the range 600-1100 ^{o}C. Average propagation velocities varied between $0.7 \cdot 10^{-4}$ and $1.2 \cdot 10^{-4}$ m/s. Intensity and velocity of the process were shown to be controlled by the rate at which oxidizer is delivered. Contaminant type and mass was observed to affect peak temperatures and propagation velocity by influencing the energy balance at the reaction front. Moreover, mass and energy balance models were demonstrated to provide reasonable predictions of the observed propagation velocities.

Overall, this research introduced an entirely new approach to the remediation of NAPL-contaminated soils and, further, advanced the understanding of the mechanisms that control the underlying process of smouldering combustion of liquids.

Acknowledgements

Financial support for this research was provided by the Engineering and Physical Science Research Council in the form of an operating grant to the author's supervisor Dr. J.I. Gerhard and in part by the BRE Centre for Fire Safety Engineering at the University of Edinburgh

The author would like to acknowledge the support and valuable guidance of Dr. Jason Gerhard and Professor Jose Torero throughout this research. The effort and constructive input of the external examiner, Dr. Bernard H. Kueper, is much appreciated. My gratitude is extended to Dr. Christine Switzer and Dr. Guillermo Rein for their advice and encouragement. For their support and invaluable scientific advice through some (of the many) difficult times, I am very much thankful to Dr. Andres Fuentes and Dr. Albert Simeoni. I am very grateful to all the CLARRC team for providing valuable technical advice. The support of Dr. John Jeffrey is also acknowledged. Thanks to Hubert, Cecilia, Adam, Rory, Wolfram, Nicolas, Joanne and all the other members of the Fire Group.

Thank you to all my friends and most of all to my family, Katya, Mamma, Babbo, Marco for their unconditional support in the last four years.

Preface

This thesis has been written in manuscript format. The material has been presented as follows:

- Chapter 1 presents a general introduction to the research and an overview of the relevant literature.
- Chapter 2 consists of a manuscript for the combustion community presenting the first successful experiments of smouldering combustion of a liquid contaminant; this has been published as:

  Pironi, P., C. Switzer, G. Rein, J.I. Gerhard, J.L. Torero, A. Fuentes, Small-scale forward smouldering experiments for remediation of coal tar in inert media. *Proceedings of the Combustion Institute* (2009) 32 1957-1964.
- Chapter 3 consists of a manuscript for the environmental engineering community focused on the first proof-of-concept for smouldering combustion as a non-aqueous phase liquid (NAPL) remediation approach; this has been published as:

  Switzer, C., P. Pironi, J.I. Gerhard, G. Rein, J.L. Torero, Self-sustaining smoldering combustion: a novel remediation process for non-aqueous phase liquids in porous media, *Environmental Science and Technology* (2009) 43 5871-5877
- Chapter 4 is a second manuscript for the environmental engineering community providing a systematic experimental investigation at the bench scale of smouldering combustion as a remediation approach; this will be submitted to Environmental Science and Technology within several weeks of completing this thesis.

- Chapter 5 is a second manuscript for the combustion community presenting an analysis, via comparison of experiments to modelling, of the processes underlying the smouldering combustion of liquids; this will be submitted to Combustion Science and Technology within several weeks of completing this thesis.
- Chapter 6 provides a summary and general conclusions of the research.
- The appendices provide supporting material that was not included in the manuscripts.

A patent application - of which the author of this thesis is a co-author - has been submitted based, in part, upon the work in this thesis (UK Patent Application 0525193.9 and PCT Application PCT/GB2006/004591, priority date December 2005).

Table of Contents

List of Figures

List of Tables

Nomenclature

Standard Notation

c_{pl}	Specific heat of the liquid
c_{ps}	Specific heat of the solid
c_{pg}	Specific heat of the gas
h	Convective heat transfer coefficient
k_T	Total thermal conductivity
$\dot{m}''_g$	Gas mass flux
$\dot{m}''_f$	Fuel mass flux
$\dot{m}''_s$	Solid mass flux
ΔH_r	Enthalpy of reaction per unit mass of fuel
CO	Carbon monoxide
CO_2	Carbon dioxide
HC	Generic Hydrocarbon
C_V	Volumetric heat capacity of solid+fuel
D_O	Diffusion coefficient of oxygen in the gas phase
D	External diameter of the column
L	Thickness of the reaction front
$\dot{Q}''_{loss}$	Heat losses to the outside
T	Temperature
T_S	Smouldering Temperature
U_S	Smouldering propagation velocity
U	Heat transfer coefficient
Y_O	Mass fraction of oxygen in the gas phase
W	Reaction rate (mass of fuel reacted per unit time and unit volume of sample)

Greek

$\rho_{b,s}$	Bulk density of the solid
ρ_f	Density of the fuel
ρ_g	Density of the gas
φ_g	Gas filled porosity
φ_f	Fuel filled porosity
ν	Stoichiometric coefficient
σ	Stefan-Boltzmann constant
ε	Emissivity

Subscripts

1	Referring to the internal surface of the column
2	Referring to the external surface of the column
amb	Referring to ambient
cc	Referring to complete combustion
co	Referring to crude oil or carbon monoxide
ct	Referring to coal tar
con	Referring to convection+conduction
e	Referring to final (in the smouldered sandpack) or external
i	Referring to initial (in the unburnt sandpack)
o	Referring to oxygen
rad	Referring to radiation
th	Referring to theoretical
tot	Referring to global

Chapter 1

Introduction and background

Non-aqueous phase liquids (NAPLs) are a class of organic compounds with a long history of extensive use in industrial processes. As the result of inappropriate disposal practices, NAPLs are now among the most frequently occurring contaminants detected in the subsurface throughout the industrialized world (Pankow and Cherry, 1996). Common NAPLs include petroleum hydrocarbons (oils, fuels), polychlorinated biphenyls (PCB, electrical transformer oils), chlorinated ethenes (solvents, degreasers), creosote (wood treaters), and coal tar (manufactured gas plants). Most of these contaminants are toxic to humans and the environment in high, acute doses and may be irritants and suspected carcinogens at low, chronic doses. Standard handling and disposal procedures resulted in widespread releases of these chemicals into the environment, creating persistent, long-term sources of groundwater contamination (Amter and Ross, 2001). Existing in soil pores as a separate liquid phase, NAPLs dissolve in groundwater in amounts high enough to render it unfit for consumption, but low enough such that its lifespan can be on the order of centuries (Mercer and Cohen, 1995). Remediation of NAPL-contaminated soil in a cost effective and robust manner remains a significant challenge.

The goal of this research is to assess the feasibility of a new remedial approach to NAPL contaminated soil, based on NAPL destruction and removal via smouldering combustion within the soil matrix.

1.1 Remedial approaches to NAPL contaminated sites

Conventional remediation technologies such as pump and treat and soil vapour extraction have proven largely inefficient in addressing substantial volumes of subsurface contamination present as NAPL. Since these techniques rely on transferring the contamination to a liquid or gaseous stream that is then extracted and treated aboveground, they are inherently limited by the rate of mass transfer from the NAPL mass to such streams. Because of the chemical properties of most NAPLs (they typically exhibit relatively low solubility and low volatility) and due to the relatively low interfacial area available for mass transfer in NAPL pools, these systems may need to be operated for extended periods, with relatively high operation and maintenance costs. Innovative treatment technologies are being developed that directly address the 'source zone' (the region of the subsurface containing the NAPL phase), thus having the potential to reduce significantly the overall time and costs for remediation (ITRC, 2002; EPA, 2003). In what follows, a brief description of the principles and applicability of some of the innovative source zone remediation technologies is presented, with a particular emphasis on thermal remediation techniques.

1.1.1 Thermal techniques

Thermal technologies represent one of the major categories of treatment technologies applicable to the remediation of source zones. The general principle on which thermal technologies are based is that increasing the temperature of the soil increases the mobility of the contaminants (in a variety of phases) and facilitates their recovery

to the surface for a subsequent treatment; in some cases the increased temperature can result in partial in-situ destruction of contaminants.

Heat typically modifies the properties of contaminants in a way that enhances their treatability (Davis, 1997). For example: the liquid viscosity decreases with increasing temperature; the solubility generally increases with increasing temperature; the partition coefficient decreases with increasing temperature (causing the contaminants to partition less preferentially to the soil); the molecular diffusion coefficient in the aqueous and gas phases increases with temperature. In addition, many common contaminants (e.g. chlorinated solvents) boil at temperatures ranging from 40 to 180 ºC thus allowing their extraction as vapour. Thermal technologies may also result in the partial degradation of the contaminants directly in the subsurface via chemical or biochemical reaction favoured by an increase in temperature (EPA, 2004). The principal thermal technologies currently available are (EPA, 2004): Steam Enhanced Extraction, Electrical Resistive Heating and Thermal Conductive Heating.

Steam Enhanced Extraction (SEE) involves the injection of steam into the subsurface to dissolve, vaporize and mobilize contaminants that are then recovered in the vapour and liquid phase. Extracted vapours and liquids are treated aboveground with conventional technologies like air stripping, carbon adsorption and thermal oxidation. Steam needs to penetrate the pore space to heat the soil, so the applicability of SEE is typically limited to zones of moderate to high permeability. If the low permeability zones are sufficiently thin they can be conductively heated from

above or below. Alternatively SEE can be combined with other technologies such as electric resistive heating (ERH, see below); the ERH technology is employed to heat the low permeability zones.

Systems for the application of SEE consist of a steam generating equipment, steam distribution system and vapour, groundwater and DNAPL extraction systems. The typical configuration of wells for a small application is with the injection wells surroundings a central extraction well. Otherwise, multiple arrays of injection and extraction wells are used, with typical spacing ranging from several to more than 10 metres.

Electrical Resistive Heating (ERH) employs an electrical current to generate heat in the subsurface; the dissipation of electric energy through resistive losses produces the soil heating. As in SEE, heating can mobilize contaminants by dissolution, desorption and vaporization if the soil is heated to the boiling point of water. ERH is suited for the treatment of low permeability zones, where steam cannot penetrate rapidly. In some cases ERH is combined with SEE, for example in an aquifer where a lower aquitard has been impregnated with DNAPL. A typical ERH setup consists of several phase electrodes surrounding a central ground electrode, which normally doubles as a vapour extraction well. Additional groundwater extraction wells may be installed to capture water prior to temperature reaching the boiling point.

Thermal Conductive Heating utilises heating elements (electrical elements within a solid casing) placed in the subsurface to generate heat, which is transferred to soil

mainly via thermal conduction and radiant heat transport. The heating elements are placed in vertical wells that act also as vacuum extraction wells; alternatively, heating “blankets” arranged horizontally over the soil can be used to treat shallow contamination. The technology is not affected by soil permeability, because the soil heat conductivities are all fairly similar in magnitude (affected only by water content, with conductivity diminishing as water content decreases); therefore it is possible to attain an almost uniform heating of the subsurface once the influence regions of adjacent heaters have superposed. The technology can achieve high temperatures (in excess of 500 ºC) and this can cause the partial in-situ destruction of the contaminants via either oxidation (if sufficient oxygen is present) or pyrolisis (chemical decomposition in absence of oxygen).

1.1.2 Other techniques

Alternative approaches to NAPL source zones employ mobilisation and/or degradation via physical, chemical or biological treatments. They can be grouped into two main categories: mass removal and (in-situ) mass destruction technologies (UKEA, 2002; NRC, 2004). Mass removal technologies include multiphase extraction, water floods and chemical (surfactants and cosolvent) flushing. Multiphase extraction employs a vacuum or pump to extract NAPL, vapour, and aqueous phase contaminants, which may then be disposed of or treated. Water floods involve the use of drains that pump both the NAPL and the water phases to produce an increased driving force to direct the NAPL towards a collection drain. In chemical flushing a liquid is introduced in the subsurface, which can increase the water solubility of NAPLs and thus increase the extraction efficiency in the water phase. Surfactants and cosolvents (typically alcohols) can also be used to reduce the water-

NAPL interfacial tension, thus increasing the NAPL mobility. This approach may be effective in the displacement of trapped NAPL and is mainly used in the remediation of LNAPLs (lighter than water NAPLs) because vertical migration will tend to be upward.

In-situ mass destruction technologies include chemical oxidation, chemical reduction and enhanced biodegradation. Chemical oxidation and reduction rely on the injection of a reactant in the subsurface (e.g. hydrogen peroxide, potassium permanganate in the case of oxidation or zero valent iron in the case of reduction), which upon contact with the NAPL mass achieve contaminant destruction via chemical reaction. Zero valent iron is typically used in the dehalogenation of chlorinated solvents, whereby the solvent is reduced to a less chlorinated compound through iron oxidation to Fe^{2+}. Enhanced bioremediation involves the stimulation of contaminant-degrading microorganisms within a subsurface aquifer or vadose zone by delivering chemical amendments to the contamination zone. Subsurface microorganisms are stimulated by delivery of substrates, electron acceptors, and/or nutrients by means of subsurface injection or surface infiltration (NRC, 2004).

Remediation technologies that remove substantial NAPL source zone mass are increasingly becoming accepted as viable – and, indeed, necessary – components of a site restoration plan. Nevertheless, solutions that are both technically practicable and cost-effective are still lacking for some of the most challenging contamination scenarios, such as those involving particularly recalcitrant compounds existing in significant NAPL volumes (e.g. coal tar, heavy petrochemicals, PCB oils). For

example, the application of thermal remediation technologies to these sites is limited by high operating costs, since a continuous external energy supply is required to reach and maintain throughout the treatment volume the minimum soil temperature (often 100°C – 150°C) over a significant duration (4 – 12 months) necessary to remove these compounds (Geosyntech, 2004). Multiphase extraction has been demonstrated to be capable of removing significant volumes of NAPL, however it typically leaves behind considerable amount of residual requiring subsequent treatment and may involve extracting significant volumes of groundwater which requires costly surface treatment. Flushing technologies are limited by issues of access and bypassing in heterogeneous formations and the potential for downward remobilization of hydrostatic DNAPL pools. Chemical oxidation, chemical reduction, and bioremediation technologies also depend on adequate delivery and mixing of surface injected fluids throughout the treatment zone and are generally ineffective for the complex, long-chain hydrocarbons contained in coal tars and heavy oils (UKEA, 2002). In this context, due to the technical or economic shortcomings of existing technologies, the dominant site remediation alternative is excavation and either disposal to a hazardous waste landfill or incineration.

1.2 Introduction to NAPL smouldering

An alternative approach to NAPL remediation, which is explored in this research, is contaminant destruction by smouldering combustion. At the basis of this concept is the observation that many common NAPLs are highly combustible and exhibit heat of combustion in excess of materials that are successfully burnt in other industries (e.g. biomass energy, waste incineration). Such industries typically employ flaming

combustion to release the heat from the fuel and often require additional energy to sustain the burning process. However, a flame cannot be sustained within a porous medium such as the soil matrix and thus is not a viable technique for in situ soil remediation. Smouldering combustion, in contrast, is the exothermic oxidation of a condensed phase (i.e. solid or liquid) occurring on the fuel surface, and is favoured by the presence of a solid matrix in which the fuel is embedded. Hence it can be hypothesised that the smouldering reaction of a liquid contaminant within the soil porous matrix may be initiated and propagate, and the process will result in destruction of NAPL and some level of soil remediation. The following sections present an introduction to smouldering combustion and summarise the scientific literature relevant to this research.

1.2.1 Background: smouldering combustion

Smouldering combustion is the flameless burning of a condensed fuel that derives its principal heat from heterogeneous oxidation reactions (direct attack of oxygen on the fuel surface) (Ohlemiller, 1985). It generally occurs within a solid porous medium, with the fuel being either a combustible component of the porous matrix or a separate substance embedded in it. The presence of a solid matrix facilitates the reaction by providing (i) a large surface area per unit volume that enhance surface reactions, (ii) thermal insulation that reduces heat losses, and (iii) permeability to oxygen transport to the reaction sites by convection (forced and natural) and diffusion. Temperature, heat losses and oxidizer availability are the limiting factors that determine the successful ignition and propagation of a smouldering reaction (Ohlemiller, 1985; Torero and Fernandez-Pello, 1996).

Smouldering combustion is commonly studied in simple, one-dimensional configurations that facilitate the analysis and the comparison between experiments and theoretical models. In this context, it is customary to distinguish two different modes of propagation: forward and opposed smouldering. These are defined according to direction of smoulder propagation relative to the direction of the oxidizer flow (Ohlemiller, 2002; Rein, 2009). In forward smouldering, the reaction propagates in the same direction as the oxidizer flow, while in opposed smouldering the reaction propagates in the opposite direction (Figure 1.1). Forward propagation is the most energy efficient mode since in this configuration the convective heat transfer is from the reaction to the virgin fuel and the energy generated is partially used to preheat the fuel and porous matrix ahead of the reaction front (Ohlemiller, 1985).

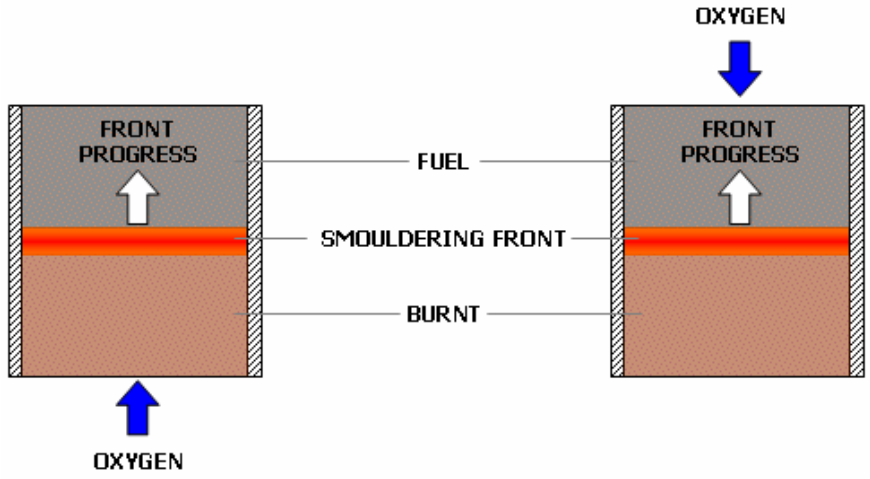

Figure 1.1 Forward propagation (left): oxidizer and smoulder propagation have the same direction; Oppose propagation: oxidizer flow and smoulder propagation have opposite directions.

One-dimensional smouldering combustion of solid fuels has been studied to a certain extent both experimentally and theoretically. Ohlemiller and Lucca (1983) conducted an experimental study to characterise the propagation of forward and opposed

smouldering in cellulose samples. The fuel was ignited at the top and a forced flow of oxidizer was established in the upward or downward direction according to the mode of propagation considered. In both cases, the oxygen was fully consumed by the reaction front so that the rate of propagation was ultimately controlled by the rate of oxygen supply. In forward mode, two distinctive reaction fronts were observed: an endothermic pyrolisis zone propagating into the virgin fuel, followed by an exothermic oxidation zone where the pyrolised fuel (char) is consumed generating the energy necessary to drive the process. In opposed mode, the front advances in an oxygen-rich region; therefore, the pyrolisis reaction (which is favoured by low concentrations of oxygen), was not observed. The oxygen availability in the char zone also resulted in the reaction being much closer to completion in forward than in opposed mode (Ohlemiller and Lucca, 1983).

Two clearly defined reactions, pyrolisis and oxidation, were also observed by Torero and Fernandez-Pello (1996) in forward smouldering experiments conducted on polyurethane foam. The experiments were conducted with upward air flow velocities ranging from 0 to 8 mm/s. A first smouldering regime was identified for very small air flows (less than 1 mm/s) where only the oxidation reaction of the virgin foam is present; at higher air flow rates two reactions take place, the endothermic pyrolisis of the virgin foam, and the exothermic oxidation of the char left behind by the pyrolisis front. The transition between the two regimes is determined by the onset of the char oxidation reactions, which deplete the oxygen from the oxidizer gas flow. Similar results were found by the same authors in natural convection forward smoldering experiments on polyurethane foam (Torero and Fernandez-Pello, 1995). In these

experiments the mass flux of oxidizer is that induced by natural draft through the duct rather than the forced-convection flux. Two regimes of smouldering propagation are identified: an initial stage when only the oxidation reaction of virgin foam is present and a later stage when pyrolisis reactions ahead of the reaction front begin to take place. This happens after the smolder has propagated into the middle to upper regions of the foam, and again appears to be generated by the onset of oxidation reactions in the char left behind by the smouldering front.

Theoretical models of the smouldering process have been presented by Dosanjh *et al.* (1987), Fatehi and Kaviany (1994) and Schult *et al.* (1995) for opposed smouldering and by Buckmaster and Lozinski (1996) and Schult *et al.* (1996) for forward smouldering. These authors employ the method of large activation energy asymptotics to derive the structure of the smouldering front and obtain analytical expressions for the burning temperature and propagation velocity. To simplify the analysis, all these models assume adiabatic, steady state conditions in a frame of reference attached to the smouldering front. Thermal equilibrium between the solid and gas phases is also assumed so that a single temperature model is possible. The reaction kinetics is generally described by a one-step global reaction model that incorporates the pyrolisis and oxidation steps. In one case (Buckmaster and Lozinski, 1996) a two-step kinetic model that considers separately the two reactions is presented.

For forward smouldering, the mode of propagation most relevant to this research, it is found that the combustion front may exist in one of two possible structures (Schult

et al., 1996). In the *reaction leading* structure the reaction zone precedes the heat transfer zone, in which the solid is cooled by the incoming gas flow. In contrast, in the *reaction trailing* structure the heat transfer zone precedes the reaction zone. For both of these structures two types of solutions can occur: stoichiometric and kinetically controlled solutions. The first type of solution occurs when the oxygen is completely consumed in the combustion front so that the reaction must wait for oxygen to arrive before moving on. These solutions display a linear dependence of the smouldering velocity on the incoming oxygen mass flux and are characterised by complete conversion of the solid fuel. Kinetically controlled solutions occur when the supply of oxygen is sufficiently high that the rate of consumption (i.e. the kinetics) limits the propagation. For these solutions, the propagation velocity is mainly influenced by total gas mass influx, through the burning temperature; incomplete fuel conversion is possible in the reaction trailing mode, if the incoming gas flux is so high that the reaction is effectively quenched before completely burning the solid.

When closed-form solutions for the combustion characteristics cannot be obtained – for example because the high activation energy approximation is not applicable – a simplified approach is to integrate the fundamental conservation equations over a control volume that comprises the reaction front to derive an approximate relation between the smouldering velocity and other parameters (Rein, 2009). This approach has proven successful in correlating the experimental data under the assumption of oxygen controlled reaction for both forward (Torero and Fernandez-Pello, 1996) and opposed (Bar-Ilan *et al.*, 2004) smouldering propagation.

While most research has focused on smouldering of solid fuels, there are several examples of combustion of a liquid fuel embedded in a porous matrix. The most relevant to the present research is the process known as in-situ combustion (ISC) (e.g. Greaves *et al.*, 2000, Sarathi, 1999, Akkutlu and Yortsos, 2003). In-situ combustion is a thermal technique for the enhanced oil recovery (EOR) from petroleum reservoirs. ISC is essentially a gas injection oil recovery process where heat is used to improve the recovery. The heat is generated within the reservoir (in-situ) by burning a portion of the oil; the burning is sustained by injecting air or an oxygen rich gas into the formation. The oil is driven toward the extraction wells by a combination gas drive (injected and combustion gases) and water drive (water from combustion and recondensed formation water). The reactions involved in enhanced oil recovery through in situ combustion are described as heterogeneous gas-solid and gas-liquid between oxygen and the heavy oil residue (Sarathi, 1999).

An important feature of smouldering combustion, common to other combustion processes occurring in a porous medium, is the effective energy recirculation from the products to the reactants that takes place within the porous matrix (Figure 1.2). In a porous burner the hot combustion gases downstream of the combustion zone transfer heat by convection to the solid matrix; the hot solid conducts and radiates heat in the upstream direction; upstream of the reaction zone heat is convectively transferred from the solid to the incoming gas (Wood and Harris, 2008).

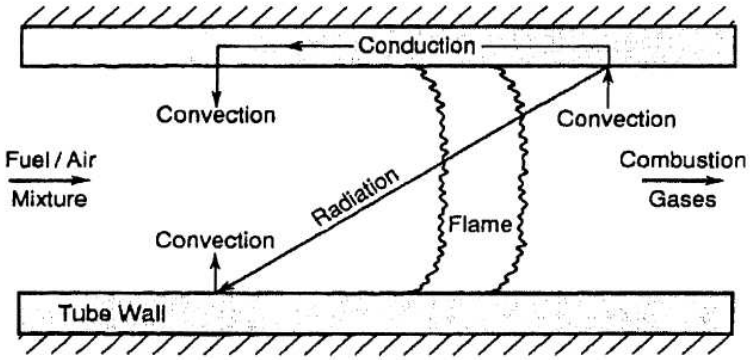

Figure 1.2 Schematic representation of energy recirculation in a porous medium idealised as an insulated refractory tube (Wood and Harris, 2008).

The solid matrix acts therefore as an internal heat exchanger, allowing the process of 'borrowing' enthalpy from the combustion products to preheat the incoming reactants. This can result in what is commonly referred to as 'super-adiabatic combustion' or 'excess enthalpy' burning, with the temperature in the combustion zone that exceeds the adiabatic combustion temperature for a given composition of reactants (Figure 1.3).

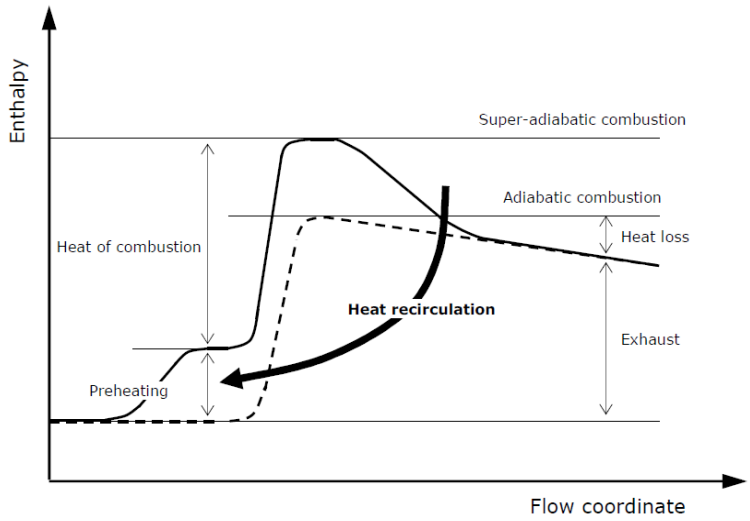

Figure 1.3 Fuel preheating and super-adiabatic combustion (adapted from Agrawal, 2008).

The mechanism of energy recirculation has several advantageous consequences on the characteristics of the combustion process in porous media. Due to the higher

temperature in the reaction zone, higher burning rates can be sustained as well as the combustion of low energy content fuels or very lean air-fuel mixtures (Howell *et al.*, 1996; Al-Hamamre *et al.*, 2006; Wood and Harris, 2008). The possibility of burning lean mixtures means lower emissions of carbon monoxide and unburned hydrocarbon from the combustion of premixed fuels. In addition, the reduced temperature in the products region suppress the formation of nitrogen oxide, which is a highly temperature dependent process (Howell *et al.*, 1996). Another characteristic of the porous burners is the increased stability against short-term fluctuations in the flow and concentration. This means, for example, that the reaction may be restarted after extinction by restoring the flow of the fuel or oxidant due to the high heat capacity of the porous bed that can maintain the temperature above the ignition temperature for some time after the flame has been extinguished (Wood and Harris, 2008).

No literature exists on the smouldering combustion of liquids in the context of NAPL remediation. However, literature research in the field of combustion in porous media and a number of technological applications suggest that NAPL smouldering is a viable concept. Many research questions need to be answered prior to the implementation of this new approach, pertaining to the mechanisms controlling the ignition and propagation of smouldering of organic liquids embedded in porous media.

1.3 Research goals

This research project had the specific goal of assessing the potential of smouldering combustion as a remediation approach for NAPL impacted soil. To this end, a series

of laboratory experiments were designed and conducted at the small and intermediate bench scale. The experimental program was organised into two main objectives. The first was to demonstrate that organic liquids embedded within an inert solid matrix can be successfully smouldered. Proof-of-concept experiments presented in Chapters 2 and 3 of the present thesis served to meet this objective. The second objective of was to characterize the behaviour of the smouldering reaction and assess its efficacy as a remediation technique under a series of contaminant, soil and oxidizer flow conditions. These results are described in Chapters 4 and 5 of this research.

1.4 References

Agrawal, A.K., Innovative combustion and emission reduction techniques, Presented at International Workshop on Advances in Combustion Science and Technology, IIT Kanpur, India, 2008. Retrieved May 28, 2009, from http://www.iitk.ac.in/comb

Al-Hamamre, A., S. Diezinger, P. Talukdar, F. von Issendorff and D. Trimis, Combustion of low calorific gases from landfills and waste pyrolisis using porous medium burner technology, Process Safety and Environmental Protection, (2006) 84 (B4) 297-308.

Akkutlu, I.Y. and Y.C. Yortsos, The dynamics of in-situ combustion fronts in porous media, Combustion and Flame, (2003) 134 229-247.

Amter, S. and B. Ross, Was contamination of southern California groundwater by chlorinated solvents foreseen? Environmental Forensics, (2001) 2 179-184.

Bar-Ilan, A. et al., The effect of buoyancy on opposed smoldering, Combust. Sci. and Tech. (2004) 176 2027-2055.

Buckmaster, J. and D. Lozinski, An elementary discussion of forward smoldering, Combustion and Flame, (1996) 104 300-310.

Davis, E.L., How heat can enhance in situ soil and aquifer remediation: important chemical properties and guidance on choosing the appropriate technique, EPA/540/S-97/502, Editor. 1997.

Dosanjh, S.S., P.J. Pagni and A.C. Fernandez-Pello, Forced cocurrent smoldering combustion, Combustion and Flame (1987) 68 131-142.

Fatehi, M. and M. Kaviany, Adiabatic reverse combustion in a packed bed, Combustion and Flame (1994) 99 1-17.

Geosyntech Consultants, Assessing the feasibility of DNAPL source zone remediation: review of case studies, 2004.

Greaves, M., et al., Air Injection into Light and Medium Heavy Oil Reservoirs: Combustion Tube Studies on West of Shetlands Clair Oil and Light Australian Oil, Chemical Engineering Research and Design, (2000) 78 (A5) 721-730.

Howell J.R., M.J. Hall and J.L. Ellzey, Combustion of hydrocarbon fuels within porous inert media, Prog. Energy Combust. Sci. (1996) 22 121-145.

Interstate Technology and Regulatory council (ITRC), DNAPL source reduction: facing the challenge, 2002.

Mercer, J.W. and R.M. Cohen, A review of immiscible fluids in the subsurface: Properties, models, characterization and remediation, J. Contam. Hydrol. 6 (2) (1990) 107-163.

National Research Council (NRC), Contaminants in the subsurface: source zone assessment and remediation. 2004, Washington, D.C., The National Academies Press.

Ohlemiller, T.J., Modeling of smoldering combustion propagation, Prog. Energy Combust. Sci. (1985) 11 277-310.

Ohlemiller, T.J., Smouldering combustion, SPFE Handbook of Fire Protection Engineering, 3rd ed., Massachusetts, 2002.

Ohlemiller, T.J. and D.A. Lucca, An experimental comparison of forward and reverse smolder propagation in permeable fuel beds, Combustion and Flame (1983) 54 131-147.

Pankow, J.F. and Cherry, J.A., Dense chlorinated solvents and other DNAPLs in ground water. 1996, Portland (Oregon): Waterloo Press.

Rein, G., Smouldering combustion phenomena in science and technology, International Review of Chemical Engineering (2009) 1 (1) 3-18.

Schult, A., B.J. Matkowsky, V.A. Volpert, A.C. Fernandez-Pello, Propagation and extinction of forced opposed flow smolder waves, Combustion and Flame (1995) 101 471-490.

Schult, A., B.J. Matkowsky, V.A. Volpert, A.C. Fernandez-Pello, Forced forward smolder combustion, Combustion and Flame (1996) 104 1-26.

Sarathi, P.S., In-situ combustion handbook – Principles and practices. Report prepared by BDM Petroleum Technologies for U.S. Department of Energy, 1999.

Torero, J.L., A.C. Fernandez-Pello, Forward smolder of polyurethane foam in a forced air flow, Combustion and Flame (1996) 106 89-109.

Torero, J.L. and A.C. Fernandez-Pello, Natural convection smolder of polyurethane foam, upward propagation, Fire Safety Journal, (1995) 24 35-52.

U.K. Environment Agency (UKEA), Source treatment for Dense Non-Aqueous Phase Liquids, Technical Report P5-051/TR/01, 2002.

U.S. Environmental Protection Agency (EPA), The DNAPL remediation challenge: is there a case for source depletion? EPA/600/R03/143, 2003.

U.S. Environmental Protection Agency (EPA), In situ thermal treatment for chlorinated solvents. Fundamentals and field applications, EPA/542/R04/010, 2004.

Wood, S. and A.T. Harris, Porous burners for lean-burn applications, Prog. Energy Combust. Sci. (2008) 34 667-684.

Chapter 2

Small scale forward smouldering experiments for remediation of coal tar in coarse sand

2.1 Introduction

Nonaqueous phase liquids (NAPLs) are a class of organic compounds with a long history of extensive use in industrial processes. As the result of inappropriate disposal practices, NAPLs are now among the most frequently occurring contaminants detected in the subsurface throughout the industrialized world [1]. Most of these contaminants are toxic to humans and the environment in high, acute doses and may be irritants and suspected carcinogens at low, chronic doses. Standard handling and disposal procedures resulted in widespread releases of these chemicals into the environment, creating persistent, long-term sources of groundwater contamination. Existing in soil pores as a separate liquid phase, NAPL dissolve in groundwater in amounts high enough to render it unfit for consumption, but low enough such that its lifespan can be on the order of centuries [2]. Remediation of NAPL-contaminated soil in a cost effective and robust manner remains a significant challenge.

A proposed NAPL remediation approach is destruction by combustion. Many common NAPLs, such as trichloroethylene, petrochemicals or coal tar have heats of combustion in excess of other wastes that are successfully burnt in other industries (*e.g.* biomass energy, waste incineration). Such industries typically employ flaming

combustion to release the heat from the waste and often require additional fuel to sustain the burning process. However, a flame cannot be sustained within the porous media that comprises the subsurface and thus is not a viable technique for soil remediation. Prior to the results of these experiments, the authors hypothesized that smouldering combustion of the organic liquid within the porous matrix can be sustained and propagate, resulting in NAPL destruction and some level of soil remediation.

Little work on smouldering combustion exists and this application has, to the knowledge of the authors, never been explored. Prior to the potential implementation of this new approach, a detailed understanding of the mechanisms controlling ignition and propagation of smouldering of organic liquids embedded in a porous medium is required. This paper presents an initial suite of bench-top experiments that describe the conditions under which a smouldering reaction will propagate in soil embedded with a NAPL. These experiments serve to characterize the reaction and to establish the conditions leading to ignition and propagation that will enable its assessment as a viable remediation technique. A sample fuel, coal tar, has been selected for this paper because it is relatively amenable to ignition and the smouldering reaction is strong (*i.e.*, can be directed away from extinction conditions). This fuel is one of many NAPLs that have been successfully ignited as part of the investigation of the burning conditions for other fuels, whose results are reported elsewhere [3].

Coal tar is a dark-colour NAPL that is typically 1.1 times denser and 160 times more viscous than water at ambient temperatures. It is a by-product of the carbonization of coal to produce coke and/or natural gas and does not occur naturally. Coal tar contains a large number of polycyclic aromatic hydrocarbons (PAHs), phenols, heterocyclic oxygen, sulphur, and nitrogen compounds and is considered carcinogenic to humans. Subsurface contamination with coal tar exists today as a result of uncontrolled disposal of process residuals at former manufactured gas plants, which were situated in most towns and cities in the industrialized world during the late 19^{th} and early 20^{th} centuries. There are more than 1,000 coal-tar contaminated sites catalogued in the United States alone [4]. Conventional remediation methods, such as direct extraction via pumping or groundwater pump-and-treat, have been demonstrated as unable to effectively restore these sites [1].

This paper presents a series of small-scale experiments conducted on sand containing coal tar to assess the potential of smouldering combustion as a novel technology for remediation of contaminated land by water-immiscible organic compounds.

2.2 Smouldering in porous media

Flaming combustion in inert porous media has been studied extensively as a mechanism to control heat losses from combustion reactions and thus allow the burning of low calorific output fuels or very lean mixtures [5]. The enabling factor is the effective retention of heat by the inert porous matrix but its most significant limitation is the need for the fuel to be in the gas phase; thus flaming is not a viable technique for soil remediation and it will not be further discussed here.

An alternative process occurring in porous media and benefiting from the same advantageous heat transfer is smouldering combustion. Smouldering combustion is the flameless burning of a condensed fuel that derives heat from surface oxidation reactions [6]. It generally burns through a wide range of temperatures, is oxygen deficient, spreads slowly and can infiltrate deep into a porous domain. It involves processes related to fluid flow, heat transfer and heterogeneous chemical reactions. In general, a smouldering fuel consists of an aggregate and permeable medium formed by particulates, grains, fibres or a porous matrix. These aggregate fuel elements provide (i) a large surface area per unit volume that enhance surface reactions, (ii) thermal insulation that reduces heat losses, and (iii) permeability to oxygen transport to the reaction sites by convection and diffusion.

Smouldering combustion of solid fuels has been the focus of fundamental research and its characteristics have been studied mostly in fire safety and material synthesis. Material synthesis studies have been reviewed by Merzanov & Khaikin [7] and fire safety researches refer mostly to polyurethane foam [8,9] and cellulose [6]. Studies on incineration processes involving smouldering are unusual; the best known are Salganskii [10] and Vantelon et al. [11].

The smouldering of liquid fuels embedded in an inert porous matrix is also possible. There are two examples of this in the literature. Well known in fire safety engineering are lagging fires, which are fires initiated inside insulating materials (the porous medium) soaked in oils and other self-igniting liquids [12]. In addition, in the petroleum industry, smouldering fronts are purposely initiated in deep underground

reservoirs to drive a fraction of the oil towards the extraction port to enhance recovery (*e.g.*, [13]). There is very little work published on the mechanisms governing the smouldering of liquids.

Once ignition occurs, the smoulder reaction advances gradually through the material. The net heat released by the reactions is partially transferred by conduction, convection and radiation ahead of the reaction and partially lost to the environment. The oxidizer is transported to the reaction zone by diffusion and convection, in turn feeding the oxidation reactions. It is well established that for most materials and typical conditions, the two limiting factors in smouldering propagation are the oxidizer flux to, and the heat losses from, the reaction zone [6,8,9]. Smouldering combustion can propagate in two distinctive modes, forward and opposed, depending on the relative direction of the oxidizer flow. Forward propagation, the mode employed in this study, is the most energy efficient mode of propagation since in this configuration the oxidizer flows through the reaction and the energy is used to preheat the fuel and porous matrix ahead of the reaction front [6,7].

2.3 Experimental set-up

For this set of experiments, a sample holder 100 mm in diameter was identified as large enough to sustain smouldering but small enough to allow for a time-efficient exploration of the phenomena. The reaction front is started by an igniter and the propagation is aided by a forced flow of air.

Figure 2.1 presents a schematic diagram of the experimental apparatus. Upward smouldering combustion tests were carried out in a 1L quartz glass cylindrical beaker

100 mm in diameter and 175 mm in height. Commercial grade fresh coal tar was employed (Alfa Aesar, Heysham, UK) exhibiting a density of 1.2 kg/L at room temperature. The inert sand (Leighton Buzzard 8/16 sand, WBB Minerals, UK) is characterized by a bulk density of 1.7 kg/L, porosity of 0.40 after packing, and grain diameters of 1-2 mm. The fuel/sand mixture was prepared by mixing coal tar and sand in a mass ratio corresponding to the desired NAPL saturation (where NAPL saturation is defined as the volume fraction of pore space occupied by NAPL). The base case NAPL saturation was 25%, corresponding to 0.12 kg coal tar per L sand.

Each sample was prepared in layers (see Figure 2.1). A layer of clean sand was placed at the bottom of the beaker up to a height of 40 mm. Then the air diffuser was installed, which consisted of a 70 mm diameter bronze porous disc, brazed to a structural support. Additional sand was used to bury the air diffuser by a few millimetres. Emplaced next was the igniter, a 3.25 mm square cross section x 762 mm length inconel cable heater (240 V, 450 W, Watlow Ltd, UK) formed into a flat spiral of 80 mm maximum external diameter. Then a 60 mm layer of the coal tar/sand mixture at the desired saturation was added. A final 30 mm layer of clean sand was emplaced at the top of the sample and in contact with the free surface. The igniter was placed at the bottom and upward propagation was chosen because buoyancy favours forward propagation. For this initial study it was chosen to explore the dependence of the process on the two dominant variables, oxidant injection rate and fuel content. Experiments were therefore conducted at different air fluxes fixing the fuel saturation, and at different NAPL saturation levels fixing the air flux. The values of the inlet air flux were calculated by referring the measured volumetric flow

rate to atmospheric pressure and dividing it by the horizontal cross-sectional area of the beaker.

Five 1.5 mm x 0.5 m inconel sheath Type K thermocouples were driven into the sand pack, with their junctions located on the beaker axis, at approximately 10 mm intervals above the cable heater. The thermocouples were connected to a data acquisition system (Multifunction Switch/Measure Unit 34980A, Agilent Technologies). Digital visual images of the process were taken every 10 s using a CCD monochrome camera (Axis 206M Megapixel Network Camera) at a 640x480 dpi resolution.

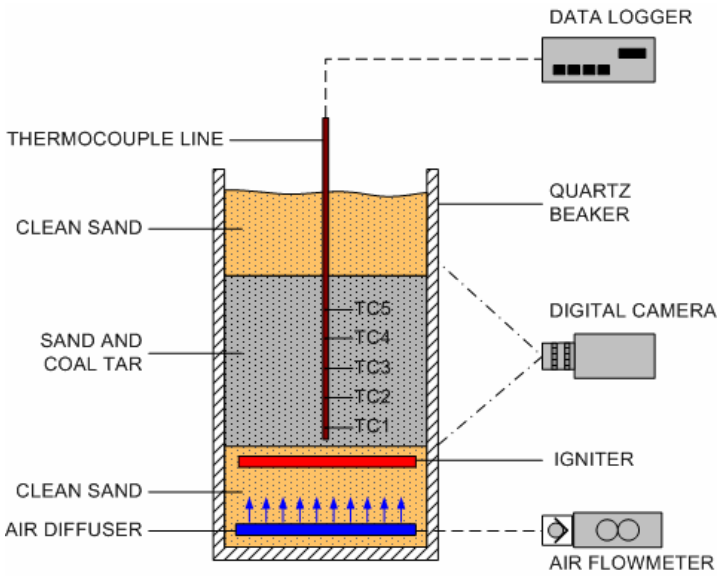

Figure 2.1 Schematic of the experimental apparatus in cross-section.

The experimental system was preheated to a starting temperature of approximately 400 °C, measured at the location of the lowest thermocouple (TC1). This starting temperature was determined from previous testing as the minimum temperature that ensures sample ignition in the selected inlet airflow range. Preheating required 1 hr on average and was carried out by supplying the igniter with progressively increasing power so as to maintain approximately constant the rate of temperature rise at TC1.

The maximum power used for these experiments was approximately 320 W, which corresponds to a heat flux of 41 kW/m^2 over the cross-sectional area of the beaker. A low air flux of 0.6 cm/s was maintained during the preheating period to prevent clogging of the air diffuser or the sand pack. Once the starting temperature was achieved, the air flux was increased instantly to the predetermined level and maintained until the end of the experiment. The igniter was turned off when the temperature measured by the thermocouple TC2 began to decrease with time (*i.e.*, post-peak). This preheating and ignition protocol is analogous to that used in [8, 9] to study the smouldering of polyurethane foam, but adapted to the new fuel characteristics.

The rate of smoulder propagation was obtained using two independent experimental measurements: temperature histories and digital images. Based on temperature histories, the smouldering velocity was calculated from the time lapse of the front arrival at two consecutive thermocouples and the known separation distance. The time of arrival of the reaction front at a certain thermocouple location in the centre of the sand pack is estimated as the average of the times at which the temperature reaches three predetermined values (either 500/600/700 °C or 600/700/800 °C depending on the peak temperature), all of which are above the observed ignition temperature.

In addition, images from the digital camera captured the movement of the glowing part of the smouldering front at the edges of the sample (Figure 2.5). The propagation of this visible front was described by processing the images to track the

movement of its leading and trailing edges. Image capture and analysis is a diagnostic technique commonly used in the study of smouldering reactions in material synthesis and filtering combustion [7]. The combined use of digital imaging and invasive thermocouple probing is a distinctive characteristic of these experiments, made possible by the strongly reacting coal tar and the unconsolidated, particulate inert media. In other contexts of smoulder research the materials under study are either reacting too weakly to be visually detected (*e.g.*, in fire safety engineering [6, 8, 9]) or not susceptible to invasive data acquisition techniques (*e.g.*, in material synthesis [7]).

During the experiment, the presence of CO and CO_2 gases at the free surface in significant amounts was measured as an indicator that a combustion reaction was occurring inside the sand pack. Post-treatment analysis of the samples was conducted to assess contaminant destruction as an indication of the remediation efficacy of the process.

2.4 Experimental observations and results

Thermocouple Results varying Air Flux at fixed NAPL Saturation

The first set of experiments was conducted at forced air fluxes of 2.29, 4.75, 7.94, and 16.2 cm/s for an initial coal tar saturation of 25%. Characteristic temperature time histories for two of these are presented in Figure 2.2. Figure 2.2b also indicates the incremental power supplied to the heater during the experiment. The preheating period lasted approximately 50 min and during this period changes in the power supplied resulted in changes of the slope of the temperature-time histories, which are particularly pronounced for the locations closer to the igniter (thermocouples TC1

and TC2). Thermocouple histories of the form presented in Figure 2.2 are the main diagnostic technique to study smouldering combustion in fire safety engineering [8,9].

Ignition of the fuel is indicated by TC1 (closest to the igniter, see Figure 2.1), and signalled by the measured rapid temperature increase. This ignition occurred either immediately or only a few minutes after the onset of air injection, but always at temperatures greater than 400 °C, This indicates that the ignition temperature for smouldering coal tar is lower and in the vicinity of 400 °C. The nature of the preheating period was explored in detail (data not shown), during which it was observed that an optimal heating rate was essential to attain ignition. Further exploratory experiments were conducted on a series of organic liquids of environmental interest, including trichloroethylene (TCE) and 1,2 dichloroethane (DCA), but in none of these cases ignition was achieved. This finding is presumably to be related to the higher volatility of these compounds as compared to that of coal tar. Vapour pressures of the above chlorinated hydrocarbons are 72 and 82 mmHg respectively at 25 ^{o}C [15] while coal tar's most significant constituents exhibit vapour pressures in the range $10^{-10} - 10^{-2}$ mmHg [16]. As a consequence, vaporization of the chlorinated compounds during the preheating period may have left an insufficient amount of fuel in the liquid phase to produce ignition.

After a location experiences the rapid heating indicative of the onset of smouldering, the temperature reaches a maximum and then starts decreasing as the reaction passes. A succession of similar temperature peaks at successive locations after the igniter is

terminated indicates the self-sustained upward propagation of the reaction away from the ignition zone. In some cases, such as the one presented in Figure 2.2b, the reaction weakens significantly before reaching the top end of the sample as suggested by the temperature history of TC5, which fails to exceed the temperature of the previous thermocouple.

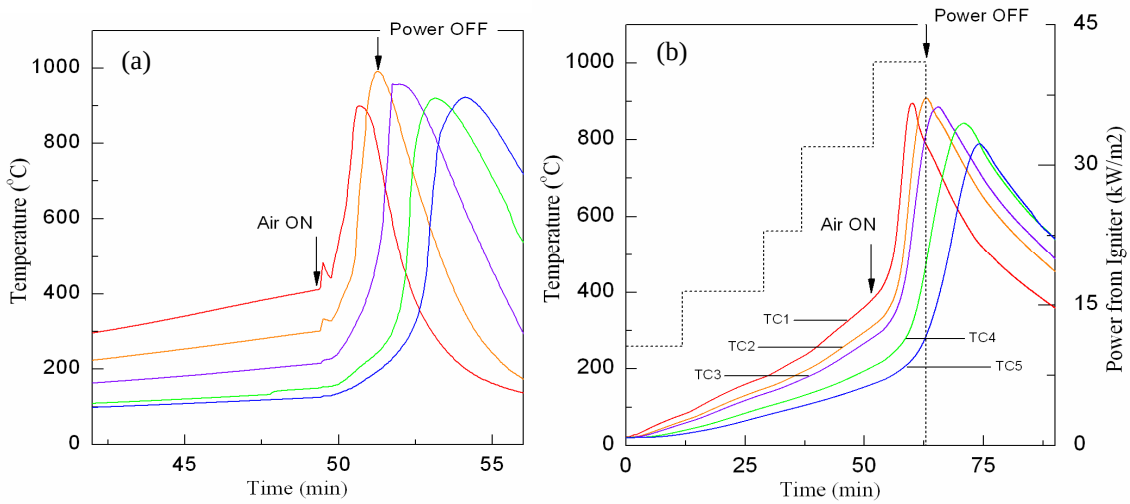

Figure 2.2 Temperature histories along the sample centre axis for a coal tar saturation of 25% and air flow rates of (a) 9.56 cm/s and (b) 2.12 cm/s. In (b) the dotted line indicates power supplied to the heater (right hand vertical axis).

The relationship between the average smouldering velocity and the air flux is presented in Figure 2.3. The results indicate a nearly linear dependence of the propagation velocity with air flux for values above 2.29 cm/s. This trend has been observed before and is typical of oxygen-limited smouldering propagation [8,9]. The variation of the peak smouldering temperature along the sample is presented in Figure 2.4 for the different air fluxes. Peak temperatures at each location ranging from 789 °C to 1073 °C were observed, with the highest values attained for the 4.75 cm/s air flux experiment. The peak temperatures for 7.94 cm/s and 16.2 cm/s are very similar and any differences observed in Figure 2.4 are within the measurement uncertainty of these experiments. These results reveal that, within the

studied range of air fluxes, higher velocities result in faster propagation but not necessarily in higher temperatures. This is typical of combustion in porous media and is mainly associated to the fine balance between oxygen consumption and heat transfer.

As indicated by Figure 2.4, peak temperatures are higher in the middle of the sample and decay towards the top. The observed decay of the peak temperatures in these experiments may be attributed to the influence of the heat from the igniter. At locations distant from the igniter heat losses have a relatively large effect and hamper smouldering propagation, reducing the peak temperature. It is therefore expected that for some of the weaker smouldering fronts obtained here, results in a taller column may show extinction of the reaction at some further distance from the igniter. Figure 2.4 suggests that only for the 2.29 cm/s air flux the reaction approaches extinction conditions as it reaches the end of the sample. This is consistent with the break-up of the linear dependence of the propagation velocity with air flux at lower values presented in Figure 2.3. It is important to note that, in such systems, the relative significance of heat losses decreases as the diameter of the sample increases; thus a stronger smouldering process is expected as the sample is scaled-up. A more detailed analysis of the effect of heat losses and sample size in smouldering processes is presented in [9].

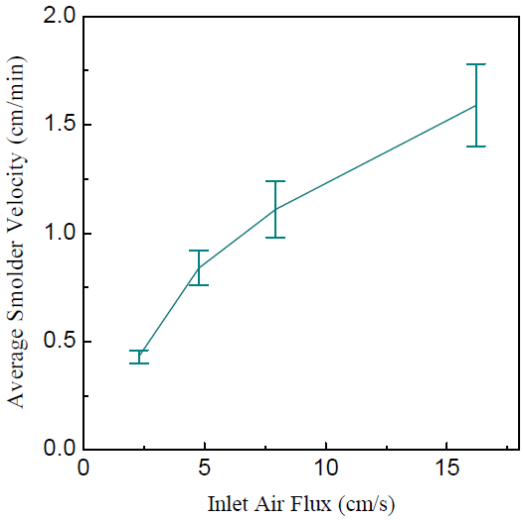

Figure 2.3 Average smouldering velocity as a function of the air flux.

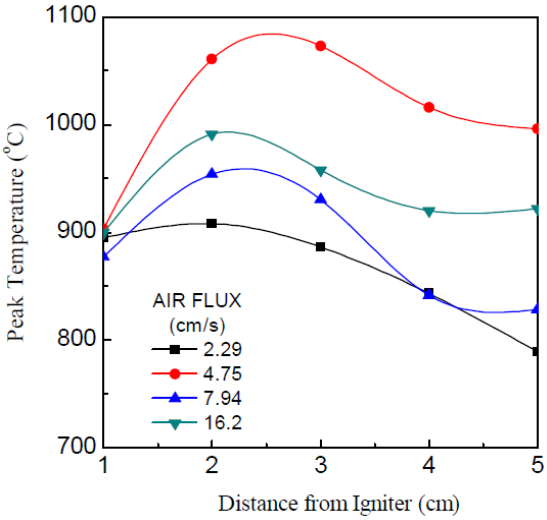

Figure 2.4 Variation of the smouldering reaction maximum temperature along the sample for several air fluxes.

The Influence of Fuel Saturation

The second set of experiments varied the fuel saturation of the sand. The amount of coal tar mixed into the soil for each case was 0.048 kg/L (10% NAPL saturation), 0.12 kg/L (25%) and 0.24 kg/L (50%). The inlet air flux was maintained at 4.75 cm/s. The propagation velocities and peak temperatures for these experiments are presented in Table 2.1. These results indicate that as the saturation increases the smoulder velocity decreases in a roughly linear fashion, which confirms that for this saturation range and air flux the reaction is oxygen limited. The results also indicate that the peak temperature increases with saturation. However, the temperature increment is much more pronounced when saturation is increased from 10% to 25% than from 25% to 50%; in other words, the temperature does not depend linearly on saturation above 25% but seems to approach an asymptotic value.

Table 2.1 Dependence of Forward Smouldering on Fuel Saturation

Saturation	10%	25%	50%
Average smoulder velocity (cm/min)	0.94	0.84	0.61
Average peak temperature (°C)	784	1010	1045

Comparison with Results from Digital Imaging

Figure 2.5 presents a sequence of images corresponding to an experiment at an air flux of 16.2 cm/s and a coal tar saturation of 25%. Similar observations could be made for other conditions. The images were chosen for temporal coincidence with the leading edge of the visible front reaching TC1 (Figure 2.5a), TC2 (Figure 2.5b), TC4 (Figure 2.5c) and TC5 (Figure 2.5d). Images from the outside of the beaker can only capture the visible phenomena taking place within a layer near the edge of the sample. Thus they do not provide a direct indication of the smouldering reaction in the core of the sample. However, they provide a qualitative description of the propagation process.

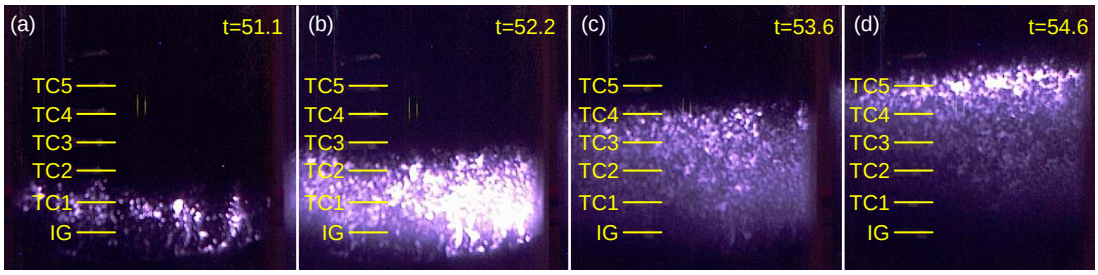

Figure 2.5 Series images showing the onset and propagation of the visible front for an air flux of 16.2 cm/s and a coal tar saturation of 25%. Numbers indicate the position of the thermocouples and the distance in cm from the igniter (IG). Times are in minutes; reaction is initiated at t=50.0 min.

Figure 2.6 compares the propagation of the visible front at the edge with the propagation of the temperature peaks at the core for two experiments, with Figure 2.6a corresponding to the experiment presented in Figure 2.2a and 2.5.

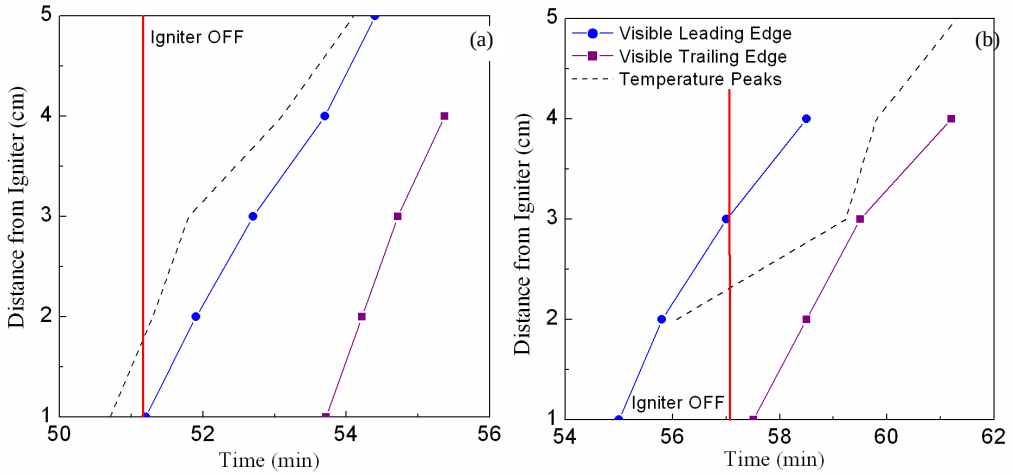

Figure 2.6 Successive positions of the leading and trailing edges of the front at the apparatus boundary obtained from image processing compared with the positions of the temperature peaks along the centre axis for air fluxes of (a) 16.2 cm/s and (b) 4.75 cm/s.

Figure 2.6 reveals that a good correlation exists between the evolutions of the two fronts, with all curves in each graph exhibiting a similar slope (i.e. spread velocity). Velocities obtained from digital images for the 4.75 cm/s and 16.2 cm/s air flux experiments in Figure 2.6 are 0.91 cm/min and 1.23 cm/min respectively. These compare well with the velocities of 0.84 cm/min and 1.59 cm/min, respectively, obtained from the thermocouples. The figure illustrates that for the lower air flux the temperature peak coincides well with the leading edge of the visible front, while for the higher air flux the temperature peak precedes the visible front. Since the visible images privilege the edges of the sample, the differences can be indirectly linked to the strength of the reaction through the curvature of the smouldering front. The visible effect of the curvature is to delay the front observed at the walls with respect to the propagation in the centre. At the lower air flux the front curvature would be lower (i.e., the front is flatter) which is indicative of a stronger reaction. This is consistent with the data presented in Figure 2.4

Post-treatment Analysis of the Sample

After each experiment the sand was excavated and the degree of remaining contamination was first visually estimated. As an illustrative example, sand resulting from one of the experiments is showed in Figure 2.7 compared to clean and contaminated sand. For all the experiments where the reaction was ignited no contamination was detected by visual inspection of sand obtained from the core (i.e., central 80 mm diameter) of the apparatus (Figure 2.7c). A change of the sand colour to red is observed in the treated core. This is attributable to iron oxidation [14] and indicative of exposure to temperatures in excess of 600 °C. Samples taken from the sand adjacent to the beaker walls revealed the presence of some visible residual contamination (Figure 2.7d). This indicates that in the periphery of the sample, heat losses to the external environment caused the quenching of smouldering very close to the wall. Several treated samples were analysed by gravimetric analysis and gas chromatography in order to measure the extent of fuel destruction and removal from the soil. Gravimetric analysis on samples following dichloromethane extraction of all organics revealed average mass removals of 99.95% for the 80-mm diameter core and 98% for the periphery. Volatile compounds (e.g., benzene, toluene, ethylbenzene, xylene) were not detected by gas chromatography-mass spectrometry either in the core nor the periphery of the sample.

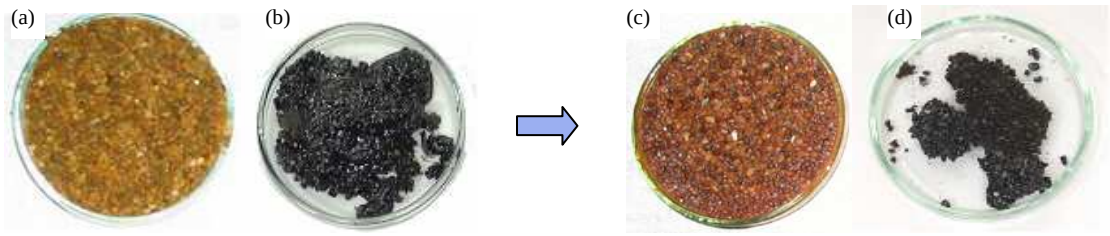

Figure 2.7 Comparison between samples of sand before and after the treatment: (a) Clean sand, (b) sand mixed with fresh coal tar, (c) treated sand from the core, and (d) treated sand from the periphery of the apparatus.

2.5 Conclusions

A set of small-scale experiments of forward smouldering combustion of liquid coal tar embedded in coarse sand has been conducted for a range of inlet air fluxes and fuel saturations. The progress of the smouldering reaction has been tracked by both thermocouple measurements and visual digital imaging. The combination of these techniques provides valuable insight into the properties of the combustion front. The process has been characterized in terms of average smouldering velocity and peak temperatures as a function of distance from igniter, air flux and initial fuel saturation. Results reveal that for all the conditions presented, ignition of the fuel occurred soon after the onset of air injection and self-sustained propagation was established after the igniter was turned off. Peak temperatures were generally highest in the middle of the sample and, decayed towards the top of the sample, but only for the lowest air flux did this appear to result in reaction extinction. The observed temperature decay away from the igniter was attributed to the consequence of igniter-assisted propagation.

Average smoulder velocity shows a nearly linear dependence on the air flux, with a decay of the velocity below the linear trend at low air fluxes. This suggests that, in the range of inlet air fluxes examined, the reaction is oxygen controlled for conditions not approaching extinction. The experiments also show that visual images can be conveniently employed as a detection tool to track the progress of the reaction and that quantitative estimates of the smouldering velocity obtained from images are in good agreement with those produced by thermocouples. Results from tests at varying fuel saturation demonstrate that ignition and self-propagation can be achieved at saturation levels as low as 10 % and show a non-linear dependence of the

peak temperature on saturation. Visual inspection and chemical analyses of the sand post-experiments indicate that smouldering combustion reduces significantly the amount of contaminant present in the soil.

These results demonstrate that smouldering combustion is a promising remediation technique for soil contaminated by organic compounds. Prior to implementing this technique in a field trial, further characterization of the reaction dynamics is underway, including the sensitivity to a range of secondary parameters such as soil type and water saturation. Soil type is considered because it is expected that changing grain size and porosity may influence the air distribution in the porous matrix, with possible formation of preferential paths. Water is considered because it represents a significant heat sink, the presence of which is expected to lead to lower reaction temperatures and lower propagation velocities. These and other additional experiments are being conducted at the bench-and field-scales to explore the sensitivity of the remediation process to a suite of in situ and operational parameters.

2.6 Acknowledgements

This work was supported by Scottish Enterprise and the Engineering and Physical Science Research Council, UK. The authors would like to acknowledge the substantial contribution of Dr. John Jeffrey to the project. The contributions of David Hedges and Wendy Hanson are also acknowledged. A patent application has been filed for this technology.

2.7 References

1. J.F. Pankow and J.A. Cherry, Dense chlorinated solvents and other DNAPLs in ground water, Waterloo Press, Portland, Oregon, 1996.
2. J.W. Mercer, R.M. Cohen, Journal of Contaminant Hydrology 6 (2) (1995) 107-164.
3. J.I. Gerhard, J.L. Torero, C. Switzer, P. Pironi, and G. Rein, In Situ Smouldering Combustion: A Novel Technique for Remediating NAPL Source Zones, Eos Transactions American Geophysical Union 87 (52) (2006), H24A-01 invited talk.
4. D.G. Brown, L. Gupta, T. Kim, H.K. Moo-Young, A.J. Coleman, Chemosphere 65 (2006) 1562–1569.
5. J.R. Howell, M.J. Hall, J.L. Ellzey, Progress in Energy and Combustion Science 22 (1996) 121-145.
6. T.J. Ohlemiller, Progress in Energy and Combustion Science 11 (1985) 277-310.
7. A.G. Merzhanov and B.I. Khaikin, Progress in Energy and Combustion Science 14 (1998) 1-98.
8. J.L. Torero, A.C. Fernandez-Pello, Combustion and Flame 106 (1-2) (1996) 89-109.
9. A. Bar-Ilan, G. Rein, D.C. Walther, A.C. Fernandez-Pello, J.L. Torero, D.L. Urban, Combustion Science and Technology 176 (12) (2004) 2027-2055.
10. E.A. Salganskii, V.P. Fursov, S.V. Glazov, M.V. Salganskaya, G.B. Manelis, Combustion, Explosion, and Shock Waves 39 (1) (2003) 37-42.
11. J.P. Vantelon, B. Lodeho, S. Pignoux,, J.L. Ellzey, J.L. Torero, Proceedings of the Combustion Institute 30 (2005) 2239–2246.

12. D.D. Drysdale, Ignition of Liquids (Chapter 18) in: P.J. DiNenno (Ed.), The SFPE Handbook of Fire Protection Engineering (4th ed.), NFPA, Quincy, MA, 2008.
13. I.Y. Akkutlu, Y.C. Yortsos, Combustion and Flame 134 (2003) 229–247
14. Q.M. Ketterings, J.M. Bigham, Soil Science Society of America Journal 64 (5) (2000) 1826-1833.
15. CRC Handbook of Chemistry and Physics (88th ed.) 2007.
16. W.J. Havenga and E.R. Rohwer, Journal of Chromatography A, 848 (1999) 279-295.

Chapter 3

Self-Sustaining smouldering combustion of Non-Aqueous Phase Liquids: Proof-of-concept experiments

3.1 Introduction

Tens of thousands of sites worldwide exhibit contamination of groundwater and surface water by historical and continuing accidental releases of hazardous non-aqueous phase liquids (NAPLs). Common NAPLs include petroleum hydrocarbons (oils, fuels), polychlorinated biphenyls (electrical transformer oils), chlorinated ethenes (solvents, degreasers), creosote (wood treaters), and coal tar (manufactured gas plants). Complex and/or long-chain compounds, such as heavy oils, PCB oils and coal tar, are particularly recalcitrant, resisting degradation via physical (e.g., volatilization), biological (e.g., dehalogenation), and chemical (e.g., oxidation) treatments that are becoming accepted remedies for more amenable contaminants. Dealing with such wastes involves excavation and either disposal to a hazardous waste landfill or incineration at substantial cost. As an alternative, this research paper proposes a new approach - NAPL smouldering - as a potential remediation process.

Combustion is the exothermic oxidation of a carbon-based compound (i.e., fuel) to primarily carbon dioxide, water, and energy. Indeed, the combustibility of NAPLs is a characteristic that has been successfully exploited through the ex situ incineration of NAPLs and contaminated soil [e.g., (1)]. Incineration is achieved primarily via

flaming combustion. Flaming combustion involves the gasification of a fuel and its exothermic oxidation in the gas phase. Incineration of NAPLs by flaming combustion is energy inefficient (i.e., high heat losses); as a result, incineration requires the continuous addition of fuel and, often, supplemental energy.

Smouldering combustion, in contrast, is the exothermic oxidation of a condensed phase (i.e., solid or liquid) occurring on the fuel surface (2). Smouldering is limited by the rate of oxygen-transport to the fuel's surface, resulting in a slower and lower temperature reaction than flaming. Importantly, smouldering can be self-sustaining (i.e., no energy input required after ignition) when the fuel is (or is embedded in) a porous medium. Self-sustaining smouldering occurs because the solid acts as an energy sink and then feeds that energy back into the un-burnt fuel, creating a very energy efficient reaction (1). Solid porous fuels such as polyurethane foam (3), cellulose (2), and charcoal are typical media that exhibit self-sustained smouldering. For these materials, studies have demonstrated that the rate of propagation of the combustion front and net heat generated are affected by the velocity (magnitude and direction) of air flow, pore diameter of the medium, and the fraction of porosity occupied by fuel, air and non-reacting materials (4). Smouldering reactions can leave a carbon-based residue (oxygen limited reactions) or can result in complete combustion of the fuel (fuel limited reactions) (5). The former is common in combustible porous media where the char minimizes heat losses and enables the reaction to propagate. The latter is common when the fuel is combined with an inert porous medium that provides the required insulation even in the fuel's absence.

While most research focuses on smouldering of solid fuels, there are several examples of combustion of a liquid fuel embedded in a porous matrix. Lagging fires occur inside porous insulating materials soaked in oils and other self-igniting liquids (6). To enhance oil recovery, combustion fronts are initiated in petroleum reservoirs to drive oil towards extraction points (7). The reactions involved in enhanced oil recovery through in situ combustion are described as heterogeneous gas-solid and gas-liquid between oxygen and the heavy oil residue (8). To the authors' knowledge, there is no work published on the mechanisms governing the smouldering of liquids and none involving smouldering as a remediation technique.

NAPL smouldering is different from existing thermal remediation techniques. In situ thermal remediation requires the continuous input of energy in order to primarily volatalize and, in some cases, thermally degrade (pyrolize) and mobilise (via viscosity reductions) the organic phase. All of these processes are endothermic and remediation continues as long as externally-supplied energy input is sustained throughout the NAPL-occupied porous medium. In contrast, NAPL smouldering has the potential to create a combustion front that (i) initiates at a single location with the NAPL-occupied porous medium, (ii) initiates with a one-time, short duration energy input, (iii) propagates through the NAPL-occupied medium in a self-sustained manner, and (iv) destroys the NAPL wherever the front passes. NAPL smouldering is different from in situ combustion for enhanced oil recovery in that the latter is designed to generate heat and pressure that will mobilise the entrapped oil towards recovery wells. NAPL smouldering, in contrast, may benefit from avoiding the recovery (and thus treatment) of NAPL and/or water.

This work presents the first experiments of liquid smouldering in the context of NAPL destruction within porous media. A base case experiment is described in detail to illustrate the viability of the process, fate of the compounds and controllability of the smouldering process in the context of coal tar remediation. A series of 23 experiments is presented to examine the potential of the process across a range of NAPL contaminants, porous media types and other relevant parameters.

3.2 Experimental methodology

A schematic diagram of the experimental apparatus is presented in Figure 3.1. Upward smouldering combustion tests were carried out in a quartz glass column 138 mm in diameter and 275 mm in height. Commercial grade fresh coal tar was employed (Alfa Aesar, Heysham, UK) in the base case, with an assumed density of 1200 kg/m^3 at room temperature (9). The base case employed commercially available quartz sand (Leighton Buzzard 8/16 sand, WBB Minerals, UK), characterized by a bulk density of 1700 kg/m^3, a mean grain size of 1.34mm and a coefficient of uniformity of 1.35. When dry packed, the average porosity of the sand is 40%. To prepare the contaminated material, NAPL and sand were mixed in a mass ratio corresponding to a desired (approximate) saturation (S_N, defined as the volume fraction of pore space occupied by NAPL). The target saturation for the base case was 25%, corresponding to 71,000 mg coal tar per kg sand. The batch was homogenized by mechanical mixing prior to packing in the apparatus.

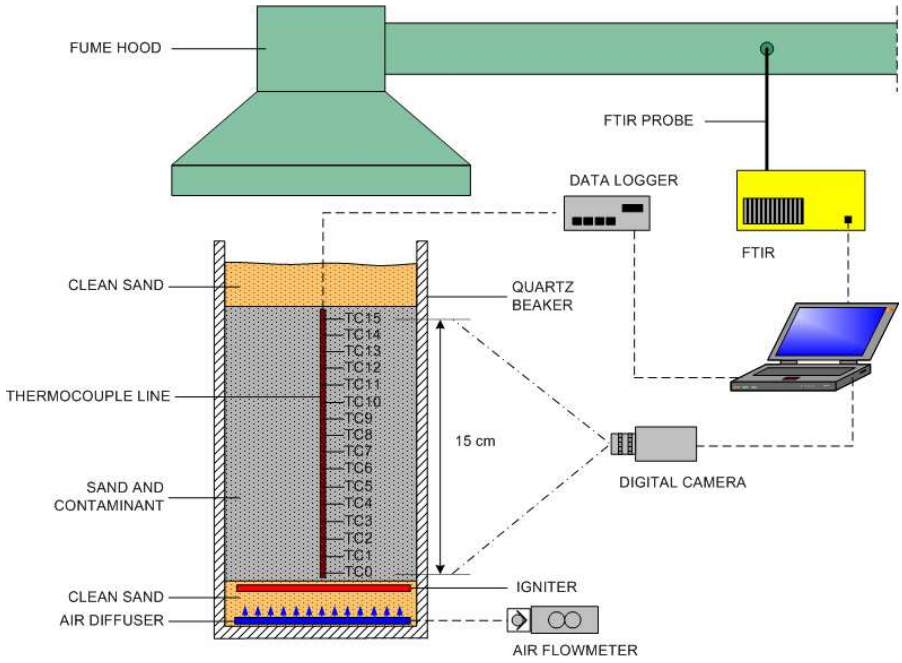

Figure 3.1 Schematic of the experimental apparatus and setup (not to scale).

The apparatus was packed each time in standard sequence (Figure 3.1). A 30 mm layer of clean sand was emplaced followed by the air diffuser, which consisted of eight perforated 6 mm tubes radiating from a central support connected to an air compressor via an air inlet tube. Clean sand was used to bury the air diffuser by a few millimetres, upon which was emplaced the igniter: a 3.25 mm square cross section x 762 mm length inconel-sheathed cable heater (240 V, 450 W, Watlow Ltd, UK) formed into a flat spiral of 130 mm maximum external diameter. The igniter was placed at the bottom and upward propagation was chosen because buoyancy favours forward propagation (3) (i.e., combustion front progressing in the same direction as the oxidizer flow). A 150 mm layer of the NAPL-contaminated sand was then emplaced. The high viscosity and cohesion of the material ensured no distinct layering or grain size separation occurred during emplacement. A final 30 mm layer of clean sand was emplaced at the top of the sample.

Fifteen 1.5 mm x 0.5 m inconel-sheathed Type K thermocouples were inserted into the sand pack along the column central axis and spaced at 10 mm intervals above the cable heater. The thermocouples were connected to a data acquisition system (Multifunction Switch/Measure Unit 34980A, Agilent Technologies). Continuous exit gas analysis was performed using a Fourier Transform Infrared (FTIR) system equipped with an onboard oxygen sensor (Analyser Dx-4000, Gasmet Technologies). At the start of each experiment, the material adjacent to the igniter (as measured at the lowest thermocouple, TC1) was preheated to 400 ^{o}C, requiring approximately 90 min. on average. Once this temperature was achieved at TC1, air injection at the predetermined level (4.25 cm/s for the base case) was initiated and maintained until the end of the experiment. The igniter was turned off when the temperature at TC1 began to decrease with time (i.e., post-peak), typically a short time (e.g., 10 minutes) after initiating the air flow. The maximum power used for these experiments was approximately 390 W, which corresponds to a heat flux of 26 kW/m^2 over the horizontal cross-sectional area of beaker. This ignition protocol was determined from a series of proof of concept experiments (10).

The rate of smoulder propagation was obtained from the temperature histories of the thermocouples embedded in the sand pack. The smouldering velocity was calculated from the time lapse of the front arrival at two consecutive thermocouples and the known distance between thermocouples. The front arrival at a thermocouple location was taken as the average of the times at which the temperature reached 500, 600, and 700 ^{o}C, all of which are above the observed ignition temperature (10).

Pre- and post-treatment analysis of the samples was conducted to assess contaminant destruction as an indication of the remediation efficacy. Accelerated solvent extraction (ASE) with a 50mL mixture of dichloromethane and acetone was conducted on 20g soil samples. The extract was analysed for total extractable petroleum hydrocarbons (TPH) in the C_{10} to C_{40} range by a gas chromatograph equipped with flame ionisation detector (Finnegan Focus GC, Thermo Electron Corporation, Hemel Hempstead, UK) and also for polycyclic aromatic hydrocarbons (PAHs) by gas chromatograph equipped with mass spectrometer (Thermo Quest Trace GC and Finnegan Trace MS, Thermo Electron Corporation, Hemel Hempstead, UK).

A second experimental apparatus was employed to obtain basic smouldering data over a wide variety of test conditions more rapidly than the base case system (Table 3.2). These demonstration experiments were conducted in a similar manner with a smaller quartz beaker (100mm diameter). The height of the contaminated soil pack was 50mm instrumented with 5 thermocouples. While not sufficient to give detailed smouldering data, this setup proved successful for evaluating NAPL/soil combinations that will smoulder successfully.

Demonstration experiments 1-7 examined the effects of contaminant concentration. Experiment 1 represents the base case of 71,000 mg/kg coal tar in coarse sand in the smaller apparatus. In experiments 2-6 the initial coal tar concentration was varied from 14,200 mg/kg coal tar ($S_N \approx 5\%$) to 284,000 mg/kg ($S_N \approx 100\%$). In

demonstration experiment 7, a mixture of 71,000 mg/kg coal tar, 100,000 mg / kg water and coarse sand was prepared ($S_N \approx 25\%$ and $S_W \approx 40\%$).

The effects of contaminant type were examined in experiments 8 – 14. The NAPLs studied were mineral oil (GTX 15W-40, Castrol UK Ltd, Swindon, UK), crude oil (Nynas, Dundee, UK), vegetable oil (Sainsbury's, London, UK), dodecane (Acros Organics, Geel, Belgium), 25% grease in dichloroethane (Acros Organics, Geel, Belgium) and 25% vegetable oil in trichloroethylene (Acros Organics, Geel, Belgium). In experiment 14, a coal tar extracted from a former manufactured gas plant (MPG) contaminated soil (Site 1, Scotland) was tested in a medium sand (Lochaline A, Tilcon Ltd, Manchester, UK; mean grain size of 0.53 mm).

Demonstration experiments 15-18 examined the effects of soil type and layering. In experiment 15, medium sand was employed at a concentration of 71,000 mg/kg coal tar. In experiment 16, natural peat (excavated at Rothiemurchus, Scotland) was mixed with coal tar at 280,000 mg/kg. In experiment 17, the apparatus was packed in two layers of equal thickness, with the coarse sand (71,000 mg/kg coal tar) overlying the medium sand (71,000 mg/kg coal tar) (Figure 3.2). In experiment 18, a 1 cm layer of clean medium sand separated 2 coarse sand layers, each exhibiting 71,000 mg/kg coal tar (Figure 3.3).

Field contaminated samples were studied in demonstration experiments 19-23. These samples were tested as received (i.e., not dewatered). Experiment 19 employed pulverised oil sands. Experiments 20 – 23 were coal tar-contaminated soil samples

extracted from three distinct former MPG sites in Scotland. In each case, the soil was a heterogeneous sample of “made ground” (i.e., artificial fill with wide assortment of materials from silt to gravel). Experiment 23 employed oil drilling cutting waste mixed at a 3:1 ratio with coarse sand.

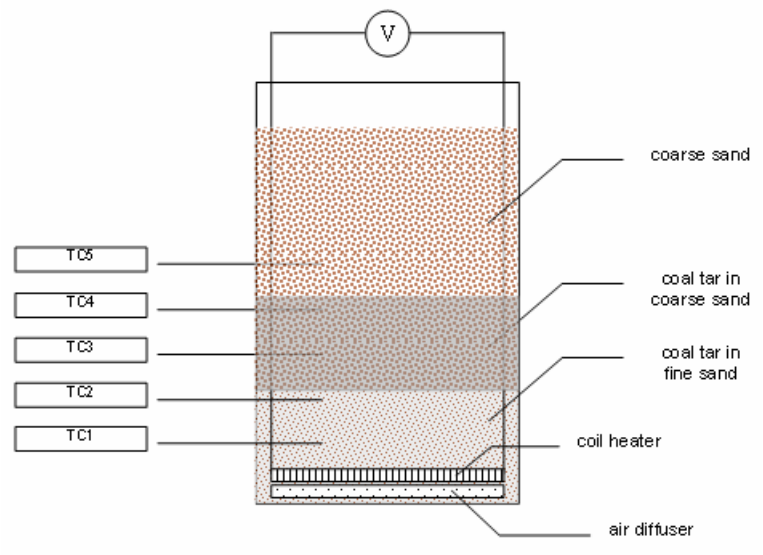

Figure 3.2 Setup for experiment 17 where the apparatus was packed in two layers of equal thickness, with the coarse sand (71,000 mg/kg coal tar) overlying the medium sand (71,000 mg/kg coal tar).

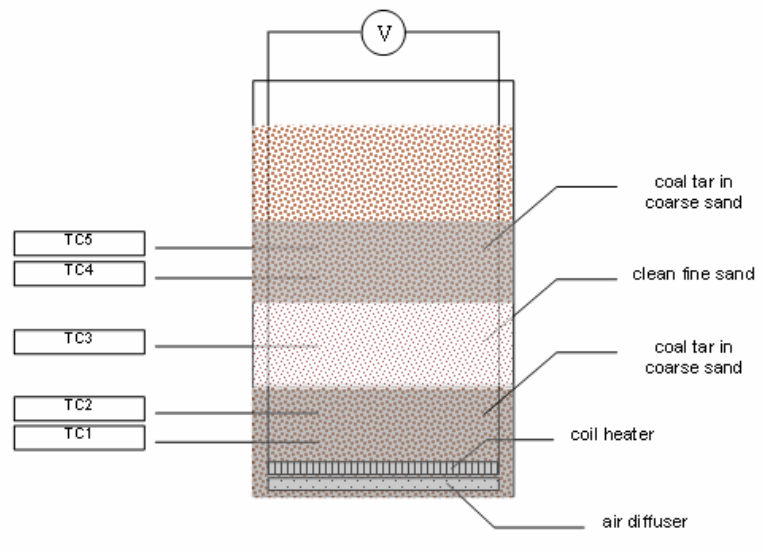

Figure 3.3 Setup for experiment 18 where a 1 cm layer of clean medium sand separated 2 coarse sand layers, each exhibiting 71,000 mg/kg coal tar.

3.3 Results and discussion

3.3.1 Base case experiment: proof of concept

Smouldering Combustion Temperature Profiles

Figure 3.4 presents the evolving temperature profiles of the base case experiment (coal tar, 71,000 mg/kg). With the ignition heater initiated at t=0, the temperature immediately adjacent to the igniter achieved 400 ^{o}C in approximately 105 minutes. The introduction of air at this time resulted in an immediate change in the rate of temperature increase, corresponding to ignition. Initiation of smouldering combustion of the coal tar at this time is confirmed by the appearance of carbon dioxide (CO_2), a combustion product, in the effluent gas stream (Figure 3.4, right axis). The temperature near the igniter achieved a maximum of approximately 1190 ^{o}C at 112 min (i.e., 8 min after ignition). The temperature at this location then decreased as the contaminant (fuel) was consumed by the smouldering reaction, reaching ambient temperature after approximately 160 min.

At the time of ignition, Figure 3.4 illustrates that the temperatures throughout the column ranged from approximately 360 ^{o}C (1 cm from the igniter) to ambient at the top of the contaminated sandpack. The power supplied to the igniter was turned off at 114 min. The energy supplied by the combustion reaction seemed sufficient to allow propagation of the reaction along the entire length of the contaminated sandpack. A continuous succession of non-diminishing peak temperatures (here approximately 1050 ^{o}C) in the absence of externally provided energy is characteristic of a self-sustaining smouldering process (11).

The smouldering velocity was calculated to be 1.3 x 10^{-2} cm/s (0.84 cm/min), a value consistent with other smouldering applications (12). Moreover, these types of temperature profiles are typical of smouldering combustion in other materials (e.g., polyurethane foam), although the observed temperatures in those materials are lower (3,13). Coal tar is a flammable substance in the absence of porous media. The ability of the porous media to trap and recirculate the heat produced by the smouldering reaction may enhance the reaction temperatures. This effect is observed in porous media burners, which can extend the flammability range of fuels and result in weakly flammable substances burning quite readily and even the attainment of super-adiabatic flame temperatures (14-17).

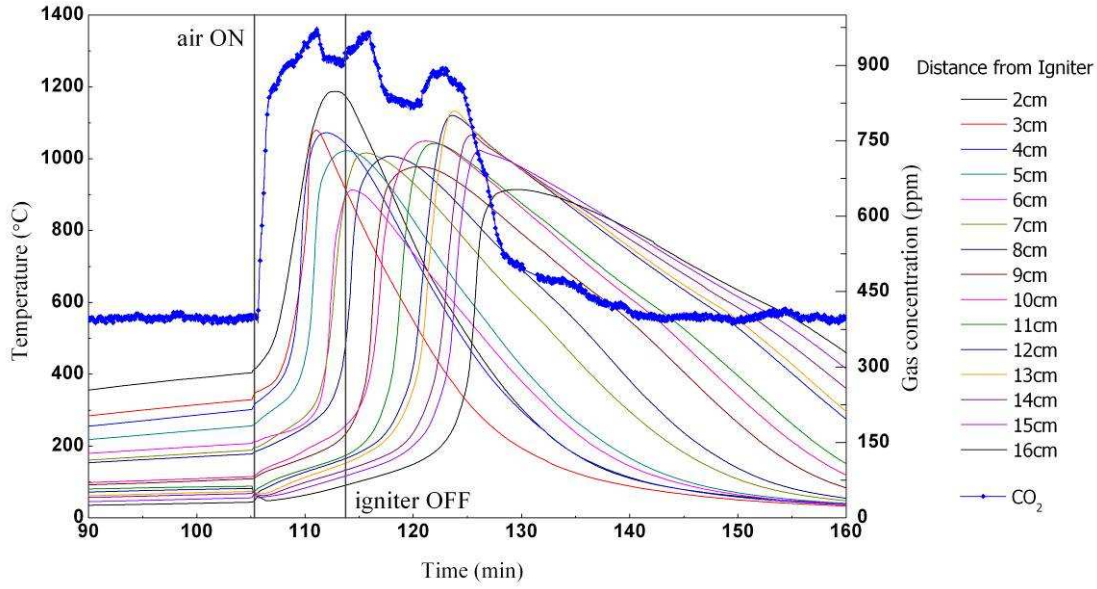

Figure 3.4 Temperature histories along the sample centre axis for the base case experiment (coal tar concentration of 71,000 mg/kg or 25% approximate saturation and air flow rate of 4.25 cm/s).

Comparison to Clean Sandpack Experiment

A comparison experiment was conducted with conductive heating only applied to sandpack with no coal tar present. In this blank experiment, the heater was left on

throughout. The temperature profiles at 10 cm from the igniter in both the base case and blank experiments were compared to determine the net energy input (Figure 3.5). The blank experiment achieved only 100 ^{o}C with constant heating, while the base case experiment achieved 1050 ^{o}C. The area under each temperature curve represents the energy accumulated at this location. Integrating the temperature profiles for the entire sandpack for both experiments quantifies the net energy input (i.e., input minus losses); this calculation reveals that the net energy input is approximately 6 times greater in the base case than the blank experiment. This difference illustrates that smouldering coal tar combustion is a strong, exothermic, self-sustaining reaction.

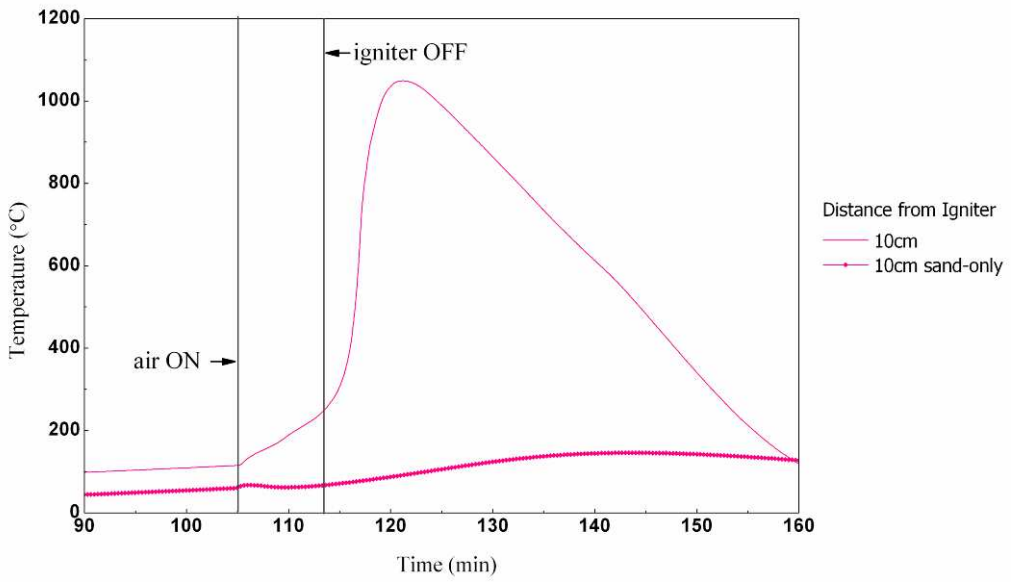

Figure 3.5 Temperature histories at 10 cm from the igniter for the base case experiment and for the corresponding blank experiment (no NAPL present) at 4.25 cm/s air flow rate.

Soil Alterations

Visual inspection of the post-treatment sand showed no apparent signs (i.e., via sight, smell, or touch) of remaining contamination throughout the sand pack (Figure 3.6). However, the colour of the sand grains had changed from yellow to red. Similar

effects are seen in soils after wildfires and slash-and-burn conversion of forest land for agricultural purposes (14,15). Severe fires have been associated with water repellancy and a number of other physical and chemical changes to the soil itself (15-17); some of these changes may be reversible if addressed directly (16). More research is necessary to understand the effects of smouldering combustion on soil properties.

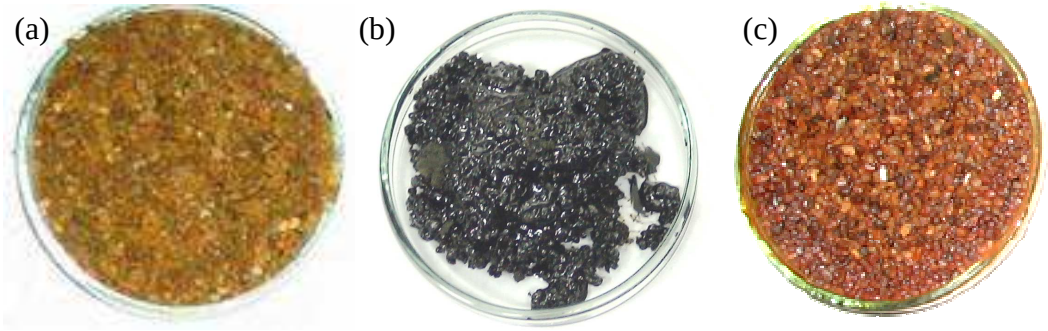

Figure 3.6 Coarse sand (a) before mixing with coal tar, (b) after mixing with coal tar and (c) after STAR treatment. The final concentration of the sand in (c) was less than 0.1mg/kg TPH.

Comparison to Conductive Heating Alone

A repeat of the base case experiment, with coal tar concentration at 71,000 mg/kg (S_N≈25%) was performed with conductive heating alone (i.e., no air injection). The same heating protocol was followed as the base case except that the power input was held constant instead of being terminated at 114 min. Similar heating of the two contaminated soil packs was observed initially, with 400 ^{o}C reached at the nearest thermocouple in approximately the same time in both the base case (Figure 3.4) and the conductive heating case (Figure 3.7). In the absence of air injection, the temperature continued to increase slowly in the conductive heating experiment with a maximum temperature of approximately 650 ^{o}C achieved in 164 minutes. Maximum temperatures decreased with increasing distance from the heater, with temperatures

near the top of the contaminated soil pack (12-16cm) reaching 100 ^{o}C at the time that the power supplied to the heater was terminated. CO_2 monitoring throughout this experiment revealed that combustion was not occurring at any time (data not shown). Thus, the higher temperatures obtained in this case as compared to the blank experiment are not due to exothermic chemical reactions but mainly due to the sustained high temperature at the heater for the duration of the experiment and the significantly higher heat capacity of coal tar relative to sand. This experiment underscores that smouldering combustion is a reaction that cannot proceed in the absence of an oxidant.

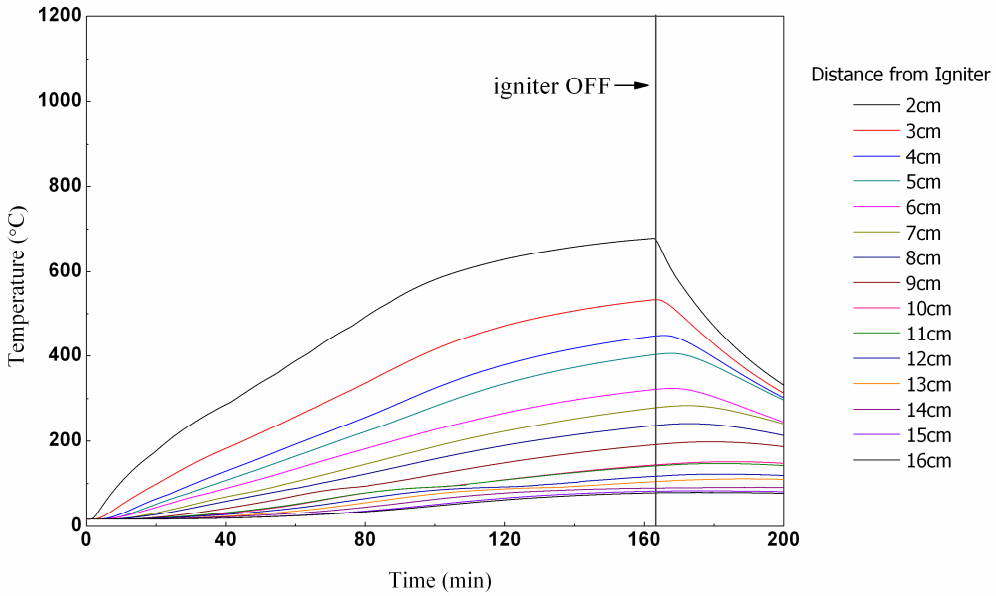

Figure 3.7 Temperature histories along the sample centre axis for a coal tar concentration of 71,000 mg/kg (25% approximate saturation) and conductive heating only (i.e., no air injected).

Terminating the Reaction

Smouldering fires of peat and coal in the natural environment have been known to burn for months or years (18,19) due to the extensive supply of fuel, the availability of oxygen, and the self-sustaining nature of the process. To investigate the ability to control NAPL smouldering in the laboratory, an experiment was conduct under

similar conditions as the base case except the air injection was terminated prior to completion. Temperature profiles in this case followed similar trends to the base case until the air was terminated (Figure 3.8). Near the bottom of the contaminated sandpack, where the smouldering reaction may have reached completion, the temperature profiles are relatively undisturbed by the termination of the air flow (except for a decrease in the rate of temperature reduction due to the loss of the cooling effect). In the centre of the sandpack, where increasing temperatures suggested that the smouldering reaction was beginning, the temperatures decreased rapidly after air termination. This shift suggests that for the fuel and conditions examined here, the smouldering reaction cannot sustain itself in the absence of supplied air, which is confirmed by the immediate reduction in CO_2 back to ambient levels (Figure 3.8). Termination experiments were conducted for a number of different conditions with identical results; the reaction did not continue in the absence of an externally supplied air flow.

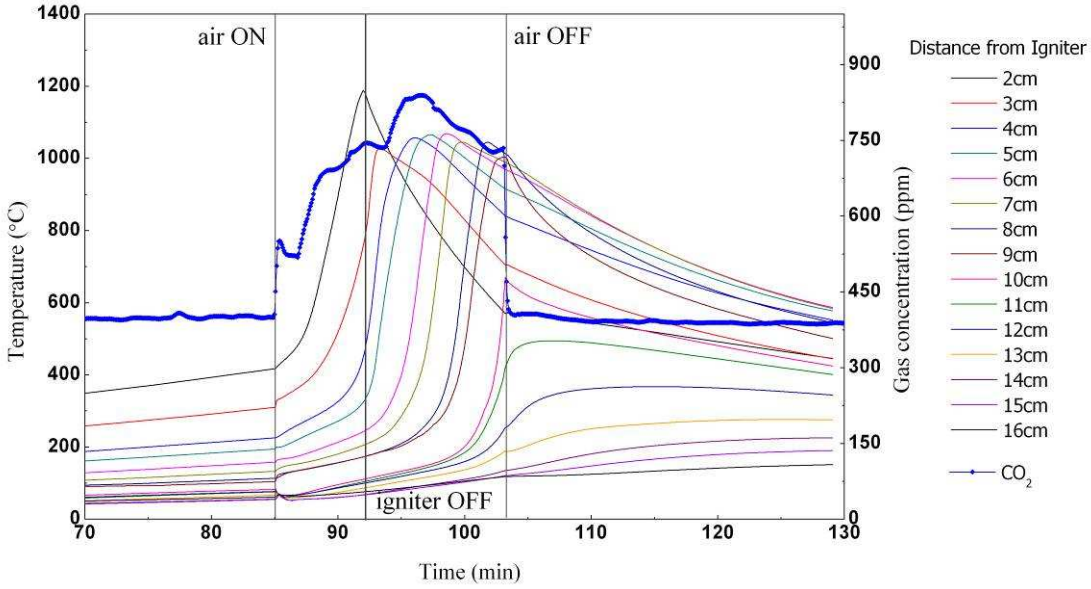

Figure 3.8 Temperature histories along the sample centre axis for a repeat of the base case experiment (coal tar concentration of 71,000 mg/kg or 25% approximate saturation and air flow rate of 4.25 cm/s) in which the air supply was terminated prematurely.

3.3.2 Fate of Coal Tar Compounds

Chemical Analysis of Post-Treatment Soil

Chemical analysis was conducted on sequential subsamples of the post-treatment sands in the three coal tar-contaminated experiments: base case, conductive heating only, and air supply terminated. Prior to the experiments, the base case coal tar sand packs exhibited TPH of approximately 38,000 mg/kg in the C_{10} to C_{40} range (71,000 mg coal tar / kg sand as prepared, $S_N \approx 25\%$) and PAH content of approximately 9,500 mg/kg. Post-experiment, the base case revealed no measurable TPH or PAH (i.e., below detection limit of 0.1 mg/kg) in the majority of locations (Table 3.1). The top of the sandpack exhibited the highest residual TPH value of 1.2 mg/kg, likely related to the condensation and deposition of volatile components or combustion products. At the same subsampling intervals, conductive heating alone was observed to reduce the coal tar concentrations significantly close to the heater (e.g., 2210 mg/kg) and residual TPH concentrations increased with increasing distance (Table 3.1, Figure 3.9). Residual TPH values are observed to increase with decreasing maximum temperature achieved during the experiment. The absence of vapour or liquid extraction to remove the coal tar suggests that conductive heating alone mobilised the coal tar, possibly below the heater and the air diffuser where subsampling was not conducted. In the termination experiment, residual TPH values increased as distance from the igniter increased (Table 3.1). Locations near the igniter did not exhibit TPH reductions as significant as the base case experiment, suggesting that despite being well along in the cooling stage, continued smouldering may have been interrupted by air termination.

Table 3.1 Summary of Chemical Analysis Results

Distance from igniter (cm)	Base Case		Heat Only		Terminated	
	TPH (mg/kg)	PAH (mg/kg)	TPH (mg/kg)	PAH (mg/kg)	TPH (mg/kg)	PAH (mg/kg)
0-1	<0.1	<0.1			580	
1-2	<0.1	<0.1	2210	680	760	730
2-3	<0.1	<0.1			330	
3-4	<0.1	<0.1	11800	5370	450	430
4-5	**0.3**	**0.3**			500	
5-6	<0.1	<0.1	29300	14100	190	170
6-7	<0.1	<0.1			980	
7-8	<0.1	<0.1			580	
8-9	<0.1	<0.1			6150	
9-10	<0.1	<0.1	33900	7730	3080	2030
10-11	<0.1	<0.1			7650	
11-12	<0.1	<0.1			36200	
12-13	**1.2**	**1.21**			42000	
13-14	<0.1	<0.1	35000	9500	29500	27800
14-15	<0.1	<0.1			30800	
15-16	<0.1	<0.1			30600	

(a)

(b)

Figure 3.9 Excavated samples taken at 1cm intervals from the top (left) to the bottom (right) after (a) the base case experiment of STAR applied to coal tar in sand and (b) conductive heating of coal tar (no air present).

Characterisation of Emissions

Emissions characterisation was conducted by real-time FTIR analysis of the exhaust gas stream. The significant gaseous products were carbon dioxide, carbon monoxide and naphthalene, with maximum concentrations of 2100, 430, and 56ppm, respectively. Trace amounts of toluene and m-xylene were identified in the exiting gas stream (maximum concentration 15ppm). Methane and hexane were also measured in trace quantities in amounts too low to quantify. Nitrogen and sulphur

oxides were not detected. In general, emissions are anticipated to be a function of the contaminant, the soil, and the operating conditions. Further emissions analysis is warranted across a range of contaminant and soil conditions to facilitate their control or capture.

Gaseous Byproduct Formation

Because NAPL smouldering involves the combustion of hazardous materials, the potential exists for the formation of harmful by-products during the smouldering process. Chemical compounds such as polychlorinated dibenzo dioxins and furans (PCDD/Fs) have been reported in the context of municipal solid waste (MSW) incineration (20,21). Optimal conditions for PCDD/F formation may include (i) temperatures of 200-400^{o}C (21,22), (ii) significant chlorine content in the starting material (22-24), and (iii) the presence of catalysts such as copper or iron (22). At temperatures greater than 400^{o}C, PCDD/Fs tend to undergo thermal decomposition (21). A standard protocol for post-treatment of incinerated MSW to remove PCDD/Fs is thermal treatment at greater than 850^{o}C for more than 2 seconds (22). In addition, the presence of sulphur either in the waste material itself or as an additive during the combustion process may inhibit PCDD/F formation (24,25).

These factors suggest that smouldering combustion of coal tar, in which the physical processes differ substantially from traditional incineration, is not likely to produce PCDD/F compounds. Coal tars typically have little or no chlorine content. In addition, the peak temperatures observed (in excess of 1000^{o}C) favour PCDD/F destruction. Further, the emission of SO_X compounds, which are anticipated in the

combustion of some coal tars, suggest further inhibition of PCDD/F production during coal tar smouldering. Nevertheless, direct testing is warranted to investigate the absence of harmful gaseous byproducts such as PCDD/Fs; however, gas emission volumes were expected to be too low in the presented experiments.

3.3.3 Demonstration Experiments

Demonstration experiments were conducted to examine the applicability of NAPL smouldering combustion across a range of typical contaminant and soil conditions, identifying important areas for future work (Table 3.2). In all cases, NAPL smouldering was initiated successfully and propagation was observed. In the cases where peak temperatures do not decay with distance from the igniter (i.e., clearly self-sustaining), a propagation velocity is reported; if peak temperature decay is observed, a propagation velocity is not reported.

Initial concentration was varied in experiments 1-6. Time to ignition seemed to increase with coal tar concentration and, except for experiment 3, the smouldering propagation velocity appeared to slow with increasing concentration. Self-sustaining smouldering was not observed in experiments 5 and 6, suggesting that at these low concentrations, heat loss effects become significant. These data suggest that in the range between 28,400 and 71,000 mg/kg coal tar ($10\% < S_N < 25\%$) in this experimental system, a critical concentration exists where self-sustaining smouldering becomes possible. Because heat loss effects decrease with increasing scale (due to reduced surface area to volume ratio), this critical concentration is expected to be lower at larger experimental scales.

In experiment 7, when coal tar (71,000 mg/kg) and water (100,000 mg/kg) were both present in coarse sand, the time to ignition appeared faster than in the base case with no water present and the peak temperatures were similar. The observed propagation velocity was slower than the base case, despite a slightly higher air flux. These phenomena are not necessarily contradictory. For ignition, conductive heat transfer is important. At the igniter, the presence of modest water contents may help to ignite the coal tar faster by acting as a heat sink helping to accumulate heat locally. At the same time, the soil moisture may slow the smouldering propagation velocity because the moisture away from the igniter continues to serve as a heat sink. At higher moisture contents, the presence of water may delay both ignition and propagation.

Experiments 8-14 varied contaminant type. All of the pure and mixed NAPLs employed exhibited ignition and propagation of the smouldering front. In all cases, except experiment 14 (field coal tar), the peak temperatures decayed with distance; however, in all cases, the final sandpack appeared clean to sight, smell, and touch. These preliminary results suggest that self-sustaining smouldering may be possible for these contaminants at a larger experimental scale.

In the experiments that varied porous media type (experiments 15-18) self-sustaining smouldering was observed in all cases and all resulted in an apparently clean sandpack. In experiment 15, ignition was achieved faster in the medium sand than the base case, but smouldering propagation was an order of magnitude slower than in the base case despite a higher air flow rate. The finer grain size may have reduced oxygen availability to the smouldering reaction, slowing propagation. In experiment

16, the peat acted as an additional fuel and both NAPL and soil were destroyed. In experiments 17 and 18, the permeability contrasts did not inhibit the continuous propagation of the smouldering front, nor did the presence of a 1 cm lens of clean material. There may be a critical thickness of clean layer, likely scale-dependent, that inhibits propagation of the reaction.

Experiments 19-23 demonstrated that successful smouldering was possible in a variety of samples obtained from NAPL-contaminated sites. Smouldering behaviour seems to correlate strongly to contaminant type and initial concentration. Heavy hydrocarbons such as coal tar and the petroleum present in the oil sands may have performed best because the smouldering reactions may have been energetic enough to overcome the severe heat losses of the small demonstration system.

Table 3.2 Demonstration Experiments conducted across a range of conditions

	Experiment	Porous Media	Contaminant	concentration (mg/kg (S_N))	ignition temp (°C)	max. temp (°C)	time to ignition (min)	air flow rate (cm/s)	propagation velocity (m/s)	Comments
saturation	1	coarse sand	coal tar	71000 (25%)	400	1010	50	4.25	1.40E-04	Base case experiment at a smaller scale.
	2	coarse sand	coal tar	280000 (100%)	400	1178	80	4.25	1.12E-04	
	3	coarse sand	coal tar	230000 (80%)	400	1277	80	4.25	2.00E-04	
	4	coarse sand	coal tar	140000 (50%)	400	1045	85	4.25	1.02E-04	
	5	coarse sand	coal tar	28000 (10%)	400	784	50	4.25		Not self-sustaining. Centre is clean but contamination is apparent near edges.
	6	coarse sand	coal tar	14000 (5%)	400	578	45	4.25		Not self-sustaining. Centre is clean but contamination is apparent near edges, more severe than experiment 5.
	7	coarse sand	coal tar water	71000 (25%) 100000 (100%)	470	1040	47	5.31	7.40E-05	Faster ignition than base case but slower propagation.
contaminant	8	coarse sand	mineral oil	210000 (near 100%)	400	890	23	4.25		Successful ignition.
	9	coarse sand	crude oil	210000 (near 100%)	400	705	53	4.25		Successful ignition.
	10	coarse sand	vegetable oil	210000 (near 100%)	203	786	44	4.25		Successful ignition.
	11	coarse sand	dodecane	180000 (near 100%)	240	660	32	4.25		Successful ignition.
	12	coarse sand	DCA/grease	290000 (near 100%)	200	688	22	4.25		75% / 25% mass ratio of DCA to grease. Successful ignition.
	13	coarse sand	TCE/oil	340000 (near 100%)	350	689	24	4.25		75% / 25% mass ratio of TCE to oil. Successful ignition.
	14	medium sand	field coal tar 1	unknown	250	1053	52	4.25	9.80E-05	Coal tar from same site as experiment 20 mixed with medium sand in the laboratory.
porous media	15	medium sand	coal tar	71000	400	822	23	5.31	1.40E-05	Faster ignition than base case but slower propagation.
	16	peat	coal tar	280000	300	1010	47	5.31	3.50E-05	Peat from Rothiemurchus, Scotland, mixed with laboratory coal tar. Self-sustaining smouldering, but peat destroyed, too.
	17	2 layers -coarse over medium sand	coal tar	71000	425	1139	43	4.25	8.30E-05	Coal tar mixed with coarse sand (71,000 mg/kg) above coal tar mixed with fine sand (71,000 mg/kg).
	18	3 sand layers (middle layer clean)	coal tar	71000	400	1139	47	4.25	8.30E-05	1cm layer of clean medium sand separating two layers of coal tar in coarse sand (71,000 mg/kg).
field materials	19	oil sands	petroleum solids	unknown	300	1066	35	4.25	1.70E-04	Oil sands of North American origin. Initial fused material pulverised prior to STAR test. Post-treatment material similar to the clean medium sand.
	20	made ground 1	field coal tar 1	unknown	400	1104	72	4.25	5.30E-05	Post-treatment material is mainly fine grain with some small aggregates.
	21	made ground 2	field coal tar 2	65000	400	795	90	4.25		Initial concentration determined by loss on ignition. Strong ignition. Possible self-sustaining smouldering (longer sample needed to verify).
	22	made ground 3	field coal tar 3	12000	400		75	4.25		Initial concentration determined by TPH and loss on ignition methods. Weak ignition observed.
	23	oil drill cutting waste	residual crude oil	unknown	415	538	70	4.5		Drill cuttings diluted with coarse sand (3:1). Successful ignition and propagation observed, but peak temperatures decayed over time.

The smouldering combustion of liquid contaminants has been demonstrated for the first time in this work. Once ignition is achieved in samples of fresh and field-derived coal tars, the process is observed to result in a self-sustaining reaction that propagates in the absence of additional external energy input. Under the employed laboratory conditions, NAPL smouldering achieves essentially complete elimination of coal tar. The self-sustaining reaction appears to depend on air injection and thus can be terminated at any time by the operator. The smouldering reaction self-terminates when the NAPL fuel in its path is consumed. Conductive heating in the absence of air injection did not produce combustion and resulted in much higher levels of residual contamination. Demonstration experiments suggest that smouldering combustion may be applicable across a substantial range of NAPLs and soil conditions. The results suggest that smouldering destruction of NAPLs has significant potential as a remediation approach. It may be particularly promising for soils exhibiting complex, long chain, and/or low volatility NAPL contamination (e.g., coal tar, heavy petrochemicals, PCB oils), where existing remediation strategies may be expensive (energy intensive), time consuming or otherwise ineffective.

As with any technology innovation, many research questions remain to be answered. There will be limits to the applicability of the process, in terms of minimum NAPL calorific output, minimum NAPL concentration, and minimum air injection rate. The influence of other practical and site-specific factors is currently being investigated at the bench scale, including the presence of (non-finite) thermal sinks such as water, soil heterogeneity, and organic carbon content. The scale-up of NAPL smouldering

as both an ex situ technique (i.e., for excavated soils) and in situ approach (i.e., on site, avoiding excavation) is currently being researched. Possible implementations of NAPL smouldering as an ex situ technique are described in (26). The study considers alternative designs for an ex situ soil treatment unit, comparing both constructive options and cost implications.

3.4 Acknowledgements

This research was supported by Scottish Enterprise and the Engineering and Physical Science Research Council (United Kingdom). The authors acknowledge the valuable assistance of colleagues Andres Fuentes, John Jeffrey and Andrew Mackenzie.

Smouldering combustion of liquids as a remediation concept is pending patent approval (UK Application 0525193.9 and PCT Application PCT/GB2006/004591, priority date December 2005).

3.5 References

(1) Howell, J. R.; Hall, M. J.; Ellzey, J. L. Combustion of hydrocarbon fuels within porous inert media. *Progress in Energy and Combustion Science* **1996**, 22, 121-145.

(2) Ohlemiller, T. J. Modeling of smoldering combustion propagation. *Progress in Energy and Combustion Science*, **1985**; 11, 277-310.

(3) Torero, J. L.; Fernandez-Pello, A. C. Forward smolder of polyurethane foam in a forced air flow. *Combustion and Flame* **1996**, 106, 89-109.

(4) DeSoete, G. Stability and propagation of combustion waves in inert porous media. In *Eleventh Symposium (Int) on Combustion*; The Combustion Institute: Pittsburgh, Pennsylvania, **1966**; pp 959-966.

(5) Schult, A.; Matkowsky, B. J.; Volpert, V. A.; Fernandez-Pello, A. C. Propagation and extinction of forced opposed flow smolder waves. *Combustion and Flame* **1995**, 101, 471-490.

(6) Drysdale, D. *An Introduction to Fire Dynamics*, 2nd Edition; John Wiley and Sons Ltd: New York, **1998**.

(7) Greaves, M.; Young, T. J.; El-Usta, S.; Rathbone, R. R.; Ren, S. R.; Xia, T. X. Air injection into light and medium heavy oil reservoirs: combustion tube studies on West of Shetlands clair oil and light Australian oil. *Chemical Engineering Research and Design* **2000**, 78, 721-730.

(8) Sarathi, P. S. *In situ combustion handbook - Principles and practices*; U.S. Department of Energy, **1999**.

(9) Lewis, R. J. S. *Hawley's Condensed Chemical Dictionary; 13 ed.*; John Wiley & Sons: New York, **1997**.

(10) Pironi, P.; Switzer, C.; Rein, G.; Gerhard, J. I.; Torero, J. L.; Fuentes, A. Small-scale forward smouldering experiments for remediation of coal tar in inert media. *Proceedings of the Combustion Institute* **2009**, 32, 1957-1964.

(11) Walther, D. C.; Anthenien, R. A.; Fernandez-Pello, A. C. Smolder ignition of polyurethane foam: effect of oxygen concentration. *Fire Safety Journal* **2000**, 34, 343-359.

(12) Ohlemiller, T. J. Smoldering Combustion. In *SFPE Handbook of Fire Protection Engineering*; Quincy, M., DiNenno, P., Beyler, C. L., Custer, R. L. P., Walton, W. D., Eds.; National Fire Protection Association, **1995**; pp 2/171-179.

(13) Torero, J. L.; Fernandez-Pello, A. C. Natural convection smolder of polyurethane foam, upward propagation. *Fire Safety Journal* **1995**, 24, 35-52.

(14) Ketterings, Q. M.; Bigham, J. M. Soil color as an indicator of slash-and-burn fire severity and soil fertility in Sumatra, Indonesia. *Soil Science Society of America Journal* **2000**, 64, 1826-1833.

(15) Certini, G. Effects of fire on properties of forest soils: a review. *Oecologia* **2005**, 143, 1-10.

(16) DeBano, L. F. The role of fire and soil heating on water repellency in wildland environments: a review. *Journal of Hydrology* **2000**, 231-232, 195-206.

(17) Robichaud, P. R.; Hungerford, R. D. Water repellency by laboratory burning of four northern Rocky Mountain forest soils. *Journal of Hydrology* **2000**, 231-232, 207-219.

(18) Aldhous, P. Borneo is burning. *Nature* **2004**, 432, 144-146.

(19) Nolter, M.; Vice, D. Looking back at the Centralia coal fire: a synopsis of its present status. *International Journal of Coal Geology* **2004**, 59, 99-106.

(20) Yasuhara, A.; Tanaka, Y.; Katami, T.; Shibamoto, T. The role of metals in dioxin formation from combustion of newspapers and polyvinyl chloride in an incinerator. *Chemosphere* **2005**, 58, 891-896.

(21) Kakuta, Y.; Matsuto, T.; Tanaka, N.; Masuda, T. Influence of residual carbon on the decomposition process of PCDD/Fs in MSWI fly ash. *Chemosphere* **2005**, 58, 969-975.

(22) Giannopoulos, D.; Kolaitis, D. I.; Togkalidou, A.; Skevis, G.; Founti, M. A. Quantification of emissions from the co-incineration of cutting oil emulsions in cement plants – Part II: Trace species. *Fuel* **2007**, 86, 2491-2501.

(23) Cunliffe, A.; Williams, P. T. De-novo formation of dioxins and furans and the memory effect in waste incineration flue gases. *Waste Management* **2009**, 29, 739-748.

(24) Preto, F.; McCleave, R.; McLaughlin, D.; Wang, J. Dioxins/furans emissions from fluidized bed combustion of salt-laden hog fuel. *Chemosphere* **2005**, 58, 935-941.

(25) Pandelova, M.; Lenoir, D.; Schramm, K.-W. Inhibition of PCDD/F and PCB formation in co-combustion. *Journal of Hazardous Materials* **2007**, 149, 615-618.

(26) McTague, J. Conceptual designs for an ex-situ Self-sustaining Treatment for the Active Remediation (STAR) reactor. *MEng dissertation, University of Edinburgh,* **2009.**

Chapter 4

Column experiments of NAPL smouldering to explore process sensitivity

4.1 Introduction

Non-aqueous phase liquids (NAPLs) are a class of organic compounds that are now among the most frequently occurring subsurface contaminants throughout the industrialized world. Common NAPLs include petroleum hydrocarbons, polychlorinated biphenyls, chlorinated ethenes, creosote and coal tar. Due to their physical and chemical properties, most of these contaminants represent a significant threat to the human health and the environment. Conventional remediation technologies such as pump and treat and soil vapour extraction have proven largely inefficient in addressing subsurface contamination present as NAPL. While new technologies are being developed and tested, remediation of the most complex, long chain and/or less volatile NAPLs (e.g. coal tar, heavy petrochemicals) remains a significant challenge.

An alternative approach to the treatment of these compounds, which has been recently introduced, is NAPL smouldering (Chapters 2 and 3). At the basis of this concept is the observation that many common NAPLs are highly combustible and exhibit heat of combustion in excess of materials that are successfully burnt in other industries (e.g. biomass energy, waste incineration). However, since NAPLs occur as liquids embedded in a solid matrix, conventional incineration techniques based on

flaming combustion (i.e. a gas phase oxidation reaction) are not applicable to NAPL destruction without the continuous supply of an external energy input. Smouldering combustion, in contrast, is the exothermic oxidation of a condensed phase occurring on the fuel surface and is favoured by the presence of a solid matrix in which the fuel is embedded (Ohlemiller, 1985). In this condition the process can be self-sustaining, that is it initiates with a one-time, short duration energy input and propagates through the NAPL-occupied medium without further input of externally-supplied energy. Since the contaminant represents the fuel being consumed by the advancing reaction, a certain degree of remediation is expected as a result of this process.

Proof-of-concept experiments conducted on coal tar were the first to demonstrate that smouldering combustion of a liquid contaminant can be initiated within a porous inert medium and that the process can become self-sustaining after the ignition source is removed. Further, they demonstrated that the smouldering process self-terminates when all of the NAPL is destroyed or when the oxygen source is removed. Nearly total elimination of the contaminant mass was observed in the employed experimental conditions (Chapters 2 and 3).

Demonstrative experiments conducted at smaller scale (50 mm sandpack) also indicated that the process may be applicable across a broad range of NAPL and soil conditions (Chapter 3). Although insufficient to adequately quantify the process, these experiments showed that NAPL smouldering is successful across a range of soil types and contaminants (including laboratory mixtures of dodecane, DCA/grease, TCE/oil, vegetable oil, crude oil, and mineral oil) as well as field-

obtained samples of materials containing coal tar, oil drill cutting waste, and oil sands.

In this work the potential of NAPL smouldering as a remediation technology was evaluated and quantified in a systematic manner through a suite of bench scale column experiments. The influence of a number of site-specific factors was investigated, including NAPL concentration, water saturation and soil type. Where possible, the work identified the parameter bounds within which the process is successful at this scale, as these may be limiting conditions in real applications.

4.2 Experimental methodology

The experiments conducted are summarized in Table 4.1. In Figure 3.1 is presented a schematic diagram of the experimental apparatus. Upward smouldering combustion tests were carried out in a quartz glass column 138 mm in diameter and 275 mm in height. Commercial grade fresh coal tar (Alfa Aesar, Heysham, UK) and crude oil (Nynas, Dundee, UK) were employed as contaminants, with densities of 1200 and 880 kg/m^3, respectively. Four types of inert porous media (two sands and two gravels, described below) were employed. To prepare the contaminated material, NAPL and the porous medium were mixed in a mass ratio corresponding to the desired (approximate) saturation. The batch was homogenized by mechanical mixing prior to packing in the apparatus.

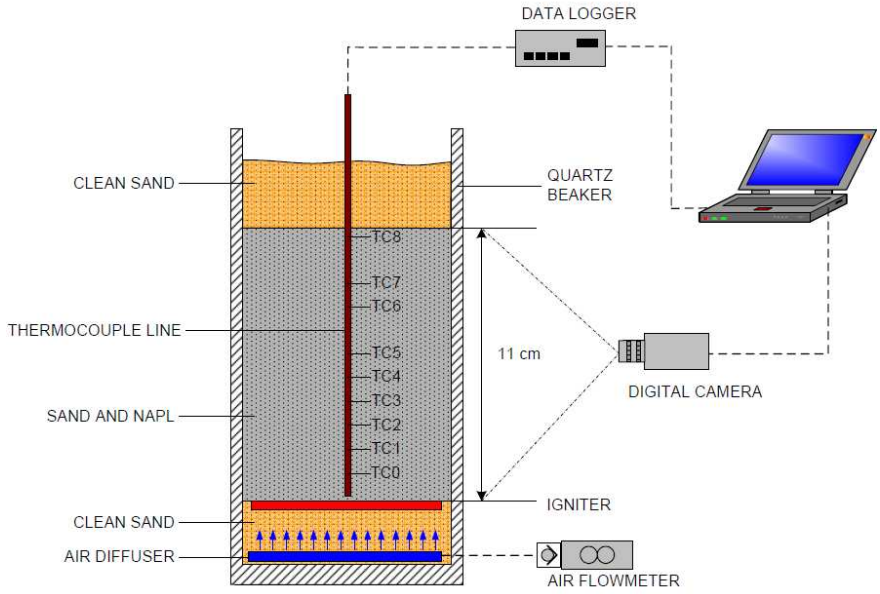

Figure 4.1 Schematic of the experimental apparatus and setup (not to scale).

The apparatus was packed each time in standard sequence (Figure 3.1). A 30 mm layer of clean sand was emplaced followed by the air diffuser, which consisted of eight perforated 6 mm tubes radiating from a central support connected to an air compressor via an air inlet tube. Clean sand was used to bury the air diffuser by a few millimetres, upon which was emplaced the igniter: a 3.25 mm square cross section x 762 mm length inconel-sheathed cable heater (240 V, 450 W, Watlow Ltd, UK) formed into a flat spiral of 130 mm maximum external diameter. A 120 mm layer of the NAPL-contaminated sand was then emplaced. The high viscosity and cohesion of the material ensured no distinct layering or grain size separation occurred during emplacement. A final 30 mm layer of clean sand was emplaced at the top of the sample.

Nine 1.5 mm x 0.5 m inconel-sheathed Type K thermocouples were inserted into the sand pack along the column central axis and spaced at 10 mm or 20 mm intervals above the cable heater (Figure 3.1). The thermocouples were connected to a data

acquisition system (Multifunction Switch/Measure Unit 34980A, Agilent Technologies).

At the start of each experiment, the material adjacent to the igniter (as measured at the thermocouple TC1) was heated to a predetermined temperature, corresponding to 400 and 300 ^{o}C for coal tar and crude oil, respectively. Once this temperature was achieved, air injection was initiated and maintained until the end of the experiment. Unless specified otherwise (i.e., Experiments 18 and 19) the air flux was maintained constant at the base-case value (9.15 cm/s) for all the experiments. The igniter was turned off when the temperature at TC1 began to decrease with time (i.e., post-peak), typically a short time (e.g., 10 minutes) after initiating the air flow. The maximum power used for these experiments was approximately 390 W, which corresponds to a heat flux of 26 kW/m^2 over the horizontal cross-sectional area of beaker. This ignition protocol was determined from a series of proof of concept experiments (Chapter 2).

The rate of smoulder propagation was obtained from the temperature histories of the thermocouples embedded in the sand pack. The smouldering velocity was calculated from the time lapse of the front arrival at two consecutive thermocouples and the known distance between thermocouples. The front arrival at a thermocouple location was taken as the average of the times at which the temperature reached three predetermined values, all of which are above the observed ignition temperature (more details on this method are available in Chapters 2 and 3).

Pre- and post-treatment analysis of the samples was conducted for the two base-case experiments on coal tar (71,000 mg/kg, Experiment 4) and crude oil (52,000 mg/kg, Experiment 9). Accelerated solvent extraction (ASE) with a 50mL mixture of dichloromethane and acetone was conducted on 20g soil samples. The extract was analysed for total extractable petroleum hydrocarbons (TPH) in the C_{10} to C_{40} range by a gas chromatograph equipped with flame ionisation detector (Finnegan Focus GC, Thermo Electron Corporation, Hemel Hempstead, UK) and also for polycyclic aromatic hydrocarbons (PAHs) by gas chromatograph equipped with mass spectrometer (Thermo Quest Trace GC and Finnegan Trace MS, Thermo Electron Corporation, Hemel Hempstead, UK).

Experiments 1-6 and 7-11 examine the dependence of the smouldering process on NAPL concentration with a range of concentrations of coal tar (14,200 to 142,000 mg/kg) and crude oil (20,800 to 104,000 mg/kg) that span an order of magnitude and are broadly representative of NAPL contents excavated from field sites. These experiments employed commercially available quartz sand (Leighton Buzzard 8/16 sand, WBB Minerals, UK), characterized by a bulk density of 1700 kg/m^3 and a mean grain size of 1.34 mm. When dry packed, the average porosity of the sand is 40%. This sand is indicated as “Coarse Sand” in Table 4.1.

The effect of varying initial water content of the contaminated soil was investigated by carrying out experiments at fixed coal tar concentration of 71,000 mg/kg in coarse sand (approximately 25% NAPL saturation) combined with initial water saturations of 0, 25, 50 and 75% (59,000, 118,000, 177,000 mg/kg, respectively) (Experiments 4

and 12-14 in Table 4.1). It is noted that in the 75% water/25% NAPL case, the initial air-filled porosity is essentially zero.

The influence of the porous media mean grain size (from approximately 0.7-0.8 mm to 10 mm) is studied in Experiments 15-17. Besides the coarse sand described above, these experiments employed a “Medium Sand” (grain size in the range 0.7-0.8 mm, porosity of 38%, bulk density of 1700 kg/m^3) and two types of gravel. The finer gravel had a grain size of 6 mm, bulk density of 1490 kg/m^3 and average porosity of 45% (this is indicated as 6mm Gravel in Table 4.1); the coarser gravel had a grain size of 10 mm, bulk density of 1580 kg/m^3 and average porosity of 41% (10mm Gravel in Table 4.1).

Experiments 18 and 19 examine the ability of the reaction to self-propagate at extremely low air flow rates. The experiments were conducted on coal tar and crude oil in coarse sand and at the base-case concentrations of 71,000 and 52,000 mg/kg respectively. The sample was ignited according to the standard procedure and using an initial air flux of 6.3 cm/s. The air flux was then lowered to the predetermined level after the reaction had propagated to approximately 4 cm from the igniter. To limit the heat losses to the outside, and thus make the experiments more representative of conditions at larger scales, in these experiments the column was covered with a flexible electric heater (240 V, 1040 W, Omega Inc., USA). The heater was operated at variable power and in such a way to maintain the temperature at the outer boundary always lower than the temperature in the centre, to ensure that the heater was not sustaining and/or driving the combustion. Such adjustment of the

boundary conditions is common in combustion experiments that try to reproduce conditions existing at the field scale (e.g., in in-situ combustion experiments, Sarathi, 1999).

Table 4.1 Summary of Experiments

Variable	Experiment	Contaminant	Porous Medium	Concentration (mg/kg)	Saturation (approx.)	Self-sustaining/ remediated[2]
Coal Tar Content	1	Coal Tar	Coarse Sand	14200	5%	✗
	2	"	"	21300	7.5%	✗
	3	"	"	28400	10%	✓
	4	"	"	71000	25%	✓
	5	"	"	99400	35%	✓
	6	"	"	142000	50%	✓
Crude Oil Content	7	Crude Oil	Coarse Sand	20800	10%	✗
	8	"	"	31200	15%	✓
	9	"	"	52000	25%	✓
	10	"	"	72800	35%	✓
	11	"	"	104000	50%	✓
Water Content	12	Coal tar/water	Coarse Sand	71000	25%/25%[3]	✓
	13	"	"	71000	25%/50%[3]	✓
	14	"	"	71000	25%/75%[3]	✓
Mean Grain Size	15	Coal Tar	Medium Sand	67000	25%	✓
	16	"	6mm Gravel	90000	"	✓
	17	"	10mm Gravel	94000	30%	✗
Air Flux	18[1]	Coal Tar	Coarse Sand	71000	25%	✓
	19[1]	Crude oil	"	52000	"	✓

[1] Air flux lowered to 0.53 cm/s soon after ignition.
[2] The definition of remediated sand is given in Section 4.3.5
[3] The second number indicates water saturation.

4.3 Experimental results

4.3.1 NAPL concentration

As identified in Table 4.1, successful self-propagating combustion was achieved for coal tar in the range 28,400 to 142,000 mg/kg and for crude oil in the range 31,200 to 104,000 mg/kg. At the scale of these experiments, the lower limit for a self-sustaining reaction in coarse sand was between 21,300 and 28,400 mg/kg for coal tar and between 20,800 and 31,220 mg/kg for crude oil. Figure 4.2 presents the temperature profiles for the two coal tar cases that bracket the lower saturation boundary. Figure 4.2(a) is representative of the 16 experiments (see Table 4.1) in which successful self-sustaining propagation was observed, as identified by the sequential, overlapping and consistent temperature peaks (Walther et al., 2000). As illustrated in Figure 4.2(b), at and below the lower bound of these concentration ranges, peak temperatures at successive locations exhibited a decreasing trend, indicating a progressive weakening of the reaction; with sufficient sandpack length, it is expected that this would lead to extinction before the reaction reached the end of the contaminated sample. Figure 4.3(a) and (b) present photographs of the excavated sand packs after treatment for the respective cases plotted in Figure 4.2. In Figure 4.3(a) the combustion front, where the essentially complete restoration of the soil is achieved, extends radially to most of the cross-sectional area of the sandpack. This contrasts with Figure 4.3(b) with insufficient coal tar, in which the combustion front extends to only a narrow region close to the centre of the sample while in the remaining area the heat generated was insufficient to overcome the lateral heat losses.

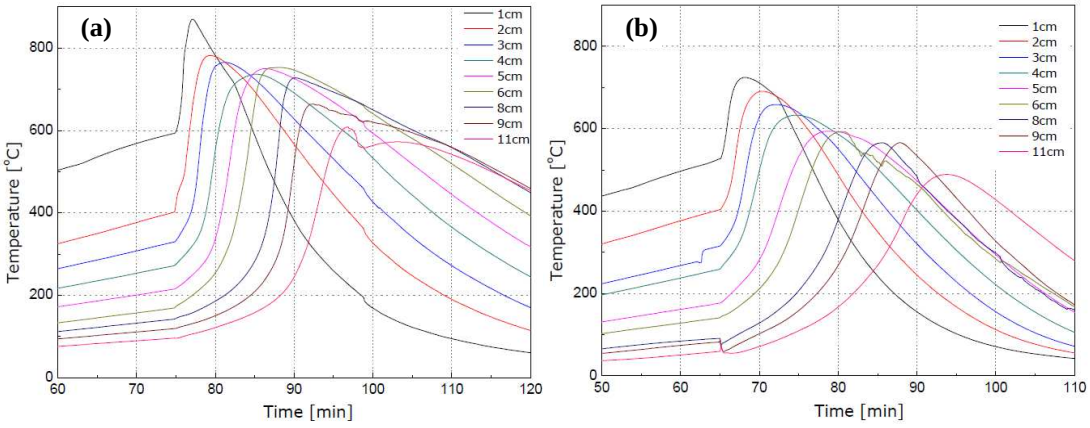

Figure 4.2 Temperature histories for coal tar in coarse sand at (a) 28400 mg/kg and (b) 14200 mg/kg .

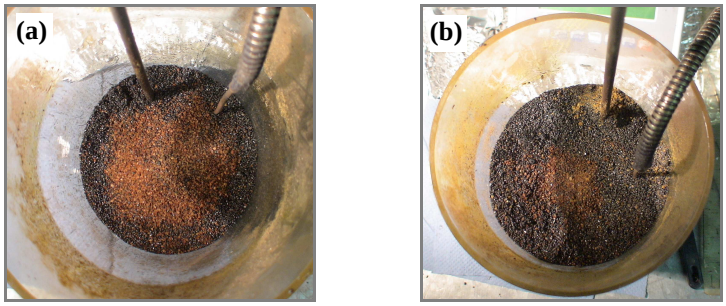

Figure 4.3 Radial extent of the reaction front for the experiments at (a) 28400 mg/kg and (b) 14200 mg/kg.

Figure 4.4 summarises the main combustion characteristics for all 11 experiments conducted at variable NAPL concentrations. Figure 4.4(a) presents the variation of the average maximum temperature recorded in the contaminated pack during propagation, while 4.4(b) presents the average propagation velocity of the reaction. Measurement uncertainty on maximum temperature values is 7%, on propagation velocity is 13%, and on NAPL content is 1% (calculations of uncertainty presented in Appendix C). The figures confirm that the transition to self-sustaining propagation occurs in the same range of concentrations for the two NAPLs; for coal tar this corresponds to a temperature of approximately 700 ^{o}C and a front velocity of approximately 4.5 cm/min; the corresponding values for crude oil are 550 ^{o}C and

4.5 cm/min. It is noted that, for coal tar, both maximum temperature and average velocity of the front increase as the NAPL concentration increases in the lower half of the range examined (i.e. until approximately 75,000 mg/kg). This suggests that for concentrations lower than 75,000 mg/kg the propagation is essentially controlled by the kinetics of fuel consumption in the reaction front: at increasing fuel concentration the increase in the rate of reaction is so high that the smouldering front can accelerate despite having to consume more fuel in order to advance. As the NAPL concentration increases further, the rate of reaction in the combustion front may become high enough to consume all the incoming oxygen; at this point the reaction would become oxygen limited and the velocity would decrease at increasing concentrations. The observed decrease of the propagation velocity above 75,000 mg/kg seems to corroborate this hypothesis.

Burning temperatures depend not only on the reaction rate but also on the thermophysical properties of the reacting medium (i.e., heat capacity and thermal conductivity), which in turn depend on both soil type and NAPL content. Thus, lower temperatures at high NAPL concentrations (above 100,000 mg/kg) may be the consequence of more energy being required to heat the contaminated sandpack.

In the case of crude oil, above the threshold concentration for self-sustaining reaction, propagation velocity remains essentially constant and the increase in peak temperature is significantly lower than for coal tar in the same range of concentrations (approximately 16% vs. 57%). This suggests that, for crude oil, the increase in reaction rate is only sufficient to compensate for the increase in fuel

concentration and that oxygen limited conditions are not reached. The overall modest increase in the burning temperature is consistent, at least qualitatively, with this observation, because it indicates that in the reaction of crude oil the increase in energy generated is nearly balanced by the increase in the energy needed to raise the temperature of the contaminated pack (due to an expected increase in volumetric heat capacity with increased NAPL content).

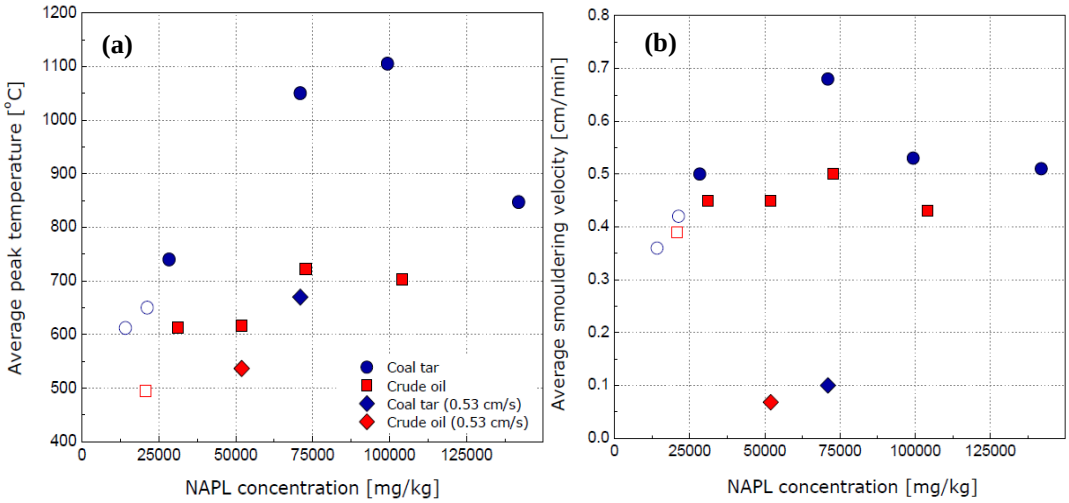

Figure 4.4 (a) Average peak temperature and (b) smouldering velocity as a function of NAPL concentration in coarse sand. Empty symbols indicate not self-sustaining combustion. Diamonds refer to experiments conducted at low air flux (Experiments 18 and 19 in Table 4.1).

4.3.2 Initial water saturation

Figure 4.5 represents the temperature histories for the experiment conducted at initial water saturation of 50% (coal tar saturation of 25%, 118,000 mg water/kg, 71,000 mg coal tar/kg, Experiment 13); similar observations were made for the other experiments in this set (Experiments 12 and 14, data showed in Appendix A). First, it is observed that the time necessary to achieve ignition increases (cf. Figure 5.2 in Chapter 5), in this case by approximately 75% (65 min to 115 min). This is due to the time lag associated with driving off the water during pre-heating of the ignition zone.

Comparing across the experiments, it is found, as expected, that ignition time increases with increasing water content since more water has to be vaporized before the temperature can rise above 100 ^{o}C and reach the ignition temperature. At the time of ignition, the upper 50% of the column still contains water (Figure 4.5, locations where temperature $\leq$ 100 ^{o}C). Comparing across experiments, the length of column containing water at the time of ignition increases with increasing initial water saturation, from about 4 cm at 25% to 6 cm at 75% water saturation. As observed in Chapter 3, the heated region of the sandpack is highly localized around the combustion front (or around the ignition point, in this case) due to the insulating properties of the porous medium; these results confirm that the igniter has a short duration influence over a limited volume of material.

In all experiments in this set, ignition is successful and, after turning off the igniter, the front is observed to propagate in a self-sustaining manner until all coal tar is destroyed. During the self-sustaining phase, the advancing front gradually vaporizes the water ahead of it via the upwards flow of hot combustion gases. Evidence of this is the marked temperature decrease, due to evaporative cooling of the sand, observed at locations where water was still present at the time of ignition (Figure 4.5). Moreover, water acts as a heat sink, absorbing energy from the reaction and thus retarding the temperature increase of the soil-contaminant mixture ahead of the combustion front. Lower burning temperatures and propagation velocities are therefore expected and there may exist a limit for the water saturation above which self-sustaining propagation is not possible. However, in all cases considered here, the

energy generated was sufficient to vaporise all the remaining water and propagate the reaction to end of the contaminated sample.

Figure 4.6a demonstrates that the maximum temperature achieved decreased in a nearly linear fashion (from 1050 to 850 ^{o}C) with increasing initial water saturation. This is a result of the corresponding increase in the net energy loss to the vaporization of water. However, the front propagation velocity does not change significantly with the water content (the differences in Figure 4.6b are within the experimental uncertainty for these experiments). This suggests that, despite the decrease in the burning temperature, the reaction remains in the oxygen-limited regime (see Section 4.3.1) where the velocity is essentially dictated by the rate of oxygen supply and the fuel concentration. As those do not change, the velocity also does not change.

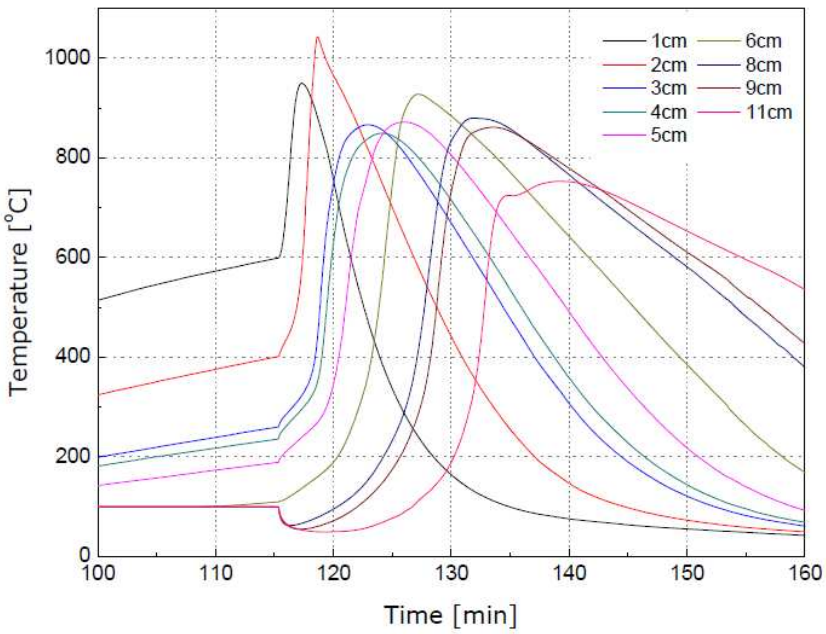

Figure 4.5 Temperature histories for coal tar at 71,000 mg/kg and 50% initial water saturation (Experiment 13).

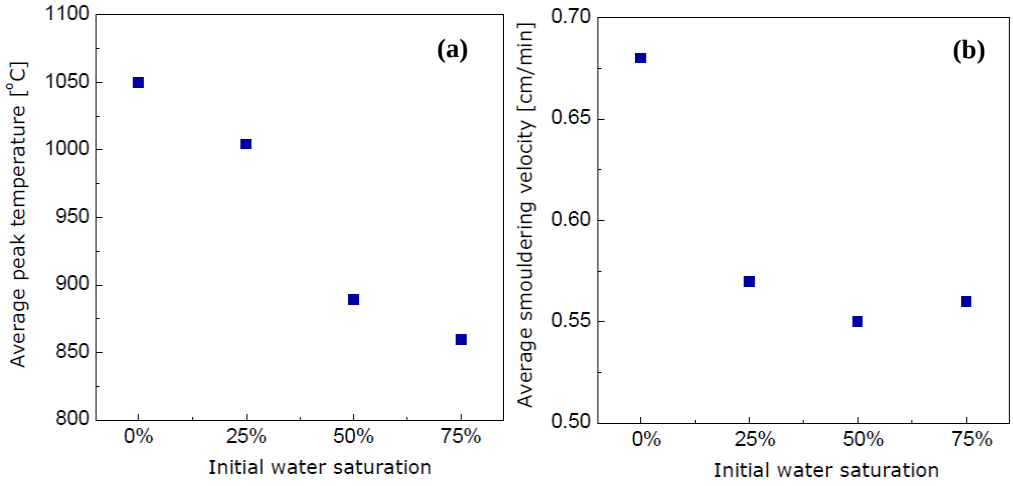

Figure 4.6 (a) Average peak temperature and (b) propagation velocity as a function of initial water saturation.

4.3.3 Mean grain size

In all cases except one (10mm gravel) a successful self-sustaining front propagated the length of the column. Figure 4.7 presents the sensitivity of the reaction peak temperature and propagation velocity with the type of sand. The graphs suggest that, among the examined media, coarse sand presents the most favourable conditions for smouldering propagation (i.e., maximum peak temperature and maximum average velocity). However, the difference between coarse sand and medium sand in both temperature and velocity is within the measurement uncertainty for these experiments. Although an increase in the smouldering reaction rate would be expected with decreased pore size, since the fuel surface area per unit volume increases, this effect may have been balanced by the decreased NAPL concentration in medium sand (recall that the NAPL concentration was selected in order to maintain the saturation constant, see Table 4.1). In 6mm gravel, the reaction is still self-sustaining and the difference in burning temperature compared to the coarse sand case is within the measurements uncertainty. However, the spread velocity is significantly lower than in coarse sand and this decrease is higher than would be

expected based on the change in NAPL concentration (see Section 4.3.1). Indeed, the decrease in propagation velocity is even more pronounced for 10mm gravel (51% compared to coarse sand) and also the average peak temperature exhibits a significant decrease (approximately 39%).

Examining the temperature histories and the excavated sand pack for this experiment reveals that the reaction is not self-sustaining in this medium at this scale (data presented in Appendix A). These results are explained by the different mechanisms acting as the grain size increases. A decrease of the smouldering reaction rate is expected with increased pore size as a result of the decreased fuel surface area per unit volume. Also, at larger solid grain size the temperature of the solid may not have sufficient time to equilibrate with the temperature of the gas phase (Whale *et al.*, 2003). This means that the solids role as a heat sink increases and may become sufficient to progressively diminish the reaction intensity with the distance from the igniter.

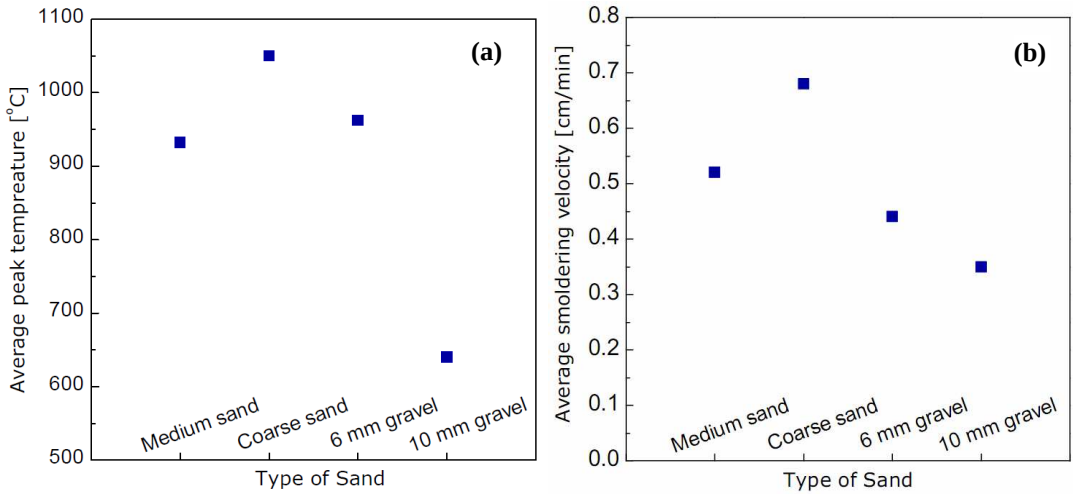

Figure 4.7 (a) Average peak temperature and (b) propagation velocity as a function of mean grain size.

4.3.4 Reduced air flux

Results for both coal tar and crude oil show that the reaction is self-propagating at least down to an air flux of approximately 0.5 cm/s (data presented in Appendix A). At this air flow rate the reaction propagated through the rest of the contaminated sandpack before extinguishing in the proximity of the top. Extinction in this region is expected at such low air flux due to the (now significant) fraction of heat lost through the upper boundary of the system. While the upper boundary normally causes relatively minor decrease in the smouldering temperature and velocity (see Chapters 2 and 5), their relative magnitude compared to the heat generated increases as the air flux decreases, until smouldering propagation can no longer occur (Rein, 2009).

As plotted in Figure 4.4, for the coal tar case, reducing the air flux by 95% (9.5 cm/s to 0.53 cm/s) caused the peak temperature to change by 36% (from 1050 to 670 ^{o}C) and the velocity of the front to change by 85% (from 0.68 to 0.10 cm/min). In crude oil, the comparable numbers are 13% temperature decrease (616 to 537 ^{o}C) and 85% reduction in propagation velocity (0.45 to 0.068 cm/min). A nearly linear decrease in propagation velocity with the air flux is expected since smouldering propagation is typically an oxygen-limited process (Chapters 2 and 5). Burning temperatures are consistent with the values observed in Figure 4.4a near the lower boundary for self-sustaining propagation.

4.3.5 Extent of remediation

While it was not feasible to conduct detailed chemical analysis on sub-samples of every experiment, it was carried out for the two base-case experiments on

coal tar (71,000 mg/kg, Experiment 4) and crude oil (52,000 mg/kg, Experiment 9). The results are presented in Table 4.2 (note that the coal tar results are reproduced from Chapter 3). Prior to the experiment, the coal tar sand pack exhibited TPH of approximately 38,000 mg/kg and PAH content of approximately 9,500 mg/kg. Note that the difference between the TPH value and the total initial concentration is a consequence of the methodology employed for the extraction and analysis of the sand (see Section 4.2), which provides a measure of the extractable hydrocarbons in the range C_{10} to C_{40} rather than the total hydrocarbons. Table 4.2 reveals that the concentrations of TPH and PAH in the treated coal tar sand are below the detection limit in the majority of the samples and never exceed 2 mg/kg (i.e., more than 99.9999% reduction at all locations). For crude oil, pre-treatment analysis revealed concentrations of TPH and PAH of approximately 18,000 and 90 mg/kg, respectively. After the experiment the concentrations were reduced more than 99.5% in all locations (average TPH = 38 mg/kg, maximum TPH = 87 mg/kg) excluding the top two centimetres where boundary effects were significant.

The higher degree of remediation in the coal tar versus the crude oil is likely due to the more exothermic reaction and higher net energy at the front (as evidenced, for example, by the higher maximum temperatures and the boundary effect only observed for crude oil). This, in turn, is likely inherent to the various properties of the two contaminants, such as the range of boiling points exhibited by the broad spectrum of compounds each contains.

As identified in Table 4.2, the contaminated sandpack was effectively remediated in every experiment that exhibited self-sustaining smouldering (i.e., all except Experiments 1, 2, 7 and 17). 'Remediated' in this context is taken to mean that no trace of contamination was evident (by sight, smell, or touch) in the treatment zone (with the exception of the top 2cm of the column, which in some cases exhibited residual contamination due to process extinction from the boundary effect). In essence, the entire set of experiments makes it clear that when self-sustaining combustion is induced, the extent of remediation is thorough. Visible traces of contamination remained only in the cases where the reaction was clearly not self-sustaining at this scale (namely, when the NAPL content was too low or the grain size was too large).

From the chemical analyses that were conducted (e.g., those presented in Table 4.2 plus numerous spot samples on other experiments), it was estimated that the lower limit of residual contamination (i.e. after treatment) that can be visibly detected is approximately 200 mg/kg TPH. Therefore, it is hypothesized that in all the successful, self-propagating cases, this represents an upper bound on the concentration after treatment (excepting the boundary effect). However, it is suspected that the actual concentration after treatment is substantially lower, particularly in the coal tar experiments (as in Table 4.2).

Table 4.2 Summary of Chemical Analysis Results

Distance from igniter (cm)	Coal tar at 71000 mg/kg		Crude oil at 52000 mg/kg	
	EPH[1] TPH (mg/kg)	PAH (mg/kg)	EPH[1] TPH (mg/kg)	PAH (mg/kg)
0-1	<0.1	<0.1	6	<0.1
1-2	<0.1	<0.1	1	<0.1
2-3	<0.1	<0.1	3	0.14
3-4	<0.1	<0.1	7	0.24
4-5	0.3	0.3	66	0.49
5-6	<0.1	<0.1	75	0.52
6-7	<0.1	<0.1	39	0.34
7-8	<0.1	<0.1	46	0.41
8-9	<0.1	<0.1	69	0.67
9-10	<0.1	<0.1	17	0.23
10-11	<0.1	<0.1	30	0.52
11-12	<0.1	<0.1	31	0.48
12-13	1.20	1.21	60	0.89
13-14	<0.1	<0.1	87	1.21
14-15	<0.1	<0.1	358	3.26
15-16	<0.1	<0.1	822	8.68

[1] EPH = Extractable Petroleum Hydrocarbons

4.4 Summary and conclusions

Self-sustaining smouldering combustion of coal tar and crude oil, corresponding to essentially complete remediation, is demonstrated across a wide range of NAPL contents, air fluxes, and several grain sizes from medium sand to gravel. The extent of remediation in the treatment zone is estimated to be at least 99.5% and 99.9999% for crude oil and coal tar, respectively. In addition, the lack of any visible traces of residual in those cases achieving self-sustaining combustion is estimated to indicate between 0.1 and 200 mg/kg TPH after treatment. At this scale, the lower concentration limits for achieving self-propagation are in the bounds of 21,300-

28,400 mg/kg for coal tar and 20,800-31,220 mg/kg for crude oil. Below this, not enough energy is generated to overcome the heat losses that are prevalent at this scale.

Non-zero initial water saturation was observed to delay the time of ignition and decrease the temperature and velocity of the reaction front. At the employed coal tar concentration (71,000 mg/kg), the process remained self-sustaining across the range of initial water saturations examined. In all cases it was observed that all the water was driven off ahead of the front by heat convection and hot gas flow. It is acknowledged that in the field, where a constant head water boundary will exist at some distance from the reaction, there will be hydraulic gradients that cause influx of water to zones where water has been displaced. It is not yet known if water influx would be enough of a heat sink to diminish an otherwise self-sustaining reaction; it likely depends on the excess energy of the system (which is, as demonstrated here, at least a function of NAPL type, mean grain size, and air flux) and on the rate of water influx versus the rate at which the reaction propagates. Experiments are planned to explore this, and thereby determine if this process is viable for contaminated sediments below the water table. Meanwhile, the presented results suggest significant promise for treating contaminated soil in the unsaturated zone as well as for contaminated soils that have been excavated (regardless of water content and without the need to dewater).

Varying the grain size of the porous medium was also observed to affect the process characteristics by modifying the NAPL-air interfacial area as well as the heat transfer

properties of the solid matrix. Results indicate that the process ceases to be self-sustaining if the mean grain size exceeds a threshold value, estimated for this scale of experiment and these contaminants to be in the range 6-10mm.

Experiments conducted at extremely low air flux indicate that the smouldering reaction of both coal tar and crude oil is self-sustaining down to an air flux of at least 0.5 cm/s (Darcy flux) when boundary conditions are modified to reduce the heat losses to the outside. This is an important result in view of full scale applications of the process, since calculations suggest that this is a value that is realistic to achieve in the field.

It is underscored that combustion behaviour is highly sensitive to scale (Rein, 2009) and therefore the results are relevant at the scale examined. In particular, the metrics of smouldering combustion are expected to be sensitive to the ratio of surface area to volume of the system, which is directly related to heat losses and thus affects the energy balance at the reaction front. For this reason, achieving self-sustaining smouldering is most challenging at the bench scale, such as that employed in this work. Thus, the limits of NAPL content and grain size observed here are expected to be conservative estimates. At the same time, it is acknowledged that real systems exhibit inherent heterogeneity of all system parameters (e.g., NAPL content, permeability, etc.) as well as multi-dimensionality that will also affect performance metrics. Larger scale experiments under controlled and pilot field conditions are currently being undertaken to address these open questions.

4.5 References

Rein, G., Smouldering combustion phenomena in science and technology, International Review of Chemical Engineering (2009) 1 (1) 3-18.

Sarathi, P.S., In-situ combustion handbook – Principles and practices. Report prepared by BDM Petroleum Technologies for U.S. Department of Energy, 1999.

Wahle, C.W., B.J. Matkowsky, A.P. Aldushin, Effects of gas-solid nonequilibrium in filtration combustion, Combustion Science and Techology (2003) 175 1389-1499.

Walther, D.C., R.A. Anthenien, A.C. Fernandez-Pello, Smolder ignition of polyurethane foam: effect of oxygen concentration. Fire Safety Journal (2000) 34 343-359.

Chapter 5

Smouldering characteristics at varying experimental conditions and comparison with theoretical models

5.1 Introduction

Smouldering combustion is an innovative approach to the remediation of soils contaminated by non-aqueous phase liquids (NAPLs). Recent studies (Chapters 2 and 3 in the present thesis) have shown that the smouldering reaction of a liquid contaminant can be initiated within the soil porous matrix and the process can become self-sustaining once the source of ignition is eliminated. Demonstrative experiments presented in Chapter 3 also suggested that the process may be applicable across a substantial range of NAPL and soil conditions. Such hypothesis was tested in a more systematic manner in Chapter 4 through a series of larger scale sensitivity experiments, which confirmed the broad range of process parameters within which the process is self-sustaining and essentially complete remediation is achieved.

The main objective of this chapter is to provide further understanding of the mechanisms governing the smouldering combustion of NAPLs by comparing the experimental results with theoretical models existing in the smouldering literature. Previous studies on the smouldering combustion of solid fuels indicate that the rate and extent of the reaction are often controlled by the rate of oxygen supply and the magnitude of the heat losses to the external environment (Ohlemiller and Lucca, 1983; Bar-Ilan *et al.*, 2004, Rein 2009). Under these conditions, analytical models

derived from global conservation of energy and oxygen mass in the reaction front have proven successful in predicting the measured propagation velocity for a range of experimental conditions (Torero and Fernandez-Pello, 1996; Bar-Ilan *et al.*, 2004). In order to apply this approach to the present study, additional experiments have been conducted to examine the combustion behaviour under varied inlet air fluxes and, further, to characterise the stoichiometry of the reaction and estimate the energy constants of the process. These and the data presented in Chapter 4 (Section 4.3.1) are used here to compare with the modelled results.

5.2 Experimental methodology

Experiments presented in this chapter are listed in Table 5.1. All the experiments were conducted at 25% NAPL saturation. Groups of experiments 1-4 and 9-12 explore the influence of the inlet air flux in coarse sand for coal tar and crude oil respectively; these experiments were repeated in medium sand to examine the sensitivity of the reaction to the porous media grain size (Experiments 5-8 and 13-16). The experimental setup and procedure employed for all the experiments is essentially the same described in detail in Chapter 4. Variations to the basic setup will be indicated in the text where necessary.

Table 5.1 Summary of the Experiments

Experiment	Contaminant	Porous Medium	Inlet air flux
1	Coal Tar	Coarse Sand	4.05 cm/s
2[a]	"	"	9.15 cm/s
3	"	"	16.6 cm/s
4	"	"	25.2 cm/s
5	Coal tar	Medium Sand	4.05 cm/s
6[b]	"	"	9.15 cm/s
7	"	"	16.6 cm/s
8	"	"	25.2 cm/s
9	Crude Oil	Coarse Sand	4.05 cm/s
10	"	"	9.15 cm/s
11	"	"	16.6 cm/s
12	"	"	25.2 cm/s
13	Crude oil	Medium Sand	4.05 cm/s
14	"	"	9.15 cm/s
15	"	"	16.6 cm/s
16	"	"	25.2 cm/s

[a] This experiment corresponds to Experiment 4 in Table 4.1
[b] This experiment corresponds to Experiment 9 in Table 4.1

5.3 Experimental results

Experimental data available for these experiments consist of thermocouple measurements and, only for Experiments 2 and 10 in Table 5.1, chemical composition data of the gaseous emissions. A detailed description of the measured results will be presented in the first part of the following subsections; derived results and their analysis will be presented later in the chapter.

5.3.1 Thermocouple data and combustion characteristics

Figure 5.1–5.4 present the temperature traces for the experiments conducted with **coal tar** in **coarse sand** at varying input air flux (Experiments 1-4); each line represents the temperature history at a specific location above the igniter, as indicated by the legend. For all the experiments, ignition of the fuel occurred either immediately or only a few minutes after the onset of the air injection, as indicated by the rapid increase of the temperature measured by the thermocouples closest to the igniter. Following ignition, a characteristic sequence of temperature peaks at successive thermocouple locations is observed as the reaction propagates upwards through the contaminated sand. Transition from igniter-assisted propagation to self-sustaining propagation of the reaction is generally signalled by a decrease in the peak temperatures at 3-4 cm from the igniter. Following this, temperatures increase and stabilise in the central part of the sample. A decrease in the peak temperatures is again observed in the last 1-2 cm of the sample as the reaction approaches the end of the contaminated material (see Figures 5.1-5.3). A somewhat different behaviour was observed at the highest air flux (Experiment 4, Figure 5.4); the reaction is here characterised by an almost constant temperature decay, from temperatures as high as 1300 ºC to approximately 1000 ºC at the end of the sample. It is further noted that the width of the temperature profiles decreases, and the peak of the profiles increases to higher temperatures, with increasing air flux; both indicate an increase in reaction intensity with increasing air flux.

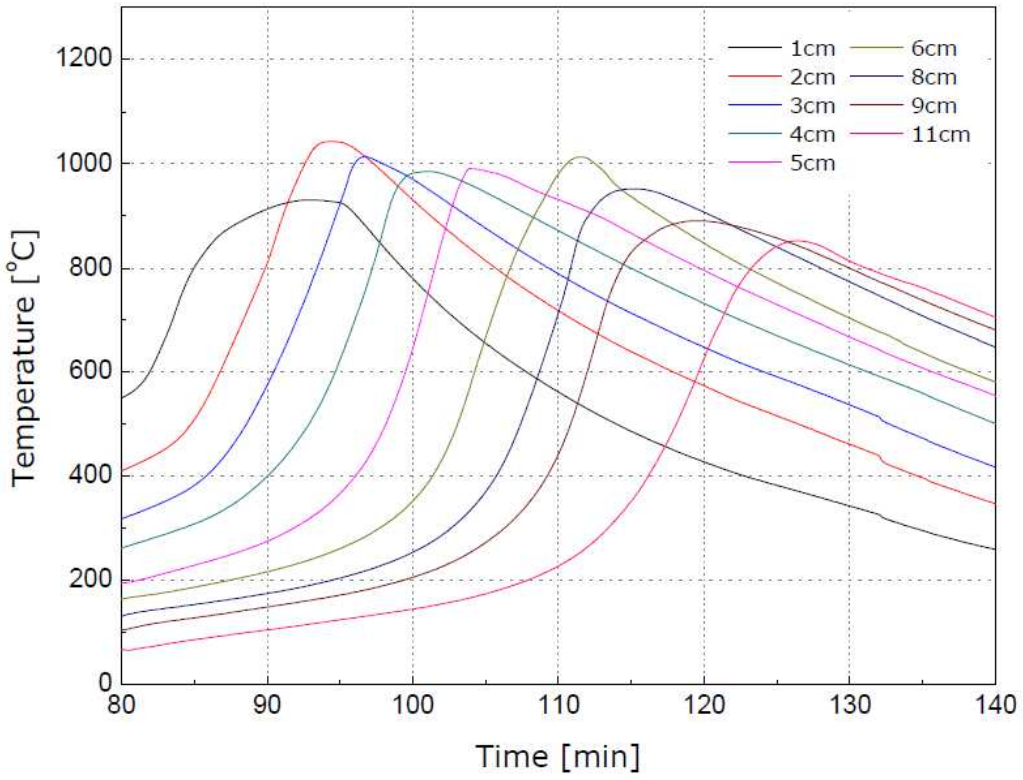

Figure 5.1 Temperature histories for coal tar in coarse sand at 25% saturation and 4.05 cm/s air flux.

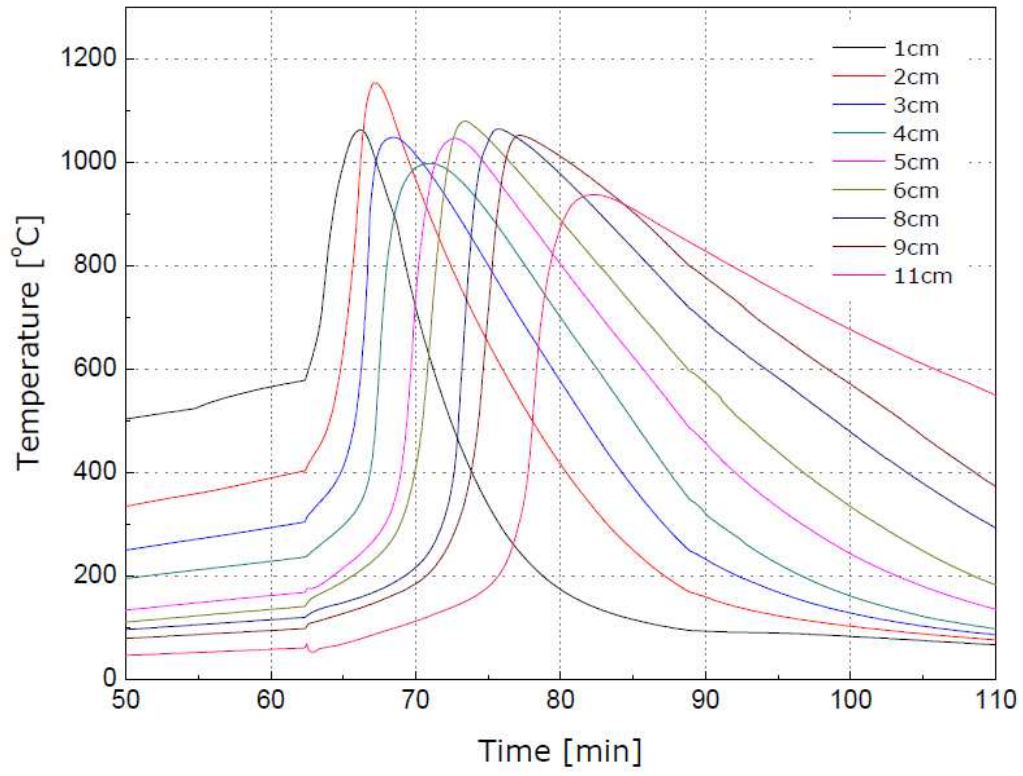

Figure 5.2 Temperature histories for coal tar in coarse sand at 25% saturation and 9.15 cm/s air flux.

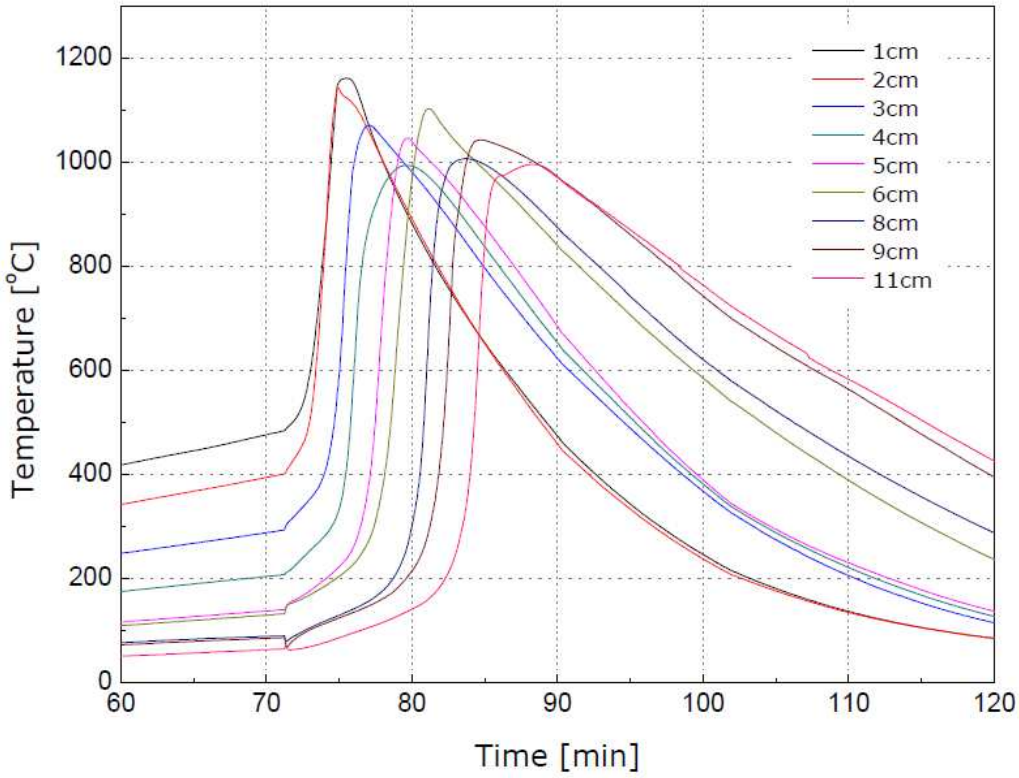

Figure 5.3 Temperature histories for coal tar in coarse sand at 25% saturation and 16.6 cm/s air flux.

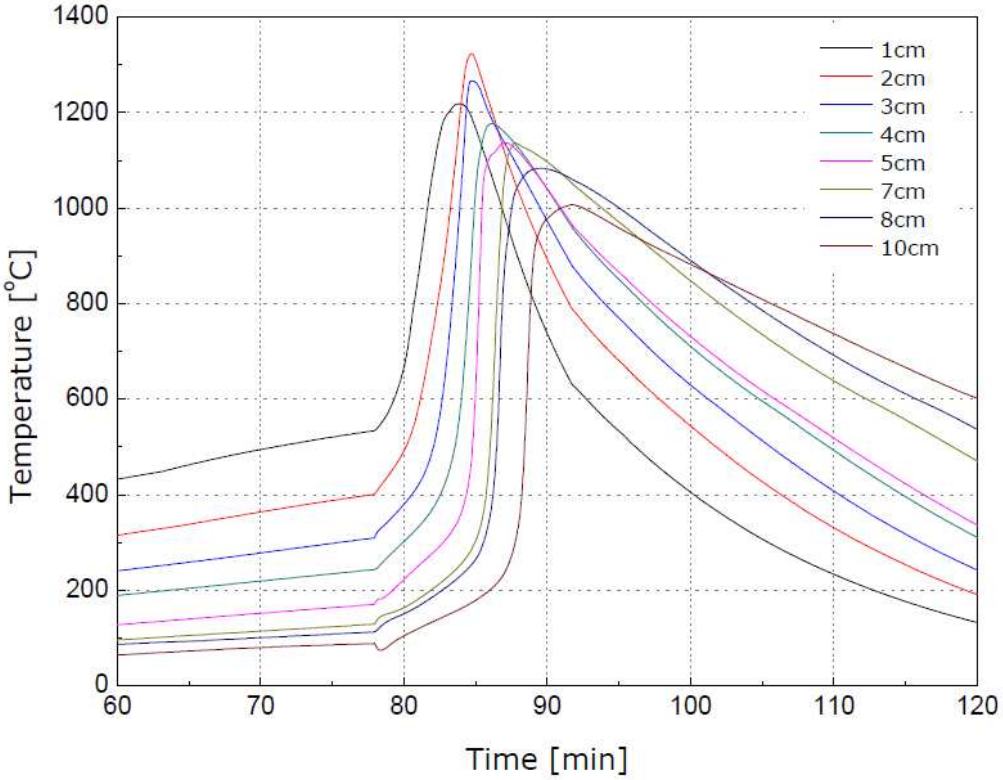

Figure 5.4 Temperature histories for coal tar in coarse sand at 25% saturation and 25.2 cm/s air flux.

Figures 5.5 and 5.6 present the temperature profiles corresponding to the experiments in Figures 5.1 and 5.2. Each line represents the temperature distribution within the sand pack recorded at a specific time after ignition; the time interval between profiles is indicated on the graphs. These plots illustrate the progression of the high temperature front associated with the advancing smouldering reaction; at the same time they show the progressive cooling of the region closer to the igniter, where the reaction is reaching completion and the cooling effect of the incoming air becomes prevalent. The comparison between the two figures confirms the increase in reaction intensity at increasing air flux: the average distance between the profiles at 9.15 cm/s is larger, and the time to reach the end of the sample is smaller, than at 4.05 cm/s. Further, the faster cooling at locations closer to the igniter is consistent with the more intense convective heat transfer at higher air flux.

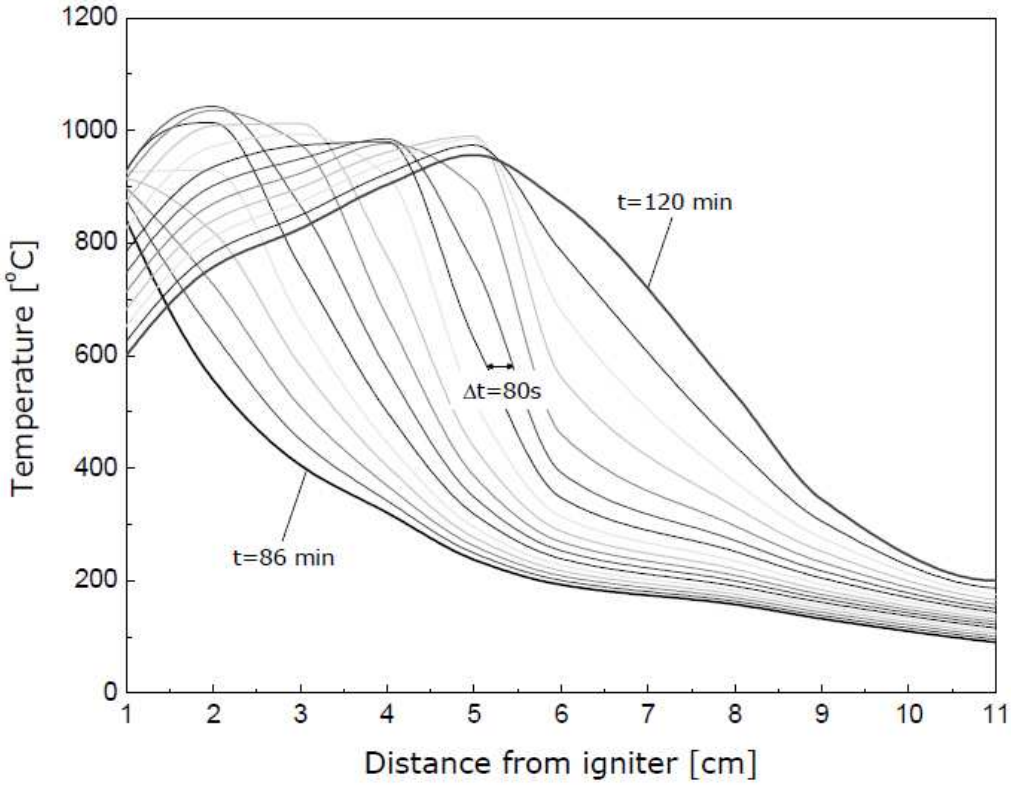

Figure 5.5 Temperature profiles for coal tar in coarse sand at 25% saturation and 4.05 cm/s air flux.

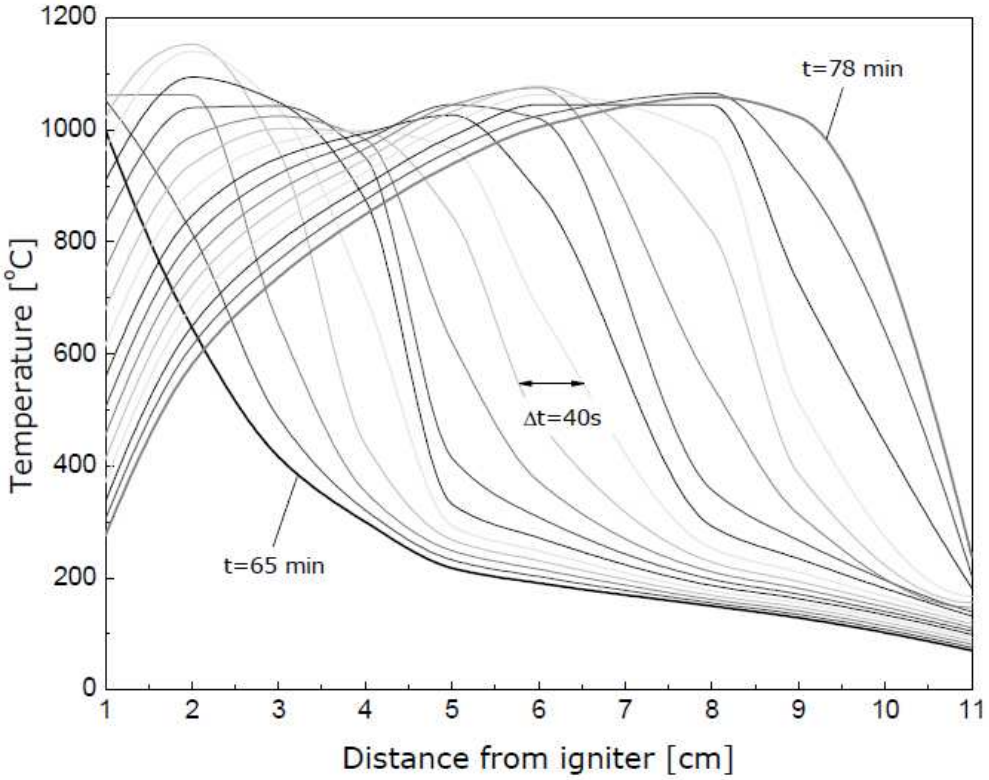

Figure 5.6 Temperature profiles for coal tar in coarse sand at 25% saturation and 9.15 cm/s air flux.

Temperature traces for the experiments conducted with **coal tar** in **medium sand** are presented in Figures 5.7-5.10 (Experiments 5-8). The graphs present similar characteristics to those observed in the coarse sand experiments, with some noticeable differences. The similarities are that in all cases ignition of the fuel occurs soon after the onset of air flow and the reaction is able to propagate itself once the igniter is turned off. However, the temperature decrease subsequent to ignition, occurring between 3 and 4 cm from the igniter, is more pronounced in these experiments than in the coarse sand case. The slope of the rising front of the temperatures peaks is lower, and their width considerably larger (nearly twice that observed in the coarse sand case, at 90% of the peak temperature), which suggests a less intense reaction. Maximum temperatures reached in the central part of the sample are significantly lower, with a decrease of about 100 to 150 ºC in comparison

to the coarse sand experiments. At the lowest air flux, temperature decay towards the upper boundary is observed, which suggests that for this experiment the reaction is approaching extinction. However, as observed with the coarse sand, increased air flux corresponds to increased reaction intensity and the differences between the sand types thus diminishes at the higher air fluxes examined.

It is noted that, for air fluxes higher than 4.05 cm/s in medium sand, partial fluidisation of the sand pack occurred towards the end of the experiment (i.e., when a small contaminated region with low permeability to air capped a large region of contaminant-free porous media). This behaviour is responsible for the sudden temperature drop and irregular trend observed in Figures 5.8-5.10, and the phenomenon is an artefact of the experimental scale.

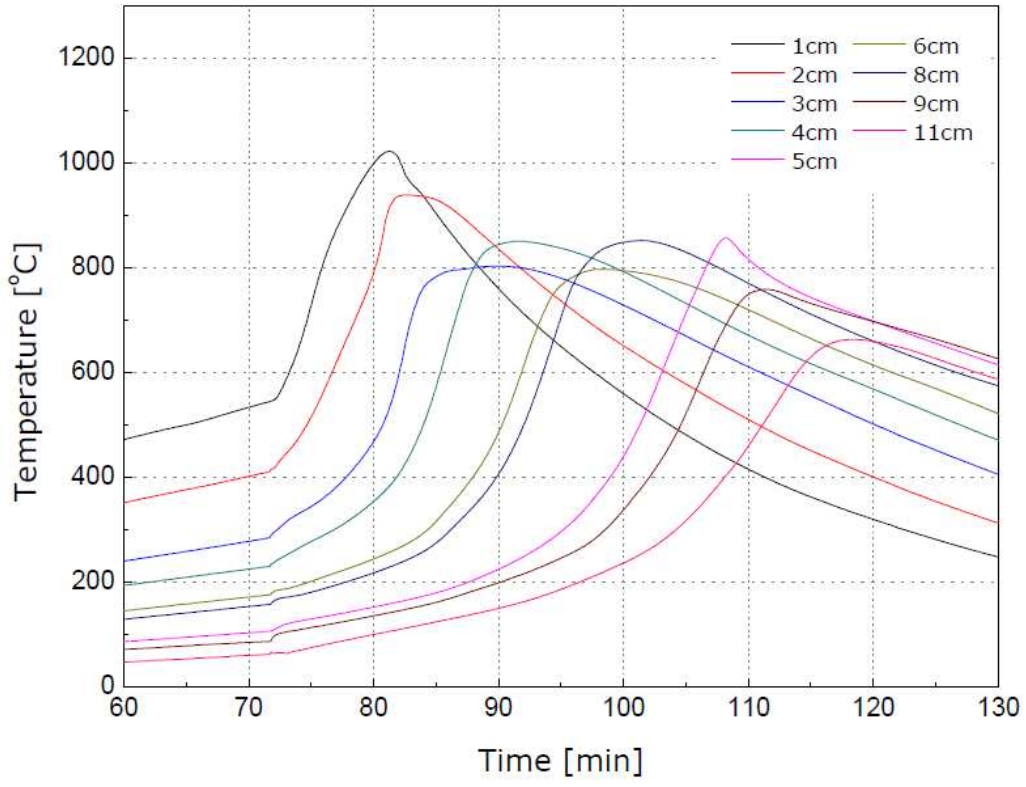

Figure 5.7 Temperature histories for coal tar in medium sand at 25% saturation and 4.05 cm/s air flux.

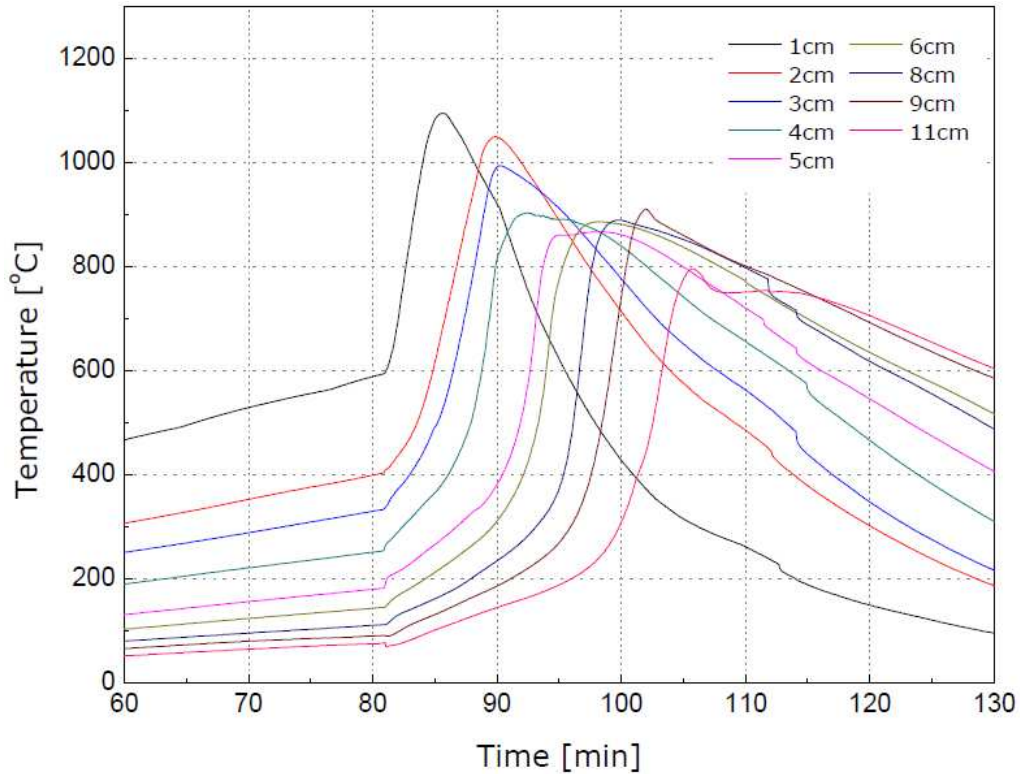

Figure 5.8 Temperature histories for coal tar in medium sand at 25% saturation and 9.15 cm/s air flux.

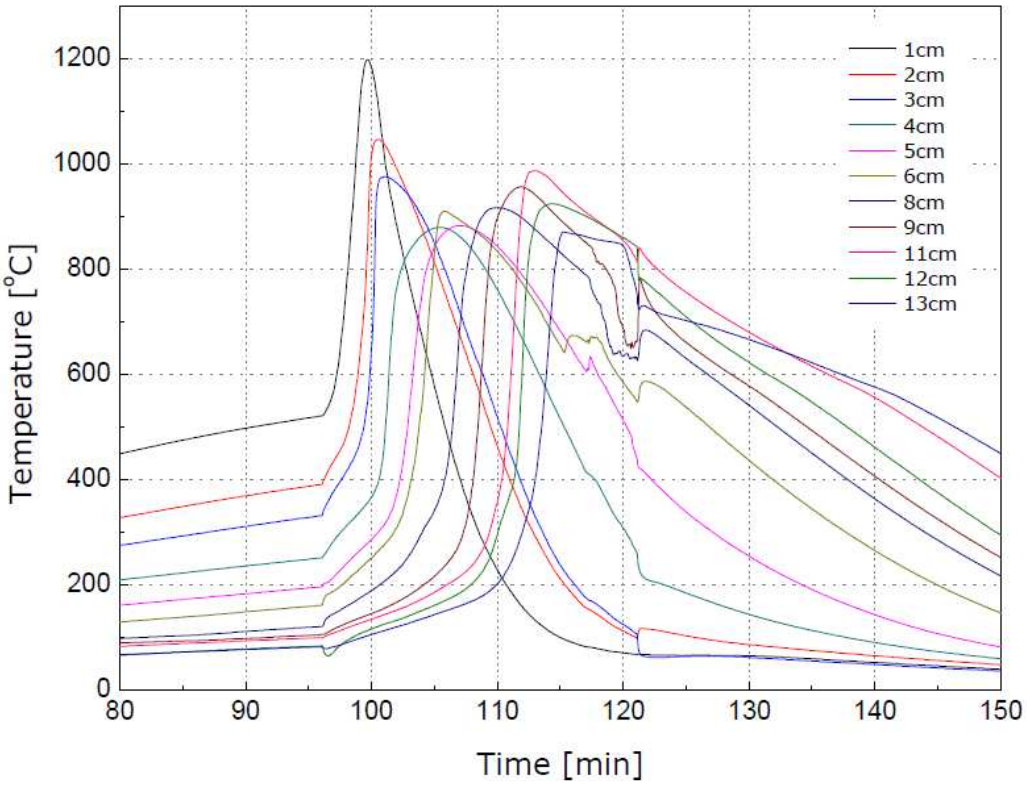

Figure 5.9 Temperature histories for coal tar in medium sand at 25% saturation and 16.6 cm/s air flux.

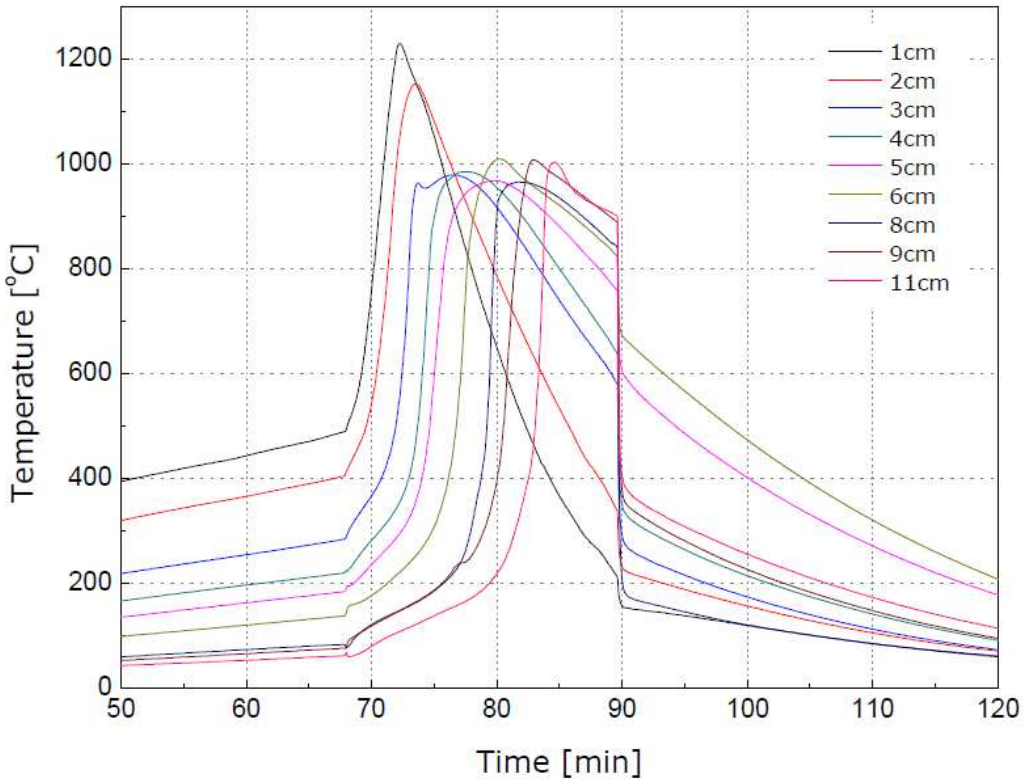

Figure 5.10 Temperature histories for coal tar in medium sand at 25% saturation and 25.2 cm/s air flux.

Temperature traces for the experiments conducted with **crude oil** in **coarse sand** are presented in Figures 5.11-5.14 (Experiments 9-12). Key similarities include the rapid onset of the reaction after air injection is started and the increase in the intensity of the reaction with increasing air flux. The most remarkable difference compared to the coal tar case is in the magnitude of the peak temperatures observed in these experiments, which are significantly lower than in the coal tar experiments. Average maximum temperatures for crude oil ranged between 630 and 680 ºC, well below the minimum observed in the coal tar experiments (nearly 840 ºC). Another noticeable difference is that the temperature peaks are much wider than those measured for coal tar (the average peak width for crude oil is about half of the propagation time, while for coal tar this is about one third on the propagation time over the same distance).

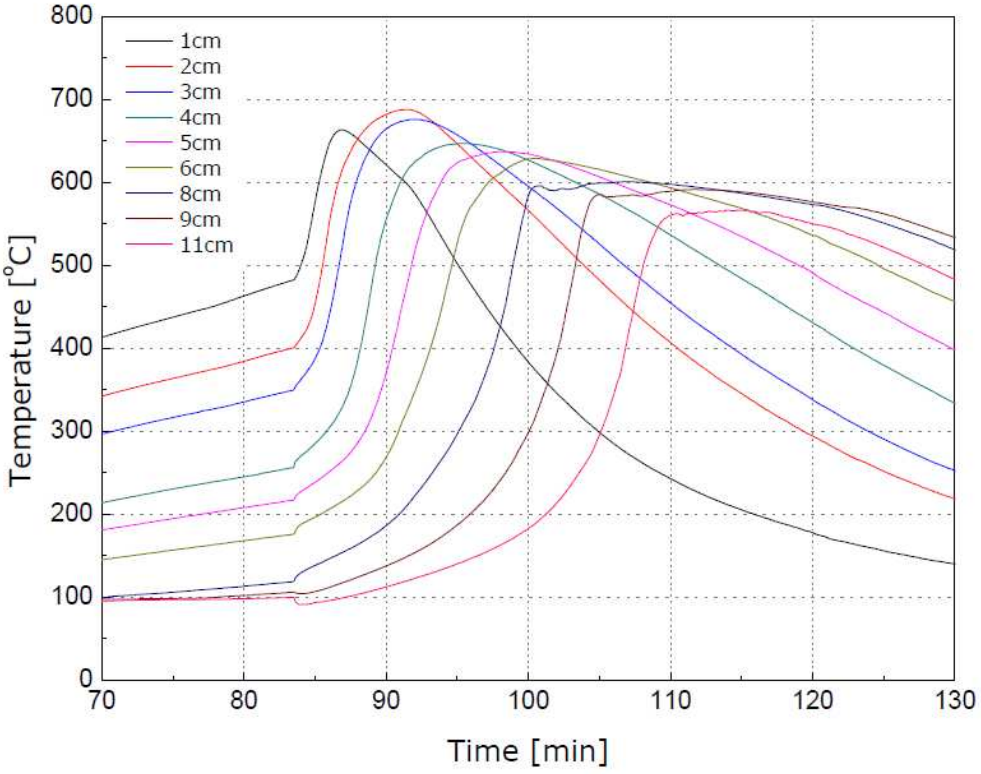

Figure 5.11 Temperature histories for crude oil in coarse sand at 25% saturation and 4.05 cm/s air flux.

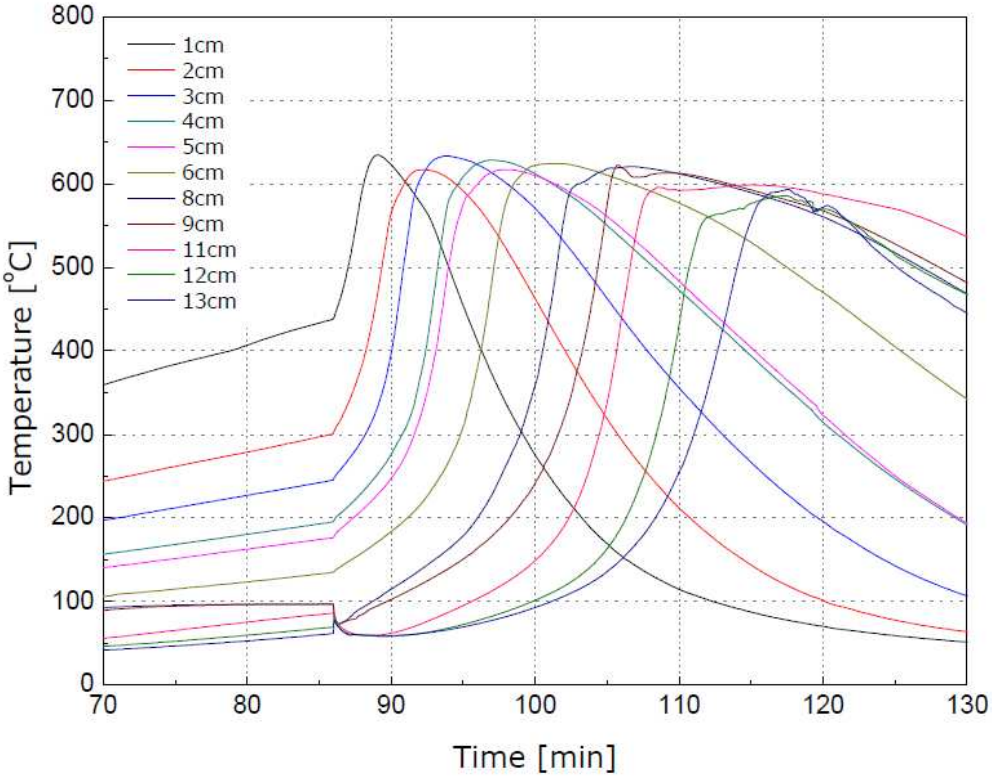

Figure 5.12 Temperature histories for crude oil in coarse sand at 25% saturation and 9.15 cm/s air flux.

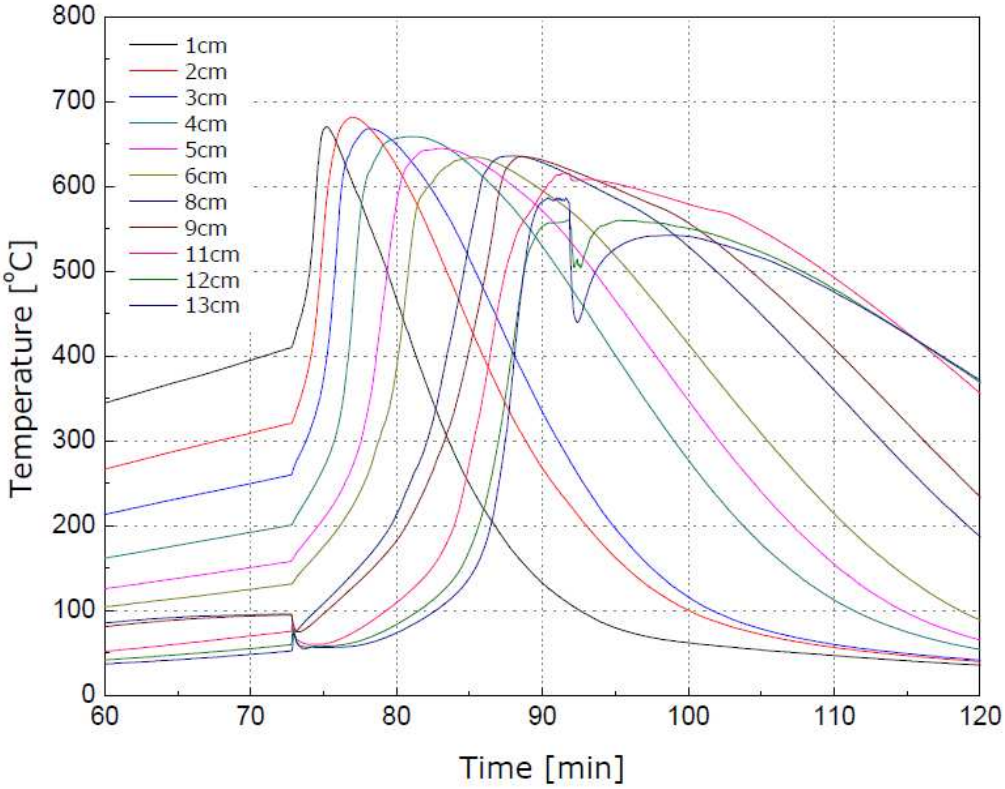

Figure 5.13 Temperature histories for crude oil in coarse sand at 25% saturation and 16.6 cm/s air flux.

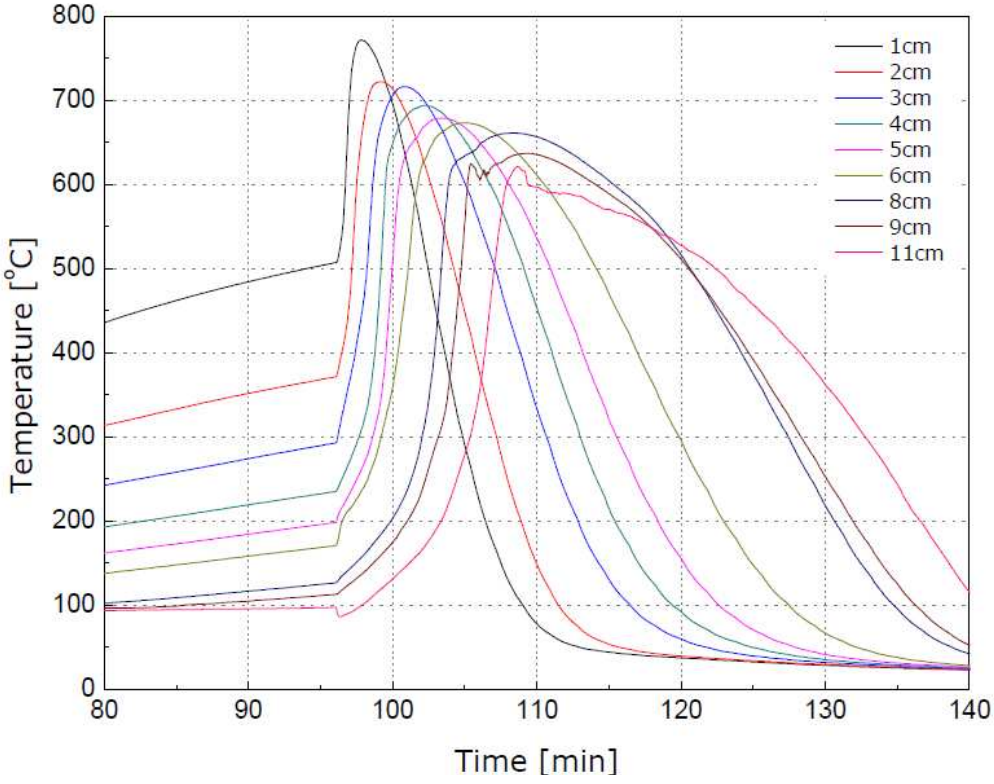

Figure 5.14 Temperature histories for crude oil in coarse sand at 25% saturation and 25.2 cm/s air flux.

The experiments conducted with **crude oil** in **medium sand** produced results similar to those for crude oil in coarse sand (data presented in Appendix A). Comparing the medium and the coarse sand experiments for crude oil, the width of the temperature profiles was similar and the average peak temperatures did not present significant variations (differences in maximum temperatures are within 3%), which contrasts with the results for coal tar in the same porous medium. This reveals that, unlike for coal tar, the strength of the reaction remained almost unchanged between the two porous media for crude oil.

The relationship between the average peak temperature and the air flux for all the experiments conducted at NAPL saturation of 25% is presented in Figure 5.15. Average peak temperatures for coal tar increase with the air flux and range between 975 and 1135 ^{o}C in coarse sand and between 840 and 1035 ^{o}C in medium sand. Peak temperatures for crude oil range between 600 and 670 ^{o}C, with no significant differences between coarse and medium sand; also, there is less of a distinct dependence on the air flux since temperature differences are within or close to the measurement uncertainty for these experiments (see Appendix C).

A clear separation is evident between coal tar and crude oil peak temperatures, the former being on average 350 ^{o}C higher than the latter. This can be in part the consequence of different fuel concentrations between the two groups of experiments because, since crude oil is less dense than coal tar, an equal saturation corresponds to a lower concentration of mass. In addition, crude oil contains a larger fraction of volatile compounds compared to coal tar, therefore it is expected that a larger amount

of it is vaporized during the smouldering process, thus reducing the effective concentration of oxidized fuel in the porous medium.

The variation of the average smouldering velocity with the inlet air flux is presented in Figure 5.16. In all but one case, propagation velocity increases with increasing air flux indicating that the reaction is, in general, oxygen limited. The exception is Experiment 12 (25.2 cm/s air flux, 25% saturation coal tar, medium sand) which exhibits essentially the same velocity as the 16.6 cm/s experiment. This behaviour was probably the result of substantial air channelling in the vicinity of the column walls, which decreased the effective air flux in the core of the sample.

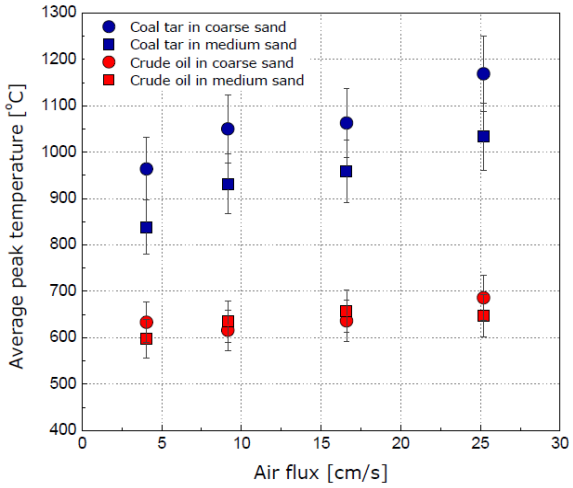

Figure 5.15 Average peak temperature as a function of the air flux for the experiments conducted at constant NAPL saturation (25% of the pore space).

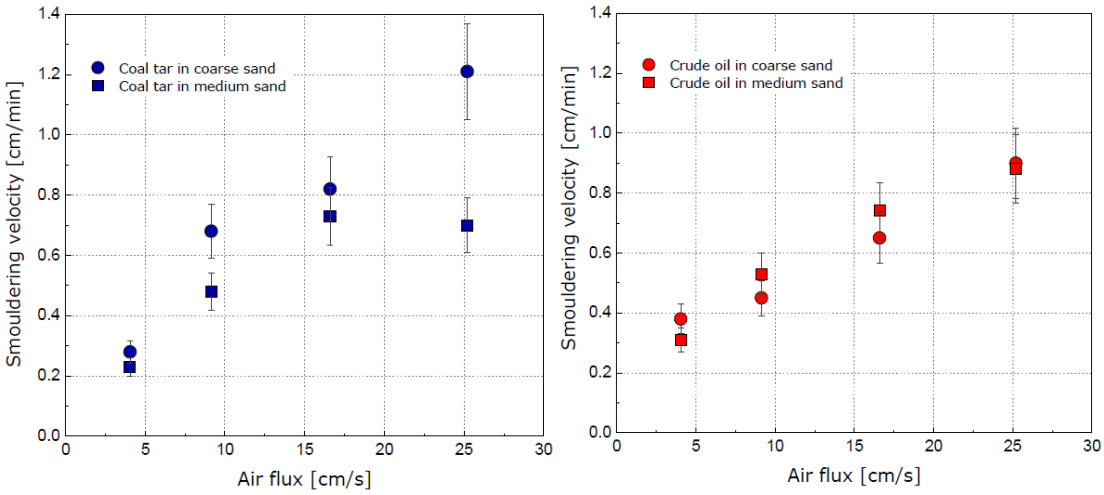

Figure 5.16 Average smouldering velocity as a function of the air flux for coal tar (left) and crude oil at constant NAPL saturation (25% of the pore space).

5.3.2 Characterisation of the gaseous emissions and reaction stoichiometry

Characterisation of the gaseous emission was carried out on a subset of the experiments (Experiments 2 and 10 in Table 5.1) through real-time FTIR analysis of the exhaust gases. At the exhausts dilution employed in these experiments (gas flow rate in extraction hood set at 150 L/s) the principal compounds detected in the emission were, in addition to carbon dioxide, carbon monoxide and water, naphthalene in the case of coal tar, hexane and methane in the case of crude oil (Figures 5.17-5.20). Trace amounts of toluene, m-xylene, methane and hexane were also measured in the emissions from coal tar while concentrations of other secondary species from crude oil were too low to be quantified. The oscillations in the concentrations of toluene and m-xylene observed in Figure 5.18 may have resulted from the instrument failing to consistently identify those compounds at each measuring time.

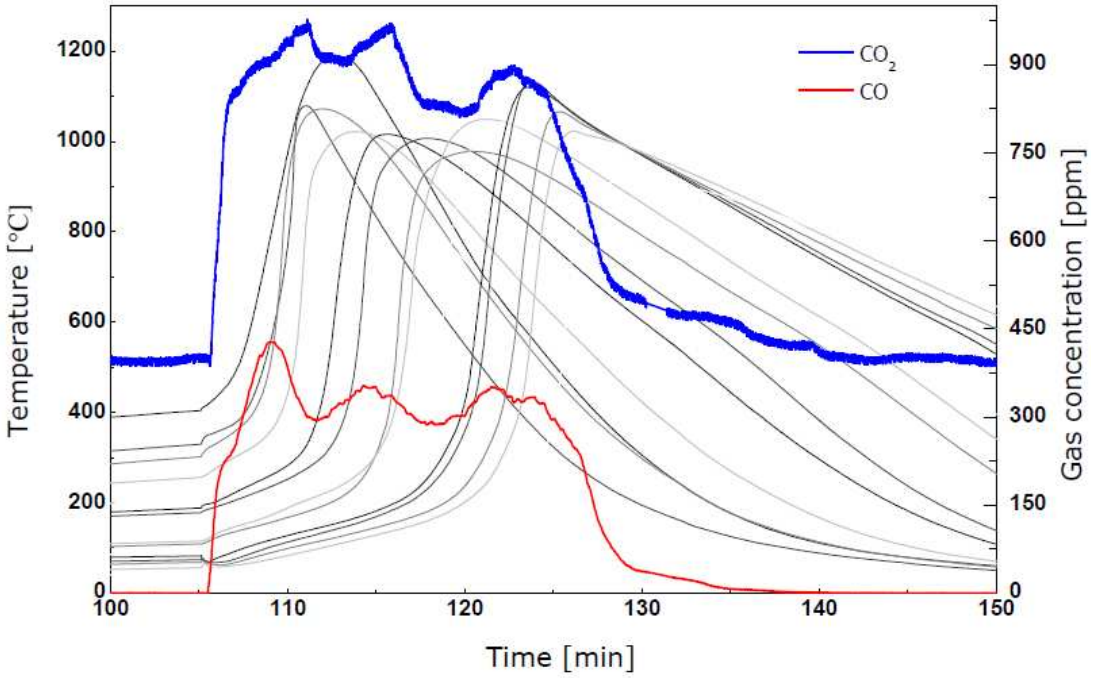

Figure 5.17 Carbon dioxide and carbon monoxide emissions for a base-case experiment on coal tar in coarse sand (reproduced from Chapter 3).

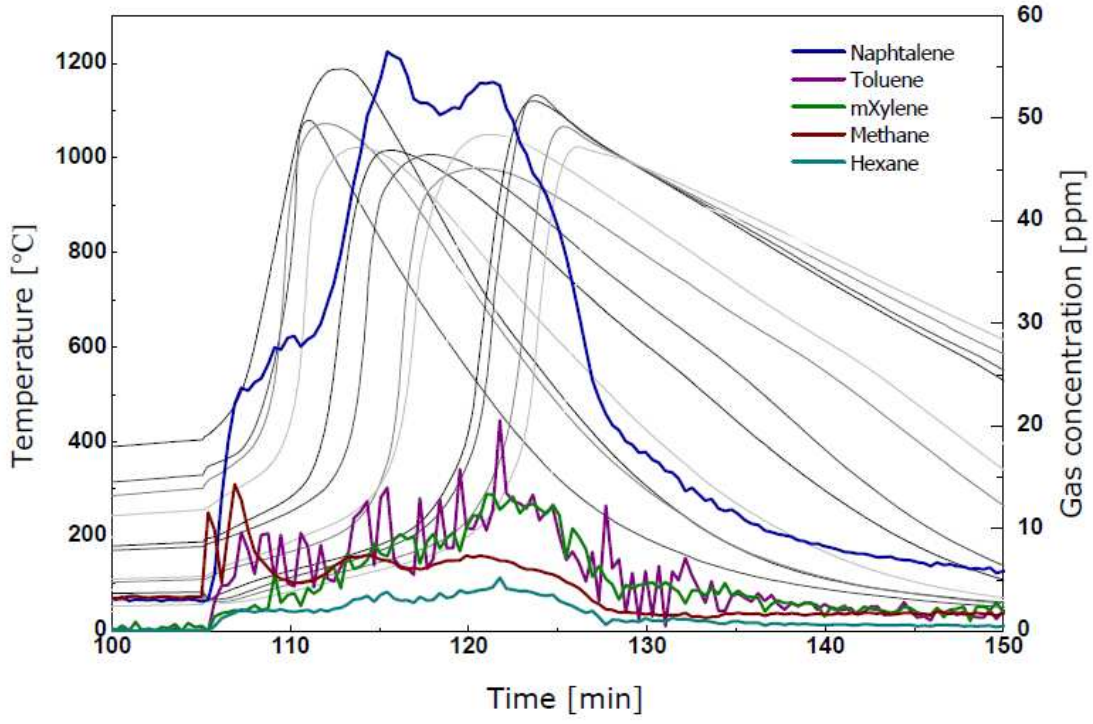

Figure 5.18 Principal volatile hydrocarbon emissions for a base-case experiment on coal tar in coarse sand.

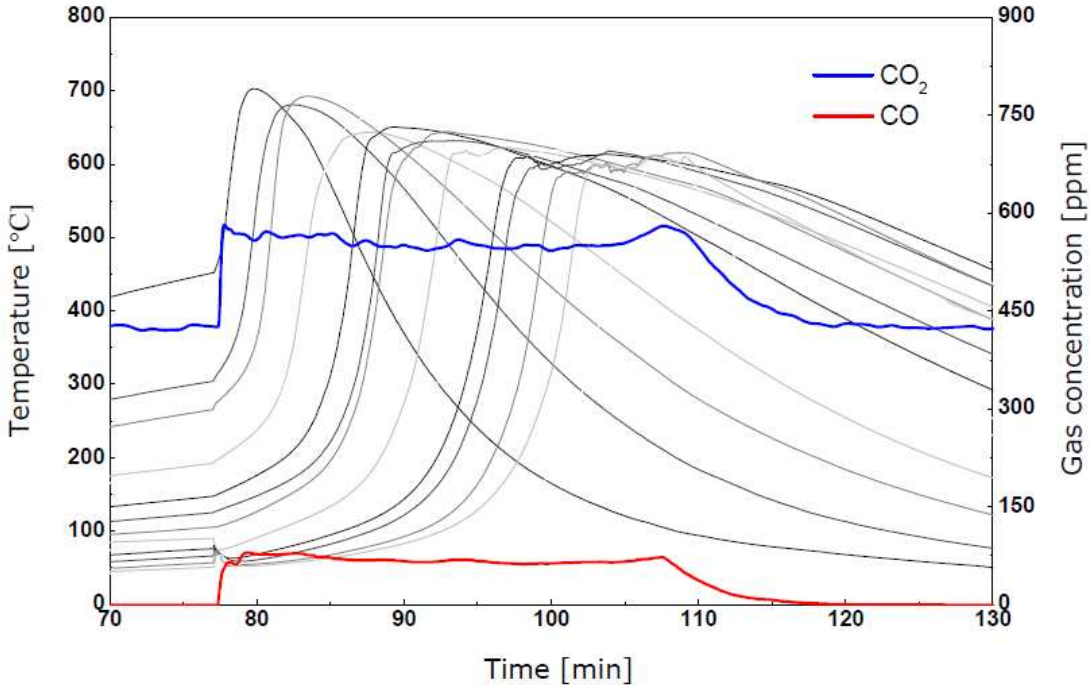

Figure 5.19 Carbon dioxide and carbon monoxide emissions for a base-case experiment on crude oil in coarse sand.

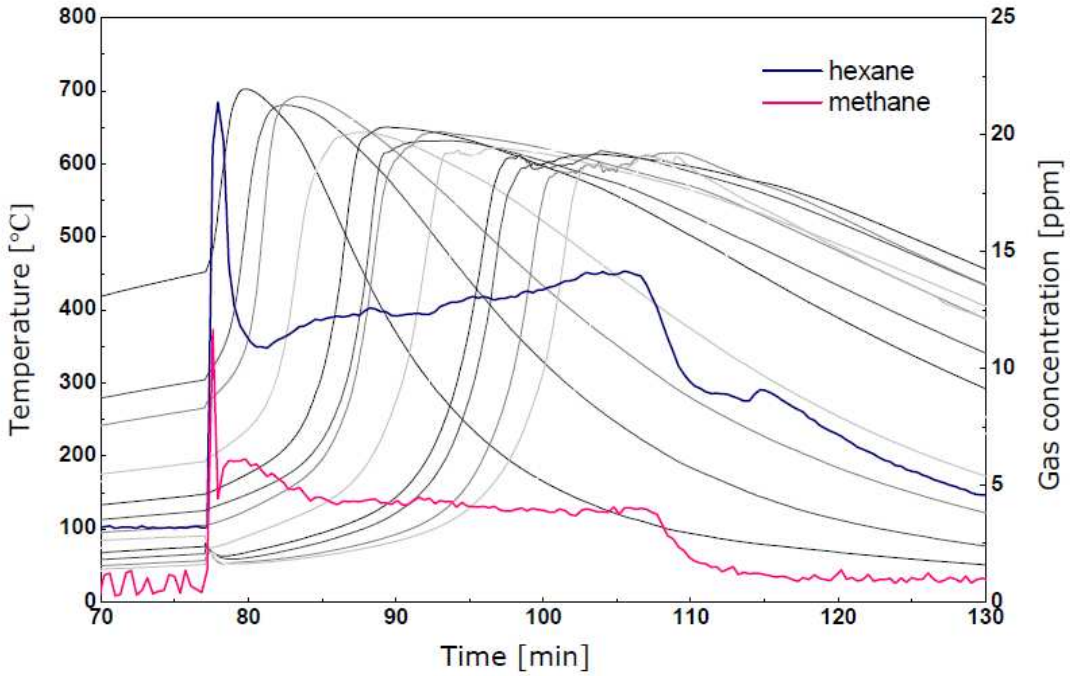

Figure 5.20 Principal volatile hydrocarbon emissions for a base-case experiment on crude oil in coarse sand.

Global stoichiometry and the heat of reaction

Based on the measured composition of the gaseous emissions, an approximate reaction mechanism is derived for the NAPL smouldering process. This will enable the estimate of the specific energy release associated with the reaction, a key parameter for both theoretical modelling and practical applications of the process.

In general, any combustion reaction can be described by a global stoichiometry of the kind

$$1 \cdot [\mathrm{NAPL}] + \nu_{O} \cdot O_2 \rightarrow \nu_{CO2} \cdot CO_2 + \nu_{CO} \cdot CO + \nu_{H2O} \cdot H_2O + \sum_{i=4}^{n} \nu_i \cdot HC_i + \Delta H_r \quad (1)$$

whereby a unit mass of fuel (the NAPL) reacts with oxygen and is converted to carbon oxides, water and lighter hydrocarbons HC_i, while releasing the amount of energy ΔH_r (enthalpy of reaction) (e.g. Glassman and Yetter, 2008).

To calculate the values of the stoichiometric coefficients present in (1), n equations are needed in the unknown coefficients ν_i. Three equations are provided by the mass balances of C, H and O; (n-3) additional relationships can be obtained from the experimental data, for example by calculating the mass ratios ν_{CO_2}/ν_{CO}, ν_i/ν_{CO} (for $i = 4 \cdots n$). The following system of equations can thus be obtained:

$$
\begin{cases}
\dfrac{1}{MW_{NAPL}} = \dfrac{\nu_{CO_2}}{MW_{CO_2}} + \dfrac{\nu_{CO}}{MW_{CO_2}} + \sum_{i=4}^{n} C_i \cdot \dfrac{\nu_i}{MW_{HC_i}} \\
\dfrac{x}{MW_{NAPL}} = 2 \cdot \dfrac{\nu_{H_2O}}{MW_{H_2O}} + \sum_{i=4}^{n} H_i \cdot \dfrac{\nu_i}{MW_{HC_i}} \\
\dfrac{y}{MW_{NAPL}} + 2 \cdot \dfrac{\nu_O}{MW_{O_2}} = 2 \cdot \dfrac{\nu_{CO_2}}{MW_{CO_2}} + \dfrac{\nu_{CO}}{MW_{CO_2}} + \dfrac{\nu_{H_2O}}{MW_{H_2O}} \\
\dfrac{\nu_{CO_2}}{\nu_{CO}} = R_1 \\
\dfrac{\nu_{HC_1}}{\nu_{CO}} = R_2 \\
\vdots \\
\dfrac{\nu_{HCn}}{\nu_{CO}} = R_{n+1}
\end{cases}
\qquad (2)
$$

In the above equations C_i and H_i are the number of atoms of carbon and hydrogen in the molecule of the hydrocarbon HC_i while x and y are the coefficients of hydrogen and oxygen respectively in the NAPL empirical formula CH_xO_y. The constants R_i are calculated from the experimental data as the ratios M_i/M_{CO} between the mass of the species i and the mass of CO produced in the reaction, taken as the net cumulative mass of these compounds produced in a given time interval in which the reaction is considered steady, so that the ratios do not depend on the interval chosen. By ‘net’ it is meant that the mass of CO_2 does not include the atmospheric CO_2 present in the ambient air entrained in the extraction hood.

By Hess’s law, the enthalpy change associated with a generic reaction can be expressed as a combination of the enthalpy changes of any number of intermediate steps that lead to the overall reaction. Thus in order to calculate the heat of combustion of the generic reaction (1) it is sufficient to represent this process as a

combination of reactions of known heat of combustions. One way to achieve this is to consider the process of complete combustion of NAPL:

$$1 \cdot [\text{NAPL}] + \nu_{O,cc} \cdot O_2 \rightarrow \nu_{CO_2,cc} \cdot CO_2 + \nu_{H_2O,cc} \cdot H_2O + \Delta H_{r,cc} \quad (3)$$

as the results of the process (1) followed by the oxidation of carbon monoxide to carbon dioxide:

$$CO + 1/2\ O_2 \rightarrow CO_2 + \Delta H_{r,2} \quad (4)$$

and the complete oxidation of the hydrocarbons HC_i:

$$HC_i + a_{i,1} \cdot O_2 \rightarrow a_{i,2} \cdot CO_2 + a_{i,3} \cdot H_2O + \Delta H_{r,i} \qquad i = 4 \cdots n \quad (5)$$

Equation (1) can thus be obtained from Equation (3) by subtracting from this the reactions (4) and (5) multiplied by the stoichiometric coefficient with which CO and the HCs occur in Equation (1). Consequently, the heat of reaction for the process (1) can be expressed as:

$$\Delta H_r = \Delta H_{r,cc} - \nu_{CO} \cdot \Delta H_{r,2} - \sum_{i=4}^{n} \nu_i \cdot \Delta H_{r,i} \quad (6)$$

The heat of complete combustion $\Delta H_{r,cc}$ can be determined experimentally, for example by bomb calorimetry testing, while the other heats of reaction on the right-hand side of equation (6) are found in the literature. Hence, the heat of reaction ΔH_r can be calculated once the stoichiometric coefficients of the reaction (1) are known.

Figures 5.21 and 5.22 present the cumulative mass of the principal gases collected in the emissions for base-case experiments on coal tar and crude oil. In both cases more than 90% of the total mass of gaseous products (excluding water) is accounted for by CO_2, CO and the most abundant among the light hydrocarbons, that is naphthalene ($C_{10}H_8$) and hexane (C_6H_{14}) for coal tar and crude oil respectively. For this reason, in

order to obtain a first-approximation estimate of the heat of combustion of the two NAPLs, only these compounds have been counted among the light hydrocarbons produced in the reaction. The general reaction scheme (1) is thus simplified into the following stoichiometries for coal tar and crude oil:

$$1 \cdot [\text{Coal tar}] + \nu_O \cdot O_2 \rightarrow \nu_{CO2} \cdot CO_2 + \nu_{CO} \cdot CO + \\ + \nu_{H2O} \cdot H_2O + \nu_{C_{10}H_8} \cdot C_{10}H_8 + \Delta H_{r,ct} \qquad (7)$$

$$1 \cdot [\text{Crude oil}] + \nu_O \cdot O_2 \rightarrow \nu_{CO2} \cdot CO_2 + \nu_{CO} \cdot CO + \\ + \nu_{H2O} \cdot H_2O + \nu_{C_6H_{14}} \cdot C_6H_{14} + \Delta H_{r,co} \qquad (8)$$

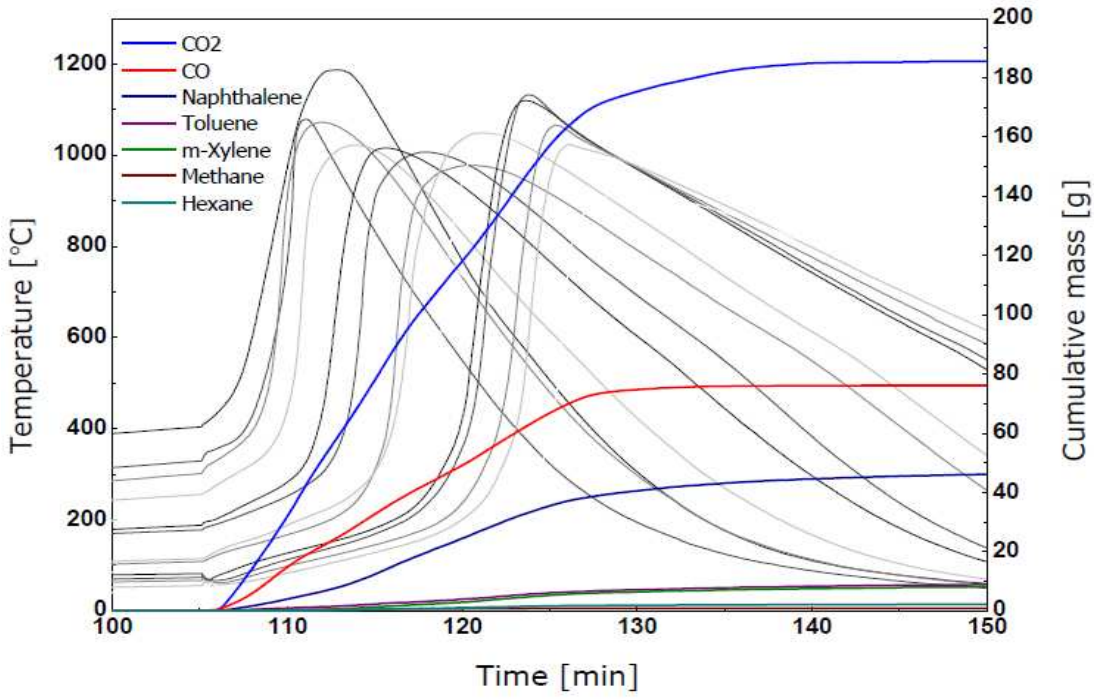

Figure 5.21 Cumulative mass of CO_x and principal volatile hydrocarbon in the emissions for a base-case experiment on coal tar in coarse sand.

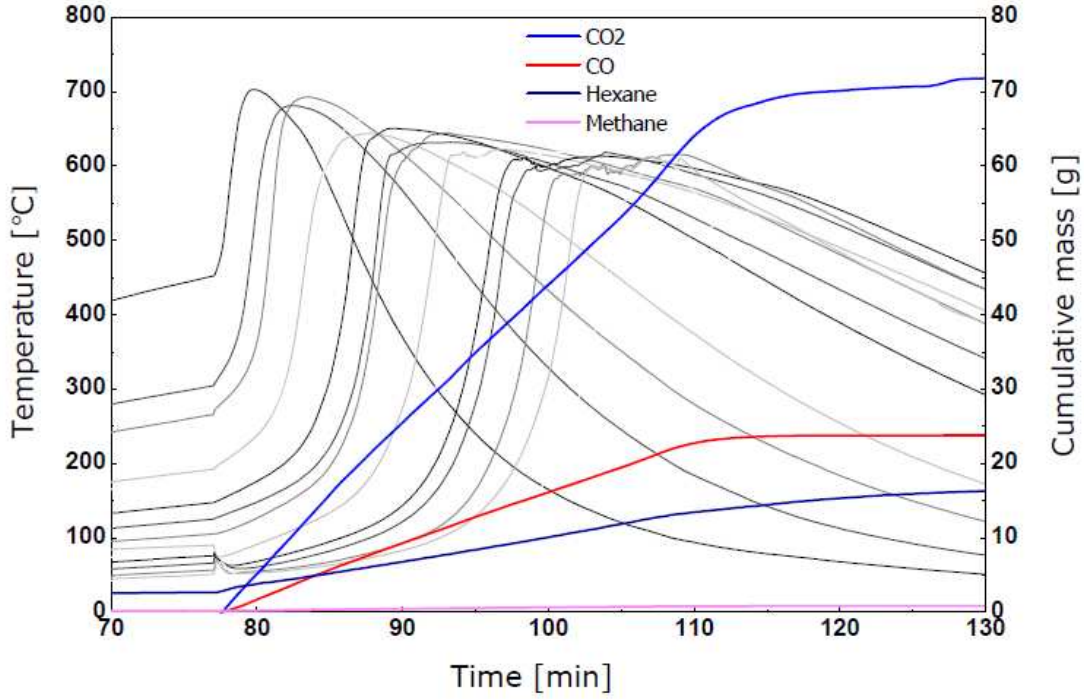

Figure 5.22 Cumulative mass of CO_x and principal volatile hydrocarbon in the emissions for a base-case experiment on crude oil in coarse sand.

The stoichiometric coefficients for the reactions (7) and (8) have been calculated using the constants listed in Table 5.2; the molar ratios x and y were determined by elemental analysis on samples of coal tar and crude oil (see Appendix C). The results are presented in Table 5.3.

Table 5.2 Values of the Constants used to calculate the Stoichiometric Coefficients

Constant	Value (coal tar)	Unit	Value (crude oil)	Unit
x	0.698	mol_H/mol_C	1.52	mol_H/mol_C
y	0.011	mol_O/mol_C	0.012	mol_O/mol_C
R_1	2.27	kg_{CO2}/kg_{CO}	2.68	kg_{CO2}/kg_{CO}
R_2	0.638	kg_{C10H8}/kg_{CO}	0.449	kg_{C6H14}/kg_{CO}

Table 5.3 Stoichiometric Coefficients obtained from System (2) (HC indicates $C_{10}H_8$ for coal tar C_6H_{14} for crude oil)

Coefficient	Value (coal tar)	Value (crude oil)	Unit
ν_O	1.62	1.98	kg_O/kg_{NAPL}
ν_{CO2}	1.39	1.53	kg_{CO2}/kg_{NAPL}
ν_{CO}	0.60	0.57	kg_{CO}/kg_{NAPL}
ν_{HC}	0.32	0.26	kg_{HC}/kg_{NAPL}
ν_{H2O}	0.31	0.63	kg_{H2O}/kg_{NAPL}

A parameter of considerable practical interest is the energy release per unit mass of oxygen consumed. As it will be shown in the following section, the balance of energy and oxygen mass at the reaction front allows to relate the rate of energy generated to the propagation velocity of the reaction. On condition that the oxygen injected is totally consumed in the reaction, the rate of energy generated and the propagation velocity of the process are controlled by the rate of oxygen injection (see Section 5.4.1). Thus the specific energy release (energy release per unit mass of oxygen) is a parameter that enables the linking between an external control parameter (the rate of oxygen injected) and the resulting behaviour of the reaction (velocity of propagation).

The heats of reaction and specific energy releases associated with the smouldering reaction of coal tar and crude oil can be calculated using Equation (6) and the stoichiometric coefficients obtained above (Table 5.3). The values of the heats of combustion appearing in Equation (6) used for the calculation are listed in Table 5.4.

Table 5.4 Heats of Combustion used to apply Equation (6)

Heat of combustion	Value (MJ/kg)	Description
$\Delta H_{r,ct,cc}$	39.4	Heat of combustion for the complete oxidation of coal tar. Determined by bomb calorimetry
$\Delta H_{r,co,cc}$	42.0	Heat of combustion for the complete oxidation of crude oil. Determined by bomb calorimetry
$\Delta H_{r,2}$	10.1	Heat of combustion for the oxidation of CO to CO_2 (SFPE Handbook, 2008).
$\Delta H_{r,C10H8}$	40.2	Heat of combustion of naphthalene - Gross value (SFPE Handbook, 2008).
$\Delta H_{r,C6H14}$	48.3	Heat of combustion of hexane - Gross value (SFPE Handbook, 2008).

The results are summarised in Table 5.5.

Table 5.5 Heats or Reaction associated with Smouldering of Coal Tar and Crude Oil

Heat of combustion	Value	Unit	Description
$\Delta H_{r,ct}$	19.9	MJ/kg	Heat of combustion corresponding to incomplete smouldering reaction of coal tar
$\Delta H_{r,co}$	22.5	MJ/kg	Heat of combustion corresponding to incomplete smouldering reaction of crude oil
$\Delta H_{o,ct}$	12.3	MJ/kg_{O_2}	Specific energy release corresponding to incomplete smouldering reaction of coal tar
$\Delta H_{o,co}$	11.4	MJ/kg_{O_2}	Specific energy release corresponding to incomplete smouldering reaction of crude oil

5.4 Analysis of the results

In what follows, an attempt will be made to explain some of the observed characteristics of the smouldering process using a simplified analysis as that developed by other authors (e.g. Dosanjh *et al.*, 1987; Torero and Fernandez-Pello, 1996; Schult *et al.*, 1995; Aldushin *et al.*, 1999). The analysis is based on a mass and energy balance across the reaction front and allows for the derivation of analytical expressions for the smouldering temperature and velocity. These will be then compared with the results obtained from the experiments.

5.4.1 Derivation of the analytical models

Analytical expressions for the smouldering velocity and temperature can be obtained from the conservation equations of energy, oxygen mass and fuel mass, under a series of simplifying assumptions (e.g. Torero and Fernandez-Pello, 1996; Schult *et al.*, 1995; Aldushin *et al.*, 1999). The reacting system is considered to be adiabatic and the energy conservation equation is written in term of a single temperature for both solid and gaseous phases (*i.e.* thermal equilibrium between phases is assumed):

$$\frac{\partial}{\partial t}\left[\left(\rho_{b,s}c_{ps}+\varphi_f\rho_f c_{pf}+\varphi_g\rho_g c_{pg}\right)\cdot T\right]=-\frac{\partial}{\partial x}\left(\dot{m}''_g c_{pg}T\right)+\frac{\partial}{\partial x}\left(k_T\frac{\partial T}{\partial x}\right)+\Delta H_r\cdot W \tag{9}$$

Oxygen and fuel mass conservation equations are

$$\frac{\partial}{\partial t}\left(\varphi_g\rho_g Y_O\right)=-\frac{\partial}{\partial x}\left(\dot{m}''_g Y_O\right)+\frac{\partial}{\partial x}\left(\varphi_g D_O\rho_g\frac{\partial Y_O}{\partial x}\right)-\nu_O\cdot W \tag{10}$$

$$\frac{\partial}{\partial t}\left(\varphi_f\rho_f\right)=-W \tag{11}$$

where

$\rho_{b,s}$ bulk density of the solid

c_{ps} specific heat of the solid

ρ_f density of the fuel

c_{pl} specific heat of the liquid

ρ_g density of the gas

c_{pg} specific heat of the gas

φ_g gas filled porosity

φ_f fuel filled porosity

k_T total thermal conductivity

$\dot{m}''_g$ gas mass flux

ΔH_r enthalpy of reaction per unit mass of fuel

W	reaction rate (mass of fuel reacted per unit time and unit volume of sample)
Y_O	mass fraction of oxygen in the gas phase
ν_O	stoichiometric coefficient oxygen/fuel
D_O	diffusion coefficient of oxygen in the gas phase

In a reference frame attached to the reaction front moving in the positive *x* direction with velocity U_S (cf. Figure 5.23), the equations (9) - (11) can be written as

$$\left(\frac{\partial}{\partial t} - U_S \frac{\partial}{\partial x}\right) \cdot \left[\left(\rho_{b,s} c_{ps} + \varphi_f \rho_f c_{pf} + \varphi_g \rho_g c_{pg}\right) \cdot T\right] = - \frac{\partial}{\partial x}\left(\dot{m}''_g c_{pg} T\right) + \frac{\partial}{\partial x}\left(k_T \frac{\partial T}{\partial x}\right) + \Delta H \cdot W \tag{12}$$

$$\left(\frac{\partial}{\partial t} - U_S \frac{\partial}{\partial x}\right) \cdot \left(\varphi_g \rho_g Y_O\right) = - \frac{\partial}{\partial x}\left(\dot{m}''_g Y_O\right) + \frac{\partial}{\partial x}\left(\varphi_g D_O \rho_g \frac{\partial Y_O}{\partial x}\right) - \nu_O \cdot W \tag{13}$$

$$\left(\frac{\partial}{\partial t} - U_S \frac{\partial}{\partial x}\right) \cdot \left(\varphi_f \rho_f\right) = -W \tag{14}$$

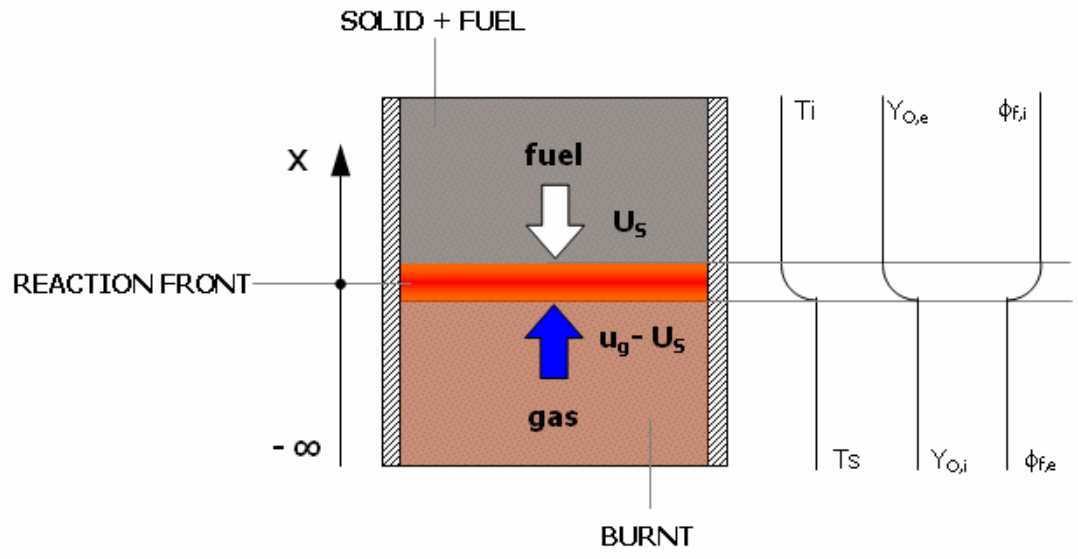

Figure 5.23 Schematic of the smouldering reaction in a reference frame attached to the reaction front.

Assuming that the smouldering reaction is steady in this reference frame, the above equations become

$$\frac{d}{dx}\left[\left(\dot{m}''_s c_{ps} + \dot{m}''_f c_{pf} + \dot{m}''_g c_{pg}\right)\cdot T\right] = \frac{d}{dx}\left(k_T \frac{dT}{dx}\right) + \Delta H_r \cdot W \tag{15}$$

$$\frac{d}{dx}\left(\dot{m}''_g Y_O\right) = \frac{d}{dx}\left(\varphi_g D_O \rho_g \frac{dY_O}{dx}\right) - \nu_O \cdot W \tag{16}$$

$$\frac{d\dot{m}''_f}{dx} = -W \tag{17}$$

where the gas, solid and fuel mass fluxes are given by

$$\dot{m}''_g = (u_g - U_S)\varphi_g \rho_g$$

$$\dot{m}''_s = -U_S \rho_S$$

$$\dot{m}''_f = -U_S \rho_f \varphi_f$$

The boundary conditions for the above equations are

at $x = -\infty$	$T = T_S$	at $x = x$	$T = T_i$
	$Y_O = Y_{O,i}$		$Y_O = Y_{O,e}$
	$\varphi_f = \varphi_{f,e}$		$\varphi_f = \varphi_{f,i}$
	$\frac{dY_O}{dx} = 0$		$\frac{dY_O}{dx} = 0$
	$\frac{dT}{dx} = 0$		$\frac{dT}{dx} = 0$

Substituting Equation (17) in Equation (16) and integrating from $x = -\infty$ to x provides a first relationship between the unknown quantities $U_S, Y_{O,e}, \varphi_{f,e}$:

$$\frac{\dot{m}''_g}{\nu_O}\cdot\left(Y_{O,i} - Y_{O,e}\right) = U_S \rho_f \cdot \left(\varphi_{f,i} - \varphi_{f,e}\right) \tag{18}$$

The above equation represents the steady state mass balance of oxygen and fuel at the reaction front. For the reaction to advance, the net rate of oxygen supplied to the reaction must be equal to the stoichiometric oxygen necessary to consume all the reacted fuel. Since it is experimentally observed that the fuel is completely consumed

in the reaction, the fuel content behind the reaction front ($\varphi_{f,e}$) can be assumed to be zero; by further assuming that the propagation of the smouldering front is oxygen-controlled (i.e. all the oxygen is consumed in the reaction) then $Y_{O,e}=0$ and Equations (18) provides the following explicit expression for the smouldering propagation velocity U_S :

$$U_S = \frac{\dot{m}''_g \cdot Y_{O,i}}{\varphi_{f,i}\rho_f \cdot \nu_O} \tag{19}$$

Equation (19) is the same obtained in (Schult *et al.*, 1995) and in (Whale *et al*., 2003) for the mode of propagation referred to as *stoichiometrically* (or *filtration*) *controlled*. In this mode of propagation the smouldering velocity does not depend on the detail of the reaction kinetics, provided this is sufficiently fast to consume all the oxygen supplied to the reaction front. Equation (19) will be herein referred to as the 'mass balance expression'.

Further derivation provides, in contrast, a more complete 'energy balance expression'. Integrating (15) and (16) with respect to *x* from $x=-\infty$ to *x* and rearranging gives:

$$U_S \cdot \left(C_{v,e}T_S - C_{v,i}T_i\right) - \dot{m}''_g c_{pg} \cdot \left(T_S - T_i\right) = \frac{\Delta H_r}{\nu_O}\dot{m}''_g \cdot \left(Y_{O,i} - Y_{O,e}\right) \tag{20}$$

where $C_v \equiv \rho_s c_{ps} + \rho_f \varphi_f c_{pf}$ is the volumetric heat capacity of solid+fuel. To obtain (20) it was further assumed that the gas mass flux $\dot{m}''_g$ is constant (*i.e.* the net gas mass production is considered to be negligible) and that the smouldering velocity is negligibly small compared to the gas velocity. Equation (20) represents the adiabatic, steady state energy balance for a control volume comprising the reaction front. The

expression on the left hand side corresponds to the net convective output energy flux while the right hand side represents the specific energy generated by the reaction in the control volume per unit time. If the propagation is oxygen-controlled ($Y_{O,e} = 0$) Equation (20) can be rewritten as (e.g. Torero and Fernandez-Pello, 1996):

$$U_S = \frac{\dot{m}''_g c_{pg} \cdot (T_S - T_i) + \frac{\Delta H_r}{\nu_O} \dot{m}''_g \cdot Y_{O,i}}{C_{v,e} T_S - C_{v,i} T_i} \tag{21}$$

Inclusion of the radial heat losses Heat losses to the external environment are a complex function of the (unsteady) temperature and fluid flow fields in and around the reacting system and cannot be accurately determined by using the simplified analysis described above. However, an approximate expression for the heat losses can be obtained by a steady-state analysis as that conducted in (Bar-Ilan *et al.*, 2004). The result is the heat losses term

$$\dot{Q}''_{loss} = \frac{4 U_{tot} L}{D} \cdot (\overline{T}_S - T_{amb}) \tag{22}$$

where

U_{tot} is a global heat transfer coefficients
L is the thickness of the reaction front
D is the external diameter of the column
$\overline{T}_S$ is the average smouldering temperature in the reaction front
T_{amb} is the ambient temperature.

After subtracting the term (22) from the right hand side of Equation (20), the expression for the smouldering velocity (21) becomes

$$U_S = \frac{\dot{m}''_g c_{pg} \cdot (T_S - T_i) + \frac{\Delta H_r}{\nu_O} \dot{m}''_g \cdot Y_{O,i} - \dot{Q}''_{loss}}{C_{v,e} T_S - C_{v,i} T_i} \tag{23}$$

The global heat transfer coefficient U_{tot} takes into account the transport of energy by convection, conduction and radiation from the inner core of the sample to the ambient air. It can expressed as the sum of two terms, the first (U_{con}) describing the heat transfer by convection and conduction only and the second (U_{rad}) the contribution of radiation (Incropera and Dewitt, 2002). An estimate of U_{con} can be obtained by equating the heat flux from the inner core at temperature T_S to the ambient air, due to convection and conduction, to the heat exchanged by natural convection between the external wall at temperature T_2 and the ambient air (Figure 5.24):

$$\frac{4U_{con}L}{D}\cdot\left(\overline{T}_S - T_{amb}\right) = \frac{4h_2L}{D}\cdot\left(\overline{T}_2 - T_{amb}\right)$$

This yields

$$U_{con} = h_2 \cdot \frac{\overline{T}_2 - T_{amb}}{\overline{T}_S - T_{amb}} \qquad (24)$$

where h_2 is the coefficient of heat transfer between the external wall and the ambient air at temperature T_{amb} and $\overline{T}_2$ is the average temperature of the external wall across the thickness of the smouldering front (see Figure 5.24).

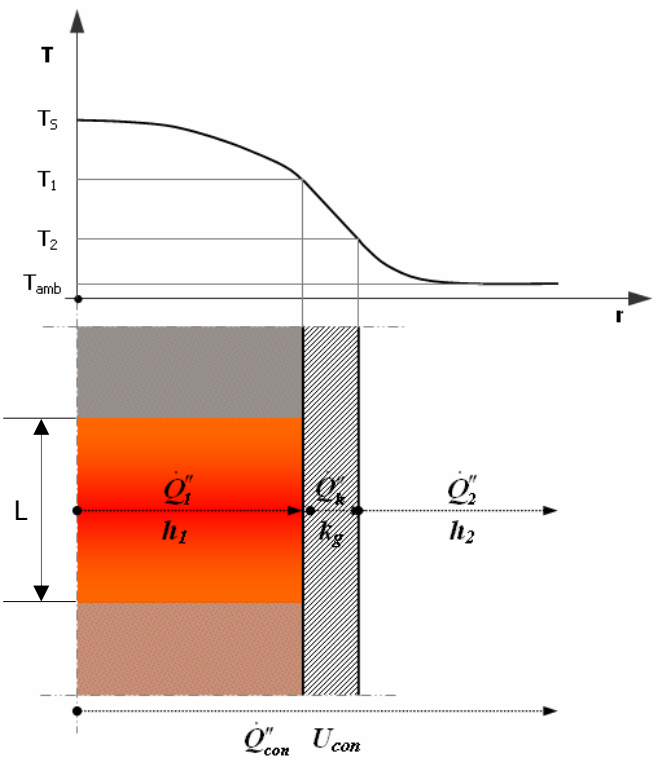

Figure 5.24 Schematic representation of the radial temperature profile and radial heat losses due to convection and conduction. In steady-state conditions the heat fluxes in the porous medium ($\dot{Q}_1''$) in the glass wall ($\dot{Q}_k''$) and in the ambient air ($\dot{Q}_2''$) are equal to each other and to the heat flux $\dot{Q}_{con}''$.

An expression for h_2 valid for natural convection between a vertical wall and a quiescent medium can be found in the literature (Incropera and Dewitt, 2002); the average temperature $\overline{T}_2$ has been obtained experimentally in a test conducted on coal tar in base-case conditions (Figure 5.25).

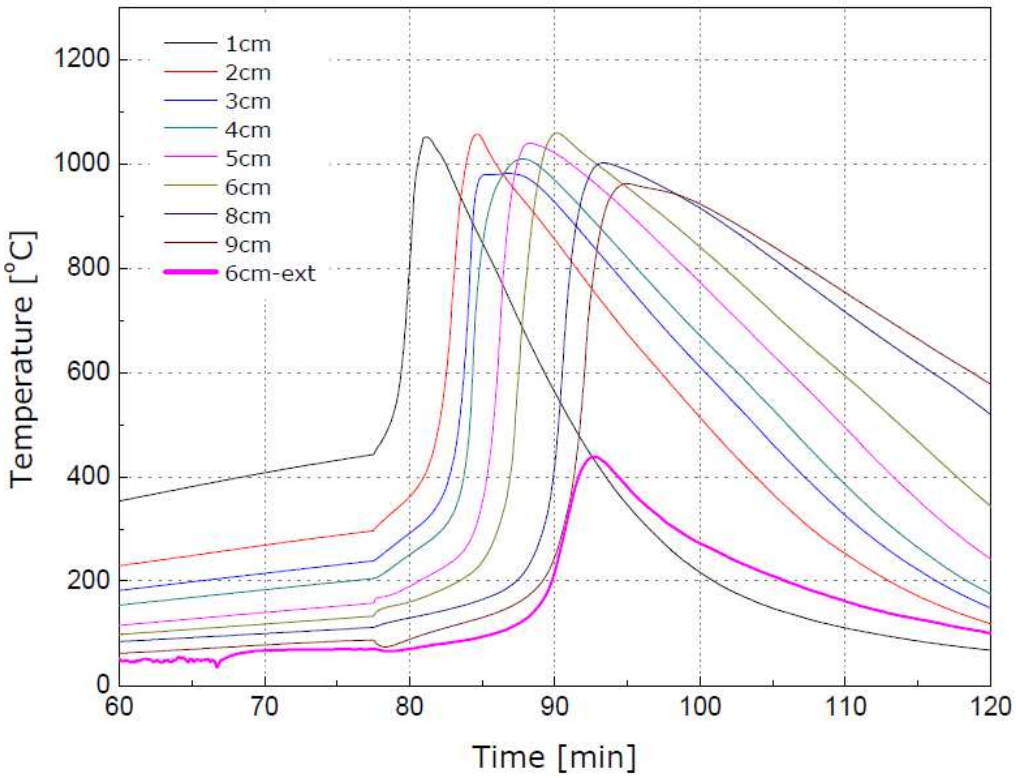

Figure 5.25 Temperature histories for coal tar in coarse sand at 25% saturation and 9.15 cm/s air flux; the thermocouple labelled "6cm-ext" measured the temperature of the external wall of the column at 6 cm from the location of the igniter.

Using the data in Table 5.6 the value obtained for U_{con} is 2.44 W/m^2/K.

Table 5.6 Data used to calculate the Heat Transfer Coefficient U_{con} from Equation (24)

Quantity	Value	Unit
$\overline{\overline{T}}_S$	799	^oC
$\overline{\overline{T}}_2$	231	^oC
T_{amb}	20	^oC
h_2	9.05	W/m^2/K

The radiation heat transfer coefficient U_{rad} is given by

$$U_{rad} = \sigma \varepsilon K \cdot \frac{\overline{\overline{T}}_S^{\,4} - T_{amb}^4}{\overline{\overline{T}}_S - T_{amb}} \qquad (25)$$

where σ is the Stefan-Boltzmann constant, ε is the emissivity of the porous medium and K is the fraction of the emitted energy that is radiated to the external environment. A value of K equal to 0.2 has been assumed for the present analysis.

5.4.2 Comparison with experimental results

The experimental data described in this Chapter and in Section 4.3.1 of Chapter 4 (influence of NAPL saturation) are compared to the theoretical smouldering velocity calculated with the mass balance (19) and energy balance (23) expressions. The values of the stoichiometric coefficient ν_O and the specific energy $\Delta H_r/\nu_O$ used in the calculation are those corresponding to the complete oxidation of coal tar and crude oil. In this way, the theoretical smouldering velocity obtained from Equation (19) is the minimum possible velocity for a reaction that propagates steadily while consuming all the fuel. In Equation (23), the temperature T_S represents the average smouldering temperature in the reaction front and is taken as the time average of the measured temperature over the duration of the reaction. Since this is not exactly known, a temperature cut-off (equal to 500 ^oC for coal tar and 400 ^oC for crude oil) has bee used to identify the beginning and the end of the reaction at each thermocouple location. The values of the heat of combustion were determined by bomb calorimetry tests conducted on the two fuels (see Table 5.4); also, the value of the volumetric heat capacity of the contaminated material is assumed to be constant and equal to that of sand alone since the heat capacity of the fuel is negligible compared to that of the sand ($C_{v,e} \cong C_{v,i}$). Table 5.7 summarises the values of the fuel and oxidizer properties used for the calculations.

Table 5.7 Property values used to apply Equations (19) and (23)

Property	Value	Unit
ν_O (coal tar)	2.89	kg_{O2}/kg_{fuel}
ν_O (crude oil)	3.21	kg_{O2}/kg_{fuel}
ΔH_r (coal tar)	$39.4 \cdot 10^6$	J/ kg_{fuel}
ΔH_r (crude oil)	$42.0 \cdot 10^6$	J/ kg_{fuel}
$Y_{O,i}$	0.235	kg_{O2}/kg_g
$C_{v,e} \cong C_{v,i}$	$2.15 \cdot 10^6$	$J/m^3/K$
c_{pg}	$1.1 \cdot 10^3$	J/kg/K

The dependent variable plotted in Figure 5.26 gives the ratio $U_S/U_{S,th}$ between the experimental and theoretical smouldering velocity calculated by the mass balance expression (Equation (19)). The graph on the left in Figure 5.26 provides this ratio versus air flux, while the graph on the right provides it versus NAPL saturation. Values significantly lower than unity indicate that not all the injected oxygen is consumed; values higher than unity may indicate incomplete fuel consumption and/or incomplete fuel oxidation (recall that Equation (19) is based on the assumptions of both complete fuel and oxygen consumption).

As Figure 5.26 shows, the ratio $U_S/U_{S,th}$ for coal tar is higher than unity in the range 4.05-9.15 cm/s inlet air flux. Since it is experimentally observed that all the fuel is consumed in the reaction, values of $U_S/U_{S,th}$ higher than unity indicate that oxidation of the fuel at these air fluxes is incomplete. This is consistent with the chemical analyses of the emissions presented in Section 5.3.2, revealing the presence in the exit gases of volatile hydrocarbons in significant amount. At higher air fluxes the values of $U_S/U_{S,th}$ are close to unity for coarse sand and lower than unity for medium sand. Since it is plausible that the reaction remains incomplete at these air fluxes,

actual values of $U_S/U_{S,th}$ would be lower than unity in this air flux range (recall that $U_{S,th}$ is minimum when calculated using the stoichiometry of complete oxidation). This suggests that as the air flux increases the reaction approaches a kinetically-controlled regime, in which it does not consume all the available oxygen but rather is limited by the intrinsic chemical reaction rate.

For crude oil, modelled propagation velocities are significantly higher than the measured ones ($U_S/U_{S,th}$ in Figure 5.26 significantly lower than unity) for all but the lowest air flux. This indicates that in the range 9.15-25.2 cm/s the smouldering reaction of crude oil does not consume all the injected oxygen (i.e. it is kinetically-controlled), while at 4.05 cm/s may be either oxygen-controlled or kinetically-controlled depending on the actual stoichiometry at this air flux.

Similar remarks hold true for the experiments at varying saturation. At low fuel saturation (less than 25% for coal tar and 35% for crude oil) the intensity of the reaction is not sufficient to consume all the available oxygen, hence propagation velocity are lower than stoichiometric ($U_S/U_{S,th}$ lower than unity). As saturation increases the fraction of the injected oxygen that is consumed also increases and the velocity becomes closer to the stoichiometric value. Velocities higher than stoichiometric at the highest saturations indicate incomplete fuel oxidation; whether the regime of propagation is oxygen-controlled or kinetically-controlled in this range again depends on the actual stoichiometry at these saturations.

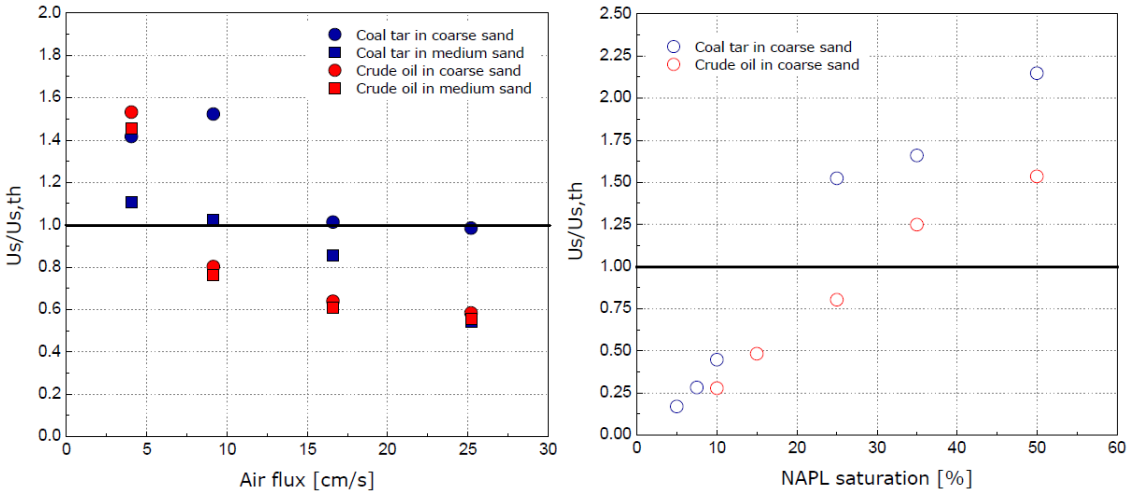

Figure 5.26 Ratio between experimental and theoretical smouldering velocity calculated by Equation (19) for different air fluxes (left) and different NAPL saturations.

Figure 5.25 represents the comparison between measured and modelled smouldering velocities, this time using the energy balance expression (Equation (23)). It is apparent that the modelled theoretical velocity is always significantly higher than the measured one. To improve the agreement between model and experiments it is necessary either to assume that not all the oxygen is consumed in the reaction (this amounts to reducing $Y_{O,i}$ in Equation (23)) or to reduce the value of the specific energy $\Delta H_r/\nu_O$ (the energy released per unit mass of oxygen consumed). The former assumption is consistent with the results of the previous paragraph, at least for a group of experiments (i.e. when the ratio $U_S/U_{S,th}$ is lower than unity). For the remaining experiments, the previous analysis suggests that a greater proportion of the injected oxygen is consumed (the ratio $U_S/U_{S,th}$ is higher than unity); thus to account for the difference between model and experiments it is necessary to assume a substantially lower value for the specific energy release. However, the stoichiometric analysis conducted in Section 5.3.2 shows that $\Delta H_r/\nu_O$ has only a weak dependence on the degree of oxidation (both ΔH_r and ν_O decrease with the degree of oxidation)

and the reduction in $\Delta H_r/\nu_O$ due to incomplete oxidation of the fuel is not sufficient to explain the discrepancy. A combination of the two effects (incomplete oxygen consumption and incomplete fuel oxidation) should therefore be considered to account for the lack of agreement in these experiments. These results may also be an indication of unsteadiness of the reaction front. Equations (19) and (23) are based on the assumption of a steady combustion front, which implies that the rate at which the front move forwards further in the fresh fuel is the same of the rate at which the fuel at the trailing edge of the front is consumed, leaving some oxygen to penetrate further (Ohlemiller and Lucca, 1983). This is no longer valid if the front is unsteady. If the thickness of the front decreases, not all the oxygen made available by the extinction of the reaction at the trailing edge will reach the leading edge of the front, because it is partially consumed to react the fuel within the front. This will result in the reduction of the observed velocity of the smouldering wave.

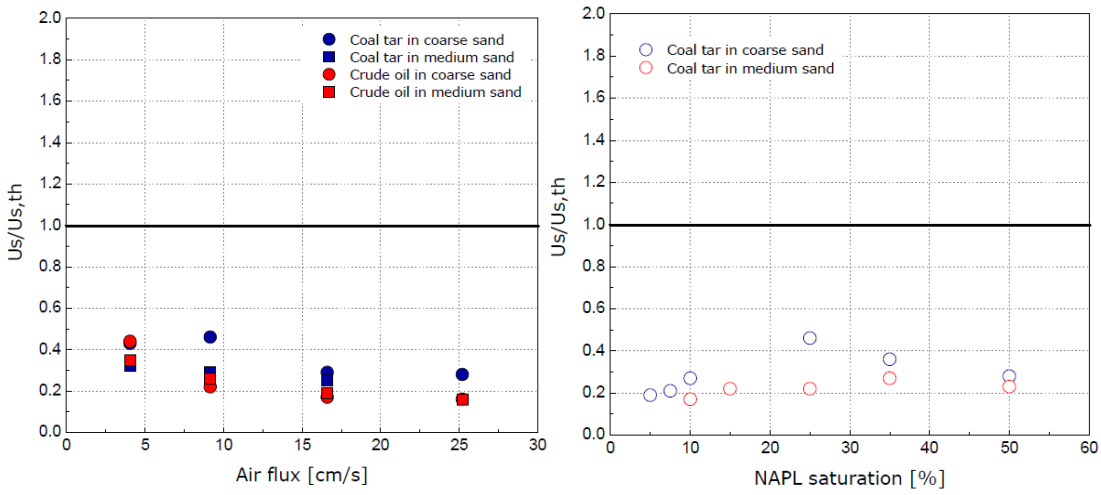

Figure 5.27 Ratio between experimental and theoretical smouldering velocity calculated by Equation (23) for different air fluxes (left) and different NAPL saturations.

Another way to analyse the results is to combine the measured and modelled variables into nondimensional groups and look for possible relationships between

these new variables. Figure 5.28 presents the result of this analysis applied to the experiments conducted at constant NAPL saturation. The variable plotted on the horizontal axis is a nondimensional velocity obtained from the measured smouldering velocity (U_S), the velocity predicted by the mass balance expression (19) (indicated as $U_{S,1}$ in the graphs) and the inlet air flux (indicated as U_g). On the vertical axis in Figure 5.28(a) is the ratio between the measured smouldering velocity and the velocity predicted by the energy balance expression (Equation (23)). The dependent variable in Figure 5.28(b) is a nondimensional temperature obtained by combining the measured average temperature in the smouldering front (ΔT_S) and a theoretical adiabatic smouldering temperature ($\Delta T_{S,ab}$). This latter is defined as the temperature at which the theoretical smouldering velocity predicted by the adiabatic energy balance expression (21) coincides with the mass balance expression (19). As Figure 5.28 shows, in terms of the new variables the experimental data are well described by a linear (Figure 5.28(a)) and a constant trend (Figure 5.28(b)). Furthermore, the correlating function is approximately the same regardless of the type of NAPL (coal tar or crude oil) and the porous medium (coarse or medium sand) used in the experiment. This result is important because it may allow to estimate the smouldering temperature and velocity for a given NAPL saturation and air flux once the enthalpy of reaction (ΔH_r) and the oxygen requirement (ν_O) for complete combustion are known. From the input data, the mass balance velocity $U_{S,1}$ (Equation (19)) and the theoretical adiabatic smouldering temperature $\Delta T_{S,ab}$ can be calculated; then, assuming that the nondimensional temperature in Figure 5.28(b) is constant, the estimate smouldering temperature can be obtained. This allows to compute the theoretical smouldering velocity $U_{S,2}$ from the energy balance

expression (Equation (23)) and then to estimate the smouldering velocity from the relationship in Figure 5.28(a). It is however to note that the linear relationship in Figure 5.28(a) seems to break outside the interval (-0.004; 0.004); therefore the estimated velocity is not to consider reliable if the corresponding nondimensional velocity lies outside this interval.

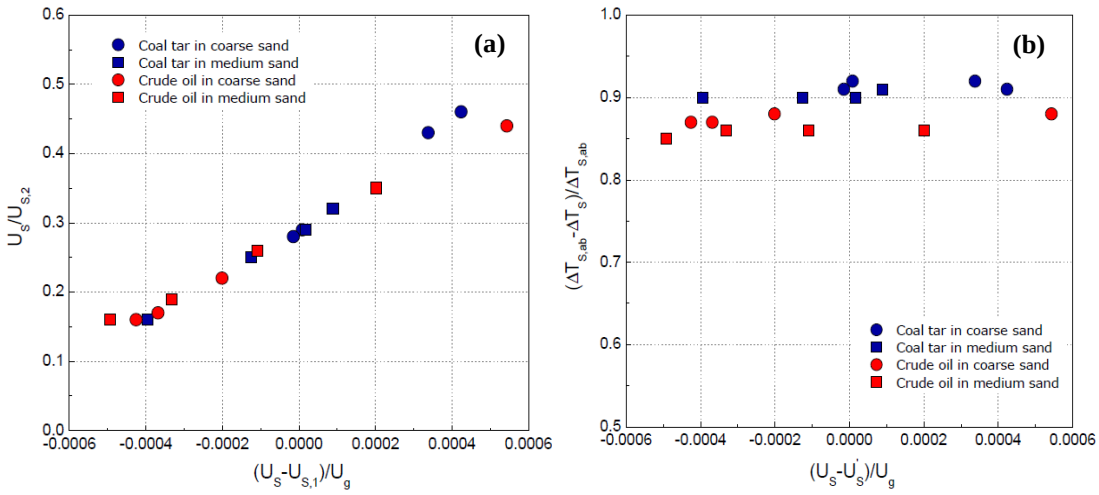

Figure 5.28 Relationship between nondimensional variables for the experiments conducted at constant NAPL saturation and variable air flux.

5.5 Summary and conclusions

An experimental study has been conducted on the dependence of the NAPL smouldering process on the inlet air flow rate and porous media grain size for coal tar and crude oil. This study extends the experimental work presented in Chapter 4 and provides additional data, including chemical composition of the gaseous emissions, necessary to conduct a theoretical analysis of the experimental results.

Tests conducted at varying input air flux indicated that propagation velocity and burning temperature always increase with the air flow rate. This suggests that, for the

experimental conditions examined, the increase of the reaction rate resulting from the increased oxygen supply prevails on the cooling effect due to enhanced convective heat transfer. Varying the porous medium from coarse to medium sand did not result in a significant variation of peak temperatures and propagation velocities for both the contaminants examined.

The experimental results have been compared to simplified analytical models based on global mass and energy balances across the reaction front. Chemical analysis of the gaseous emissions helped to interpret the observed discrepancies between measured and modelled results. Comparison with the ‘mass balance’ expression suggests that smouldering propagation transitions from oxygen-controlled to kinetically-controlled as air flux increases and NAPL saturation decreases. The exact location in the parameter space where the transition occurs depends on the actual stoichiometry of the reaction. In general, this is expected to shift towards lower air fluxes and higher saturations as the stoichiometry changes to less complete oxidation. The fit with the ‘energy balance’ expression is poor across the whole range of parameters examined, which suggests that the assumptions embedded in the model are inadequate to describe the entire range of complex, interacting processes affecting the reaction. However, when combined with the measured results into conveniently defined nondimensional variables, the modelled results are shown to correlate well the experimental data across the whole suite of experiments conducted at constant saturation.

5.6 References

Aldushin, A.P., I.E. Rumanov, B.J. Matkowsky, Maximal energy accumulation in a superadiabatic filtration combustion wave, Combustion and Flame 118 (1999) 76-90.

Bar-Ilan, A. et al., The effect of buoyancy on opposed smoldering, Combustion Science and Technology (2004) 176 2027-2055.

Dosanjh, S.S., P.J. Pagni, A.C. Fernandez-Pello, Forced cocurrent smoldering combustion, Combustion and Flame (1987) 68 131-142.

DiNenno, P.J. (Ed.), The SFPE Handbook of Fire Protection Engineering (4th ed.), NFPA, Quincy, MA, 2008.

Incropera, F.P. and D.P. Dewitt, Fundamentals of heat and mass transfer (5th ed.), J. Wiley & Sons, N.Y., 2002.

Glassman, I. and R.A. Yetter, Combustion (4th ed.), Academic Press, 2008.

Ohlemiller, T.J. and D.A. Lucca, An experimental comparison of forward and reverse smolder propagation in permeable fuel beds, Combustion and Flame (1983) 54 131-147.

Rein, G., Smouldering combustion phenomena in science and technology, International Review of Chemical Engineering (2009) 1 (1) 3-18.

Schult, A., B.J. Matkowsky, V.A. Volpert, A.C. Fernandez-Pello, Forced forward smolder combustion, Combustion and Flame (1995) 101 471-490.

Torero, J.L., A.C. Fernandez-Pello, Forward smolder of polyurethane foam in a forced air flow, Combustion and Flame (1996) 106 (1-2) 89-109.

Wahle, C.W., B.J. Matkowsky, A.P. Aldushin, Effects of gas-solid nonequilibrium in filtration combustion, Combustion Science and Techology (2003) 175 1389-1499.

Chapter 6

Conclusions

This research has been carried out to investigate a novel concept: the potential of smouldering combustion as a remediation approach for soils contaminated by non-aqueous phase liquids (NAPLs). An experimental program was designed and executed to achieve two main objectives: (i) evaluate the concept in principle and (ii) characterise the process under a range of natural (e.g., contaminant, soil, concentration) and engineering (e.g., oxidizer flow rate) conditions.

To meet the first objective, more than 25 proof-of-concept experiments were conducted involving the controlled ignition of a variety of NAPLs in a small-scale (~ 15 cm) apparatus. Temperature measurements and digital images were employed in these experiments to identify the onset of the reaction and track the progression of the combustion front. Results demonstrated that liquid contaminants embedded in an inert porous medium can be successfully smouldered and this process results in a significant reduction of the original contamination. Further, they suggested that NAPL smouldering may be viable across a variety of conditions relevant to engineering applications (e.g., soil types, NAPL types, heterogeneities, presence of water).

This hypothesis was evaluated in a more systematic manner in the second phase of the experimental program, which examined the sensitivity of the process to a series

of fluid-media system variables and engineering control parameters. This investigation was carried out through more than 30 intermediate-scale (~ 30 cm) column experiments. Results confirmed the broad range of process parameters, including contaminant type, contaminant mass, water content, soil type and oxidizer flow rates, within which the process is self-sustaining. Moreover, when the process is self-sustaining then the degree of remediation achieved for crude oil and coal tar was demonstrated to be essentially complete. They further demonstrated that the intensity and velocity of the process can be controlled by the rate at which oxidizer is delivered. Contaminant type and mass was observed to affect peak temperatures and propagation velocity by influencing the energy and oxidizer balance at the reaction front; soil grain size was observed to affect them by influencing the thermal properties of the porous medium while water content was observed to influence the time to ignition and the peak temperature by acting as an energy sink.

A simplified theoretical analysis was employed to assist in explaining some of the observed characteristics of the smouldering process. Based on mass and energy conservation across the reaction front, two analytical expressions were obtained relating peak temperature and propagation velocity to parameters characteristic of the reaction such as specific oxygen consumption and specific energy release. Comparison of experimental data with the ‘mass balance’ expression suggests that smouldering propagation transitions from an oxygen-controlled process to a kinetically-controlled process as air flux increases and as NAPL saturation decreases. The exact location in the parameter space where the transition occurs depends on the actual stoichiometry of the reaction. The ‘energy balance’ expression performed

poorly in predicting experimental results across the whole range of parameters examined, suggesting that the assumptions embedded in the model are inadequate to describe the entire range of complex, interacting processes affecting the reaction.

Overall, this research has contributed to the fields of (i) environmental engineering, by introducing an entirely new approach to the remediation of industrial sites contaminated by non-aqueous phase liquids and (ii) combustion engineering, by exploring a new technological application of the relatively unknown process of liquid smouldering. Laboratory experiments and a simplified theoretical analysis have provided the proof-of-concept and developed an understanding of the mechanisms that control the underlying process. Based in part upon this work, the concept of NAPL smouldering for remediation is patent-pending (UK Patent Application 0525193.9 and PCT Application PCT/GB2006/004591, priority date December 2005).

By the nature of starting research in a relatively new area, this work contains some considerable limitations and simplifying assumptions. For example, the experiments were designed to approach one-dimensional conditions (uniform air injection and uniform heating across the horizontal section of the apparatus); most of the experiments employed homogeneous porous media and homogeneous NAPL saturation; no water influx was allowed into the reaction zone from an external source; due to the reduced experimental scale, soil permeability did not limit the ability to inject air at the desired rate. Most real applications may not exhibit such ideal conditions and this could reduce the range of natural and operating conditions

in which the process is successful in the field. On the other hand, achieving self-sustaining smouldering is most challenging at the scale employed in this work, because heat losses can significantly reduce the amount of energy available for propagation. For this reason, the process may become more robust as the system is scaled-up towards field applications.

Many unresolved questions need therefore to be answered before this new approach can be implemented at full scale, and these should be explored with experiments of increasing dimension and complexity moving from the current scale to intermediate two-dimensional experiments and eventually pilot field trials.

Appendix A

Additional Data

A.1 Temperature histories for coal tar in coarse sand at varying concentrations

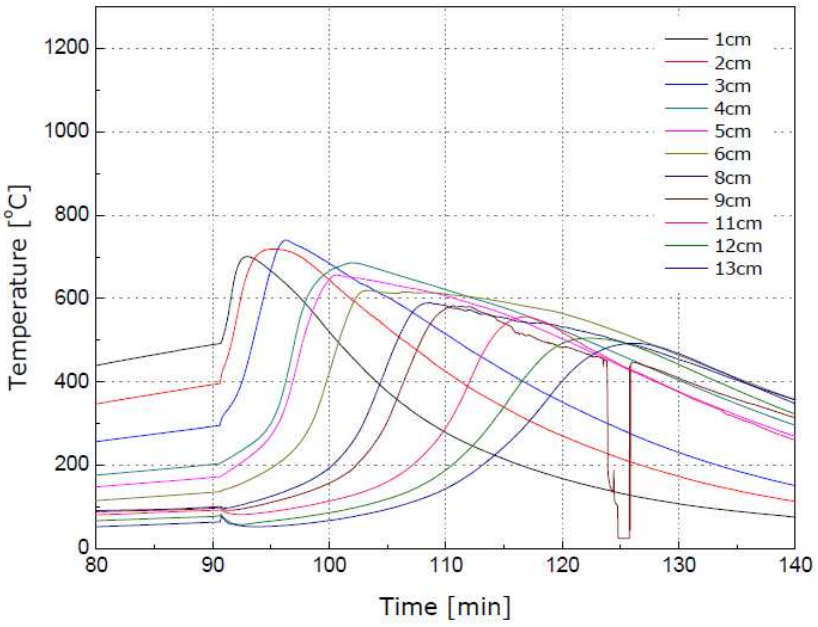

Figure A.1 Temperature histories for coal tar in coarse sand at 21,300 mg/kg.

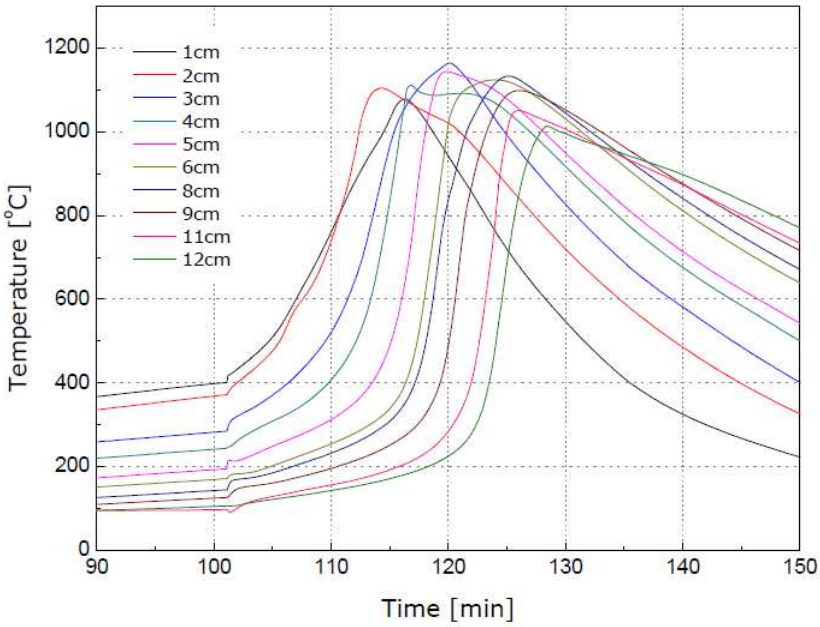

Figure A.2 Temperature histories for coal tar in coarse sand at 99,400 mg/kg.

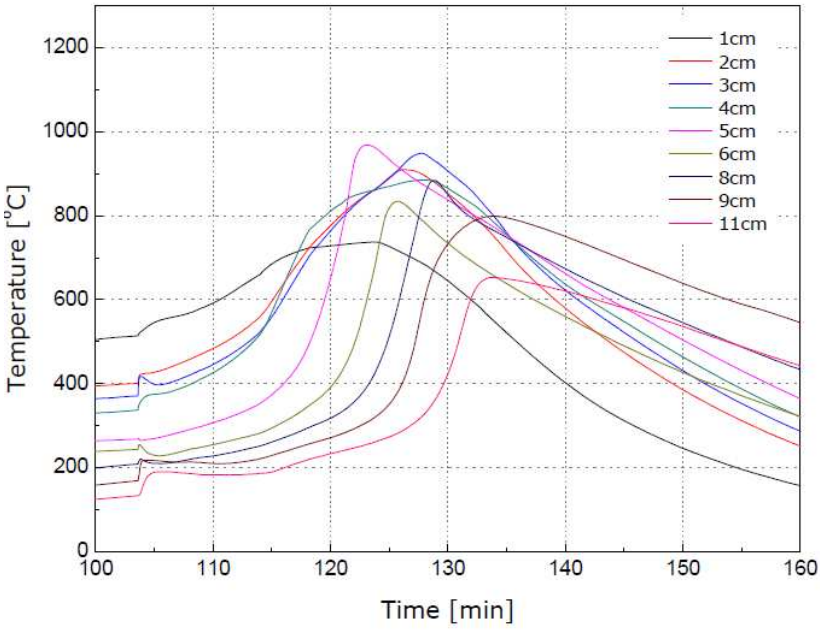

Figure A.3 Temperature histories for coal tar in coarse sand at 142,000 mg/kg.

A.2 Temperature histories for crude oil in coarse sand at varying concentrations

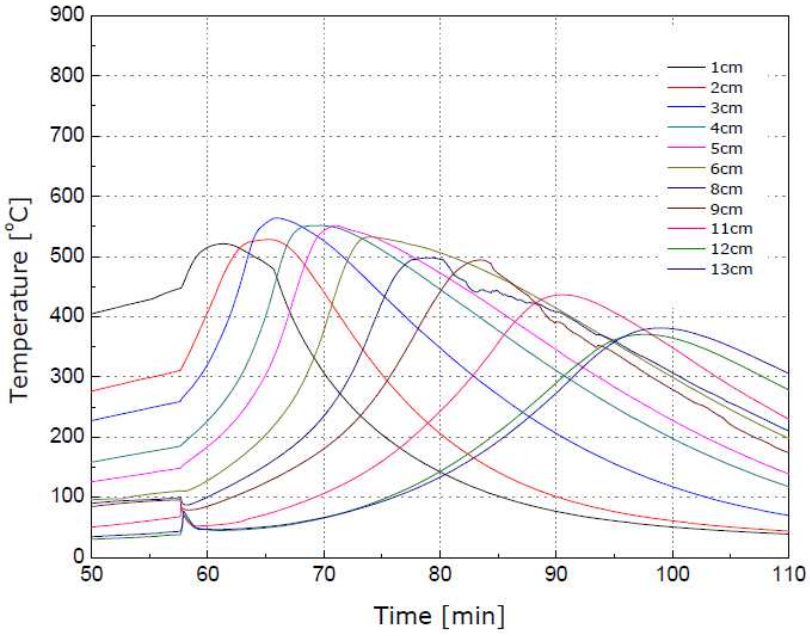

Figure A.4 Temperature histories for crude oil in coarse sand at 20,800 mg/kg.

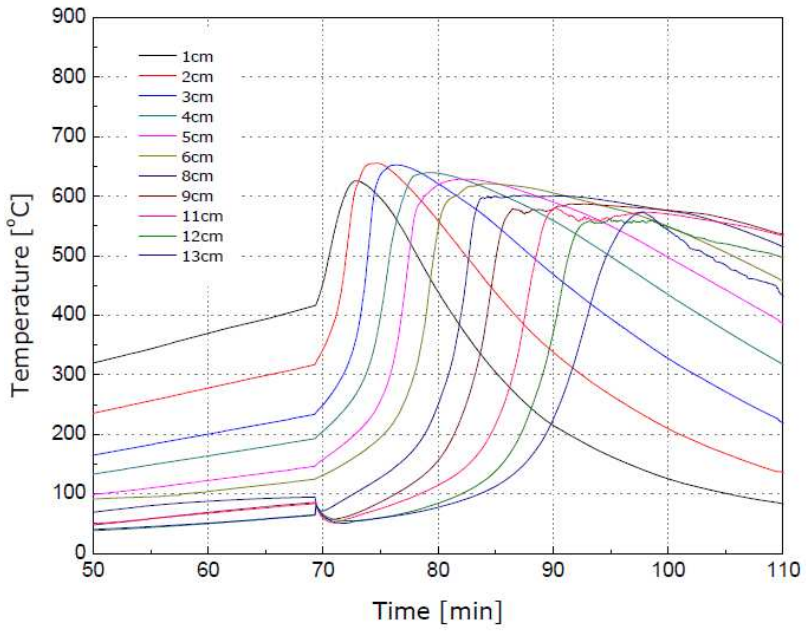

Figure A.5 Temperature histories for crude oil in coarse sand at 31,200 mg/kg.

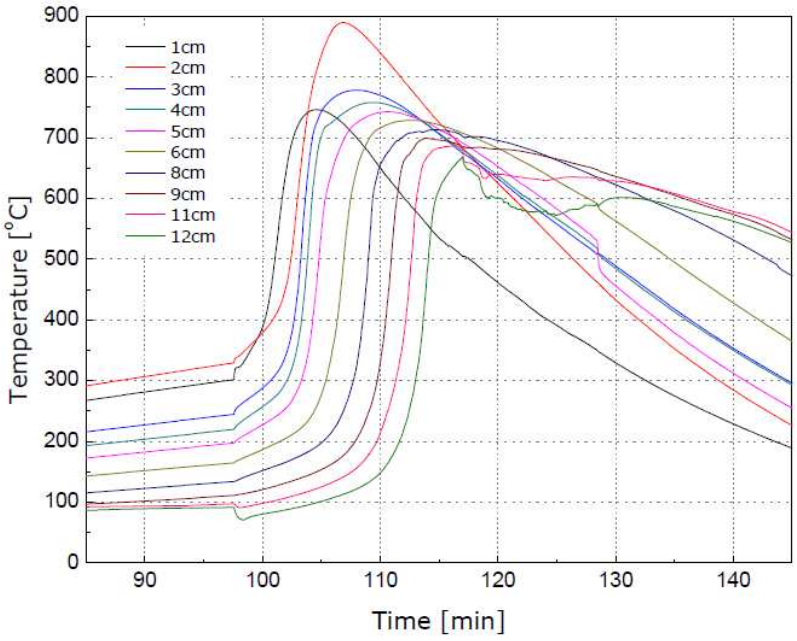

Figure A.6 Temperature histories for crude oil in coarse sand at 72,800 mg/kg.

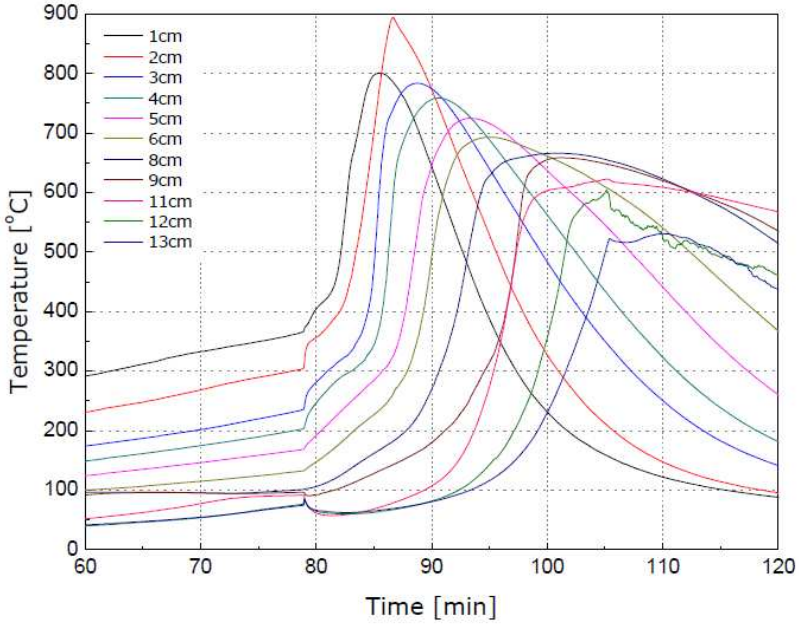

Figure A.7 Temperature histories for crude oil in coarse sand at 104,000 mg/kg.

A.3 Temperature histories for coal tar in coarse sand at varying initial water content

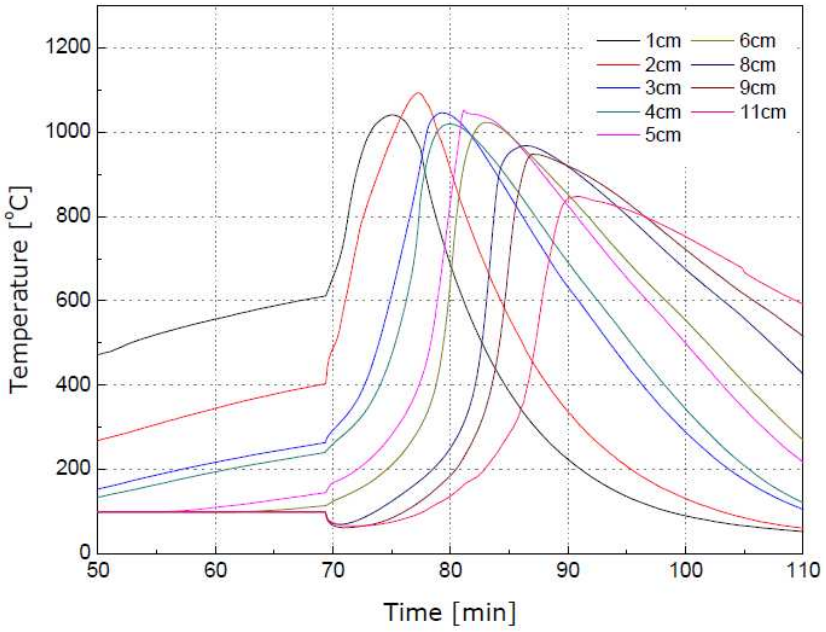

Figure A.8 Temperature histories for coal tar in coarse sand at 71,000 mg/kg and initial 25% water saturation.

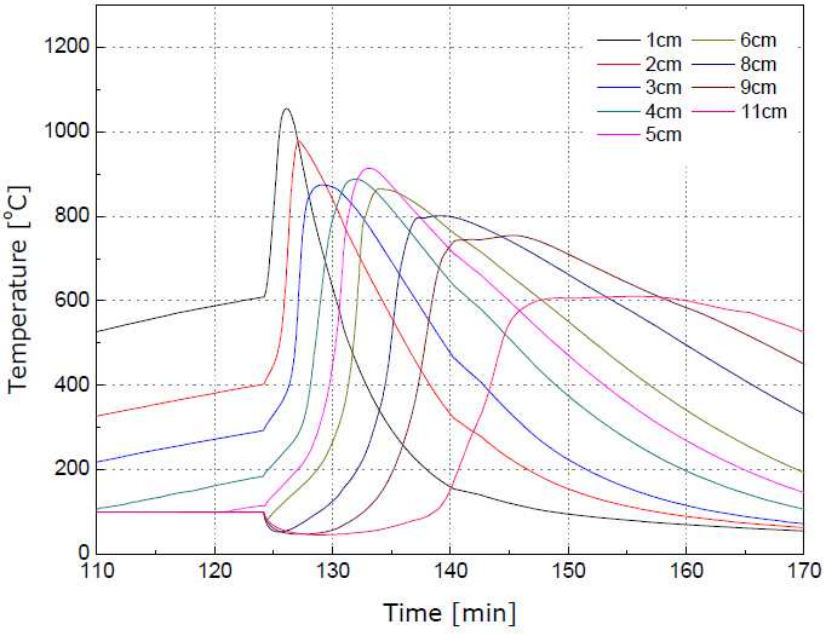

Figure A.9 Temperature histories for coal tar in coarse sand at 71,000 mg/kg and initial 75% water saturation.

A.4 Temperature histories for coal tar in different porous media

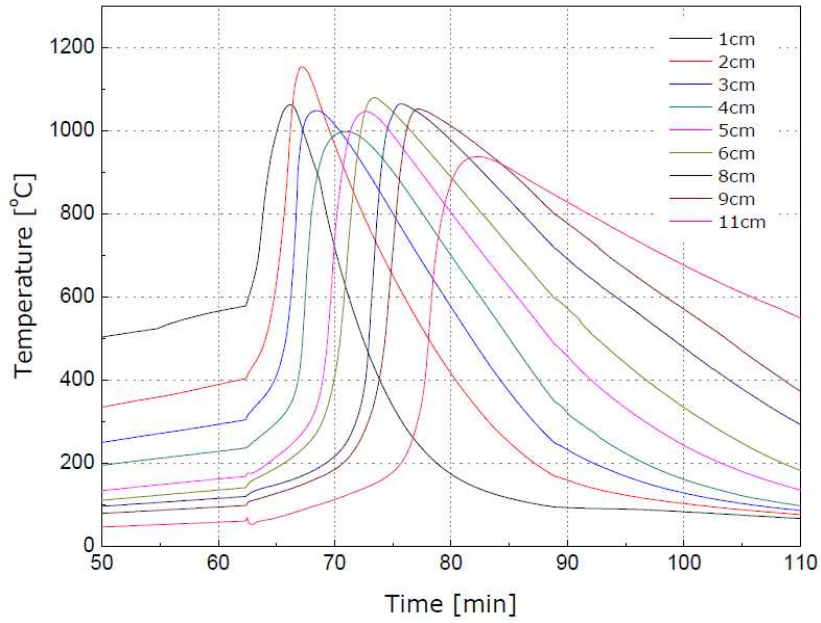

Figure A.10 Temperature histories for coal tar in coarse sand at 71,000 mg/kg.

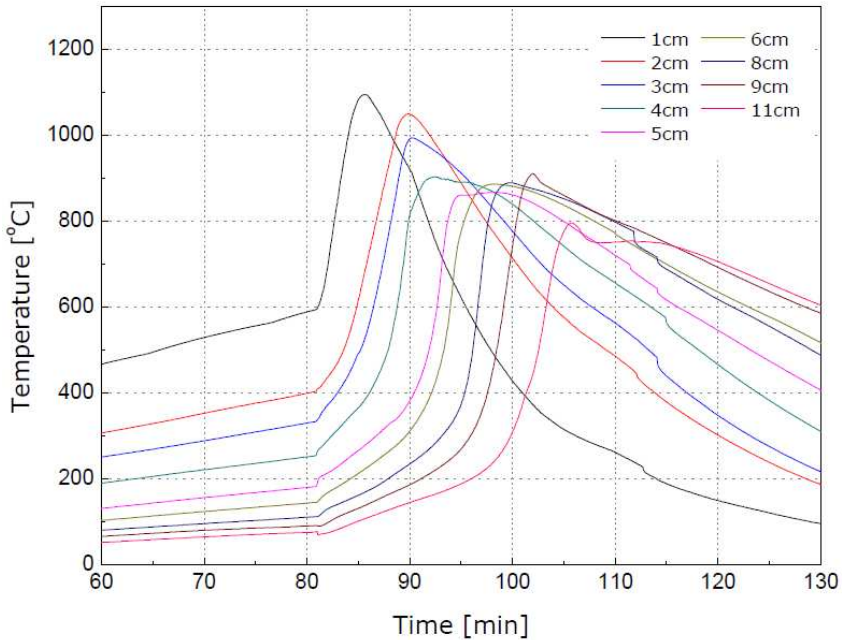

Figure A.11 Temperature histories for coal tar in medium sand at 67,000 mg/kg.

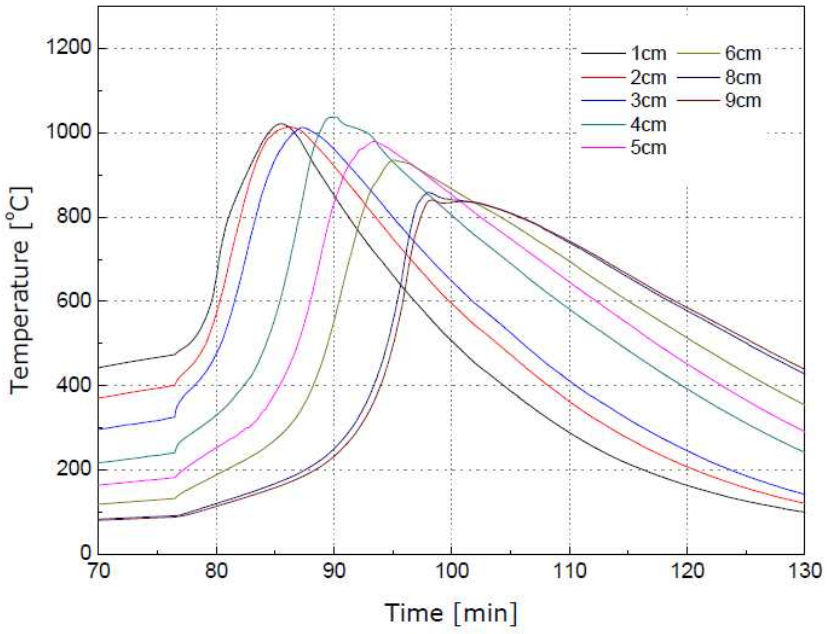

Figure A.12 Temperature histories for coal tar in 6 mm gravel at 90,000 mg/kg.

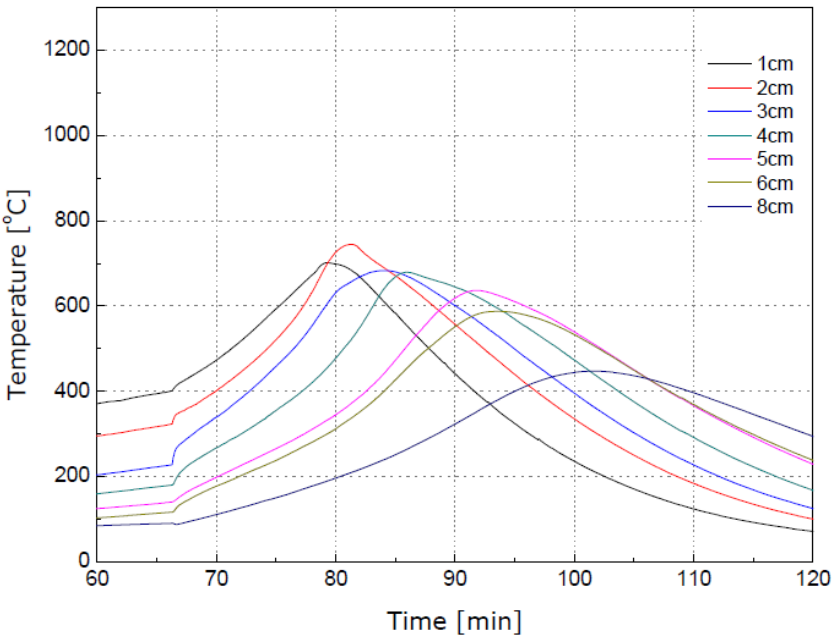

Figure A.13 Temperature histories for coal tar in 10 mm gravel at 94,000 mg/kg.

A.5 Temperature histories for coal tar and crude oil in coarse sand at low air flux

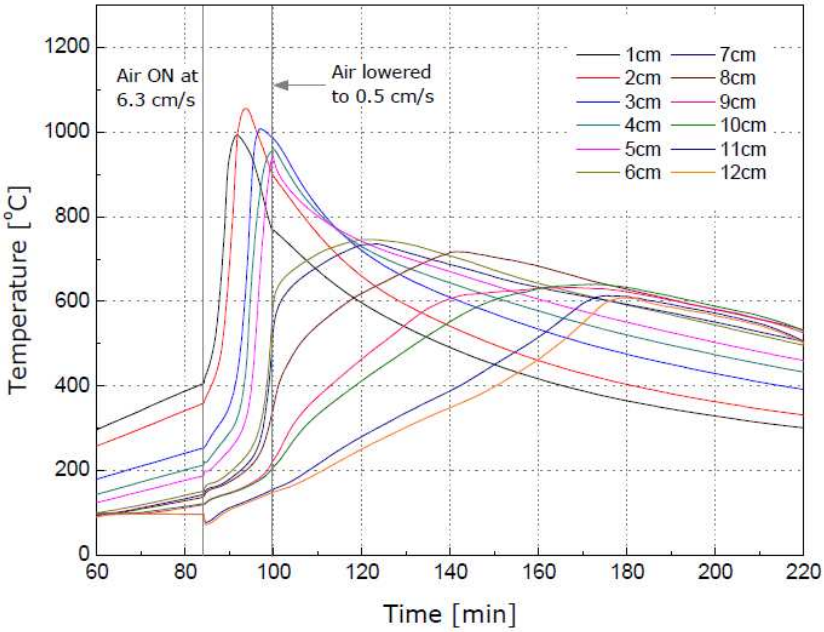

Figure A.14 Temperature histories for coal tar in coarse sand at 71,000 mg/kg and air flux lowered to 0.5 cm/s after ignition.

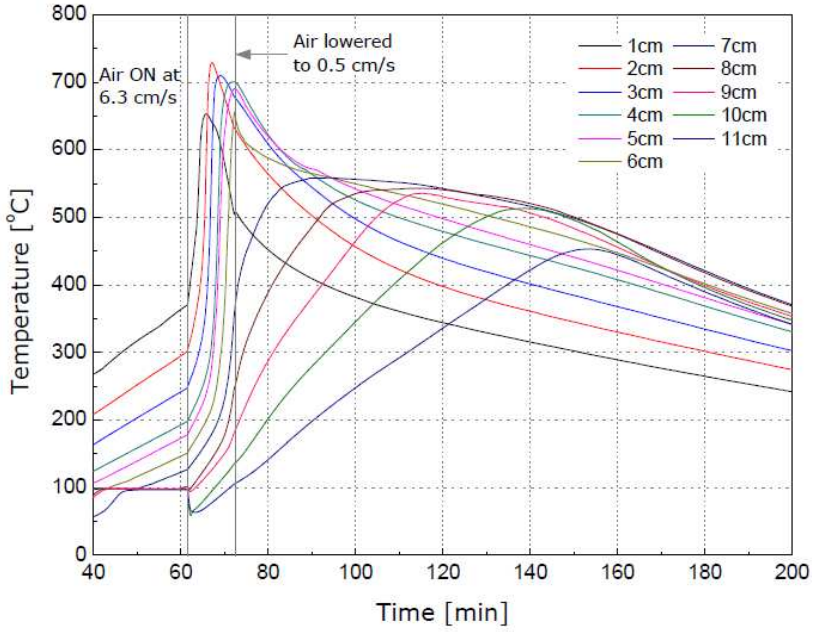

Figure A.15 Temperature histories for coal tar in crude oil at 67,000 mg/kg and air flux lowered to 0.5 cm/s after ignition.

A.6 Temperature histories for crude oil in medium sand at varying air flux

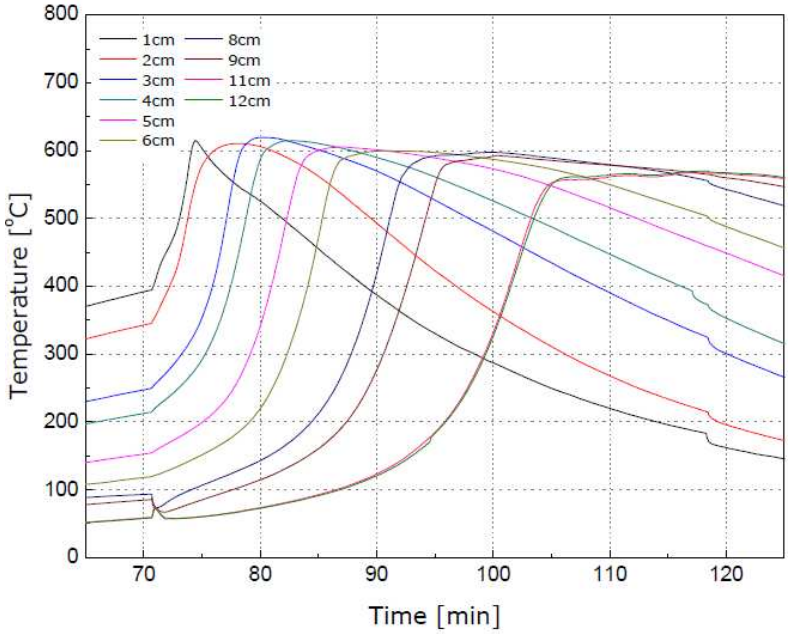

Figure A.16 Temperature histories for crude oil in medium sand at 67,000 mg/kg and 4.05 cm/s air flux.

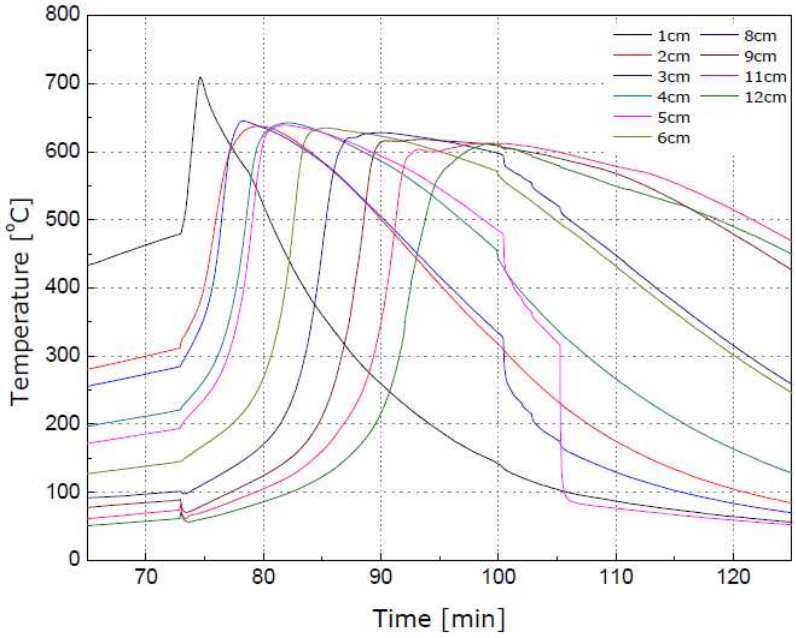

Figure A.17 Temperature histories for crude oil in medium sand at 67,000 mg/kg and 9.15 cm/s air flux.

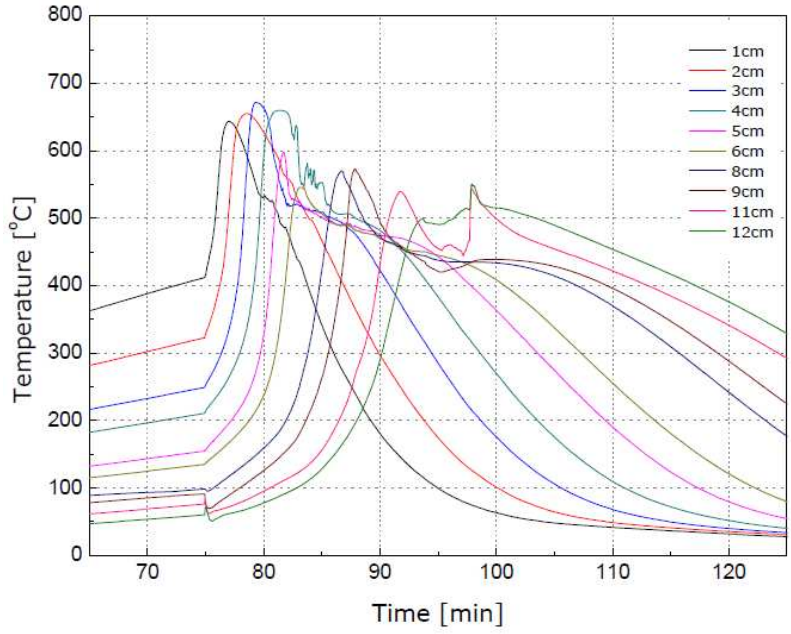

Figure A.18 Temperature histories for crude oil in medium sand at 67,000 mg/kg and 16.6 cm/s air flux.

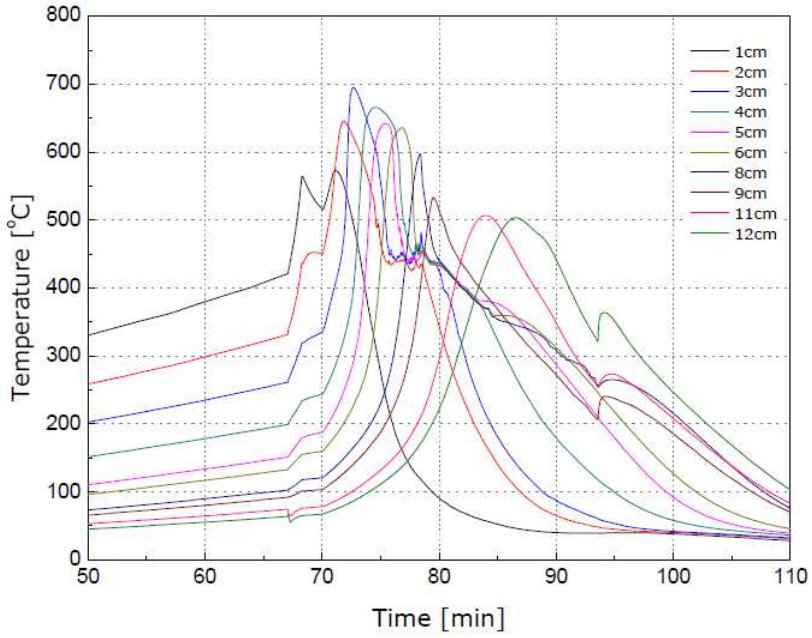

Figure A.19 Temperature histories for crude oil in medium sand at 67,000 mg/kg and 25.2 cm/s air flux.

A.7 Repeatability experiments for coal tar in coarse and in medium sand

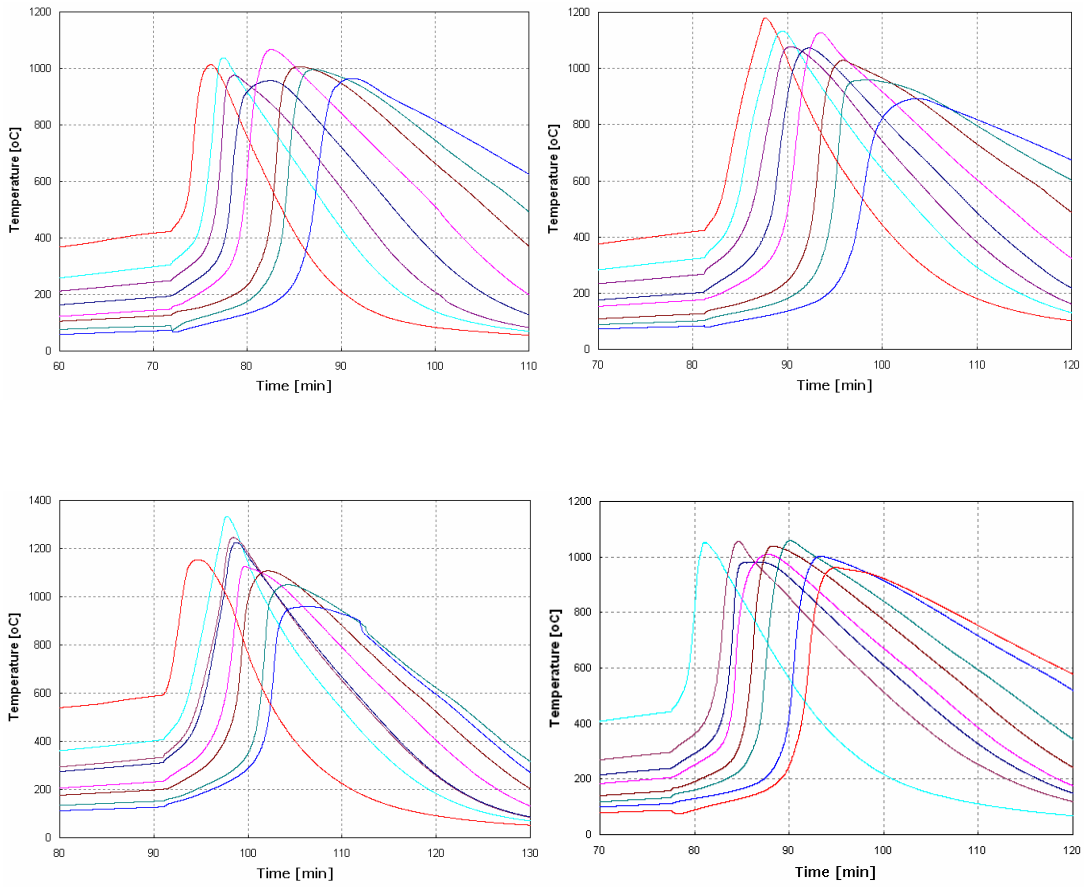

Figure A.20 Four repetitions of the base-case experiment on coal tar in coarse sand (Experiment 2 in Table 5.1).

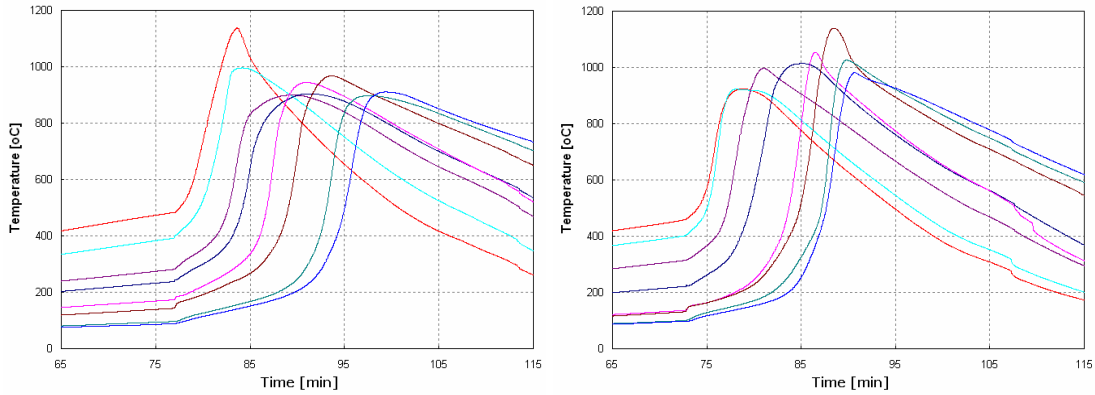

Figure A.21 Two repetitions of the experiment on coal tar in medium sand at 9.15 cm/s air flux (Experiment 6 in Table 4.1).

A.8 Experiments conducted using enriched air as inlet gas

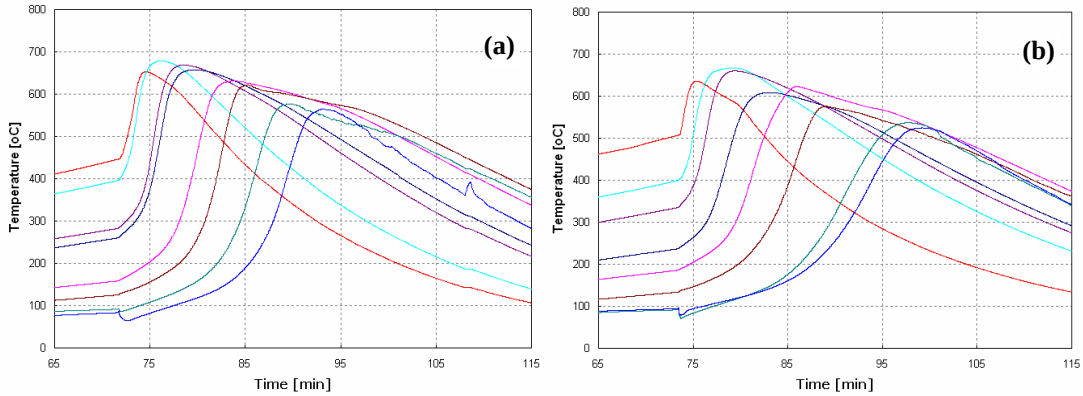

Figure A.22 Temperature histories for coal tar in coarse sand at 21300 mg/kg and 35% vol. oxygen in the inlet gas. (a) Same total inlet mass flow rate as in the base-case; (b) same total inlet oxygen flow rate as in the base-case.

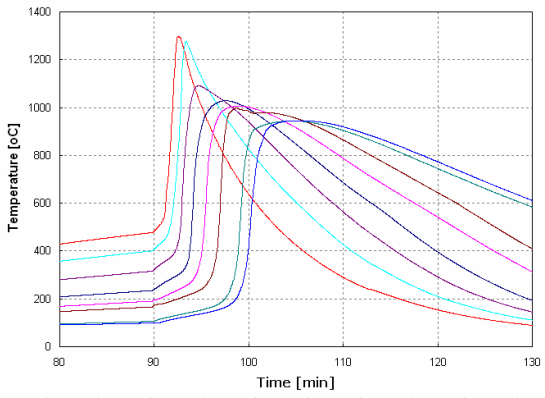

Figure A.23 Temperature histories for coal tar in coarse sand at 71000 mg/kg and 35% vol. oxygen in the inlet gas. Same total inlet mass flow rate as in the base-case.

A.9 Additional experiments at the small scale

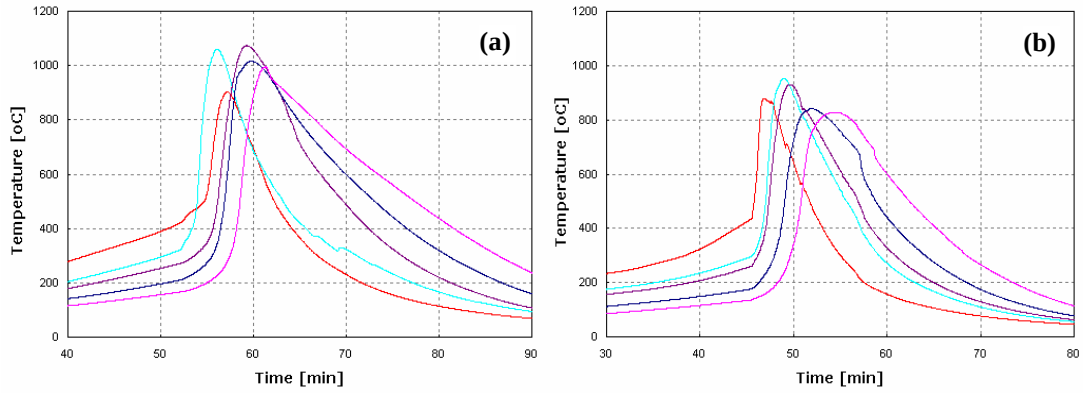

Figure A.24 Temperature histories for coal tar in coarse sand at 71000 mg/kg and (a) 4.75 cm/s air flux and (b) 7.94 cm/s air flux.

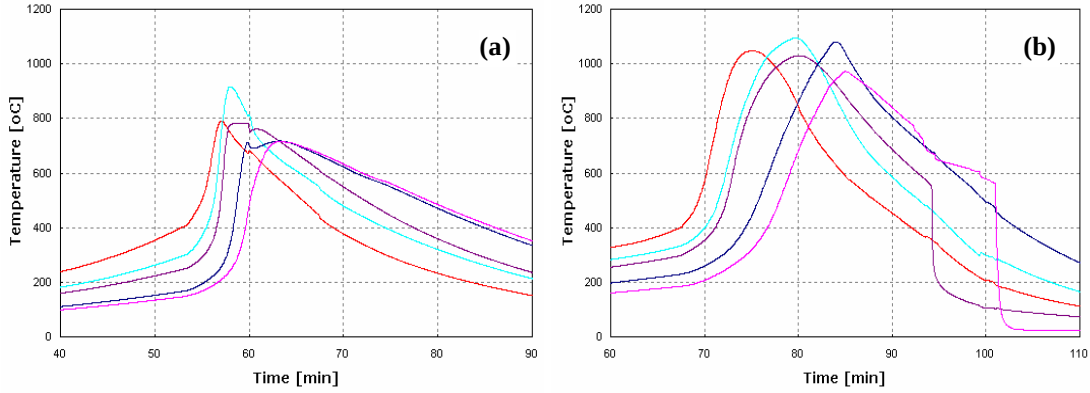

Figure A.25 Temperature histories for coal tar in coarse sand at 4.75 cm/s air flux and (a) 28400 mg/kg and (b) 142000 mg/kg NAPL concentration.

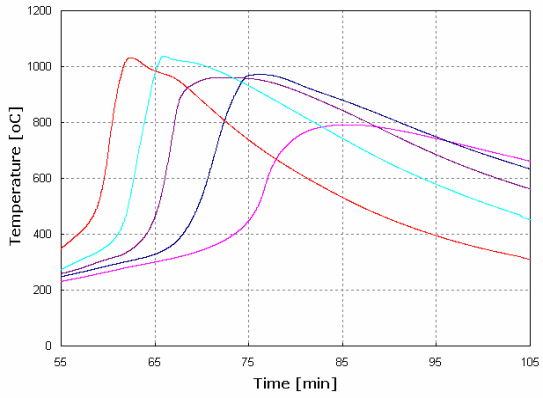

Figure A.26 Temperature histories for coal tar in coarse sand at 4.75 cm/s air flux and 284000 mg/kg NAPL concentration.

Appendix B

Uncertainty analysis

The uncertainties associated with the average peak temperature and smouldering velocity have been estimated as the 95% confidence intervals of the mean calculated from five repetitions of the base-case experiment on coal tar (Experiment 2 in Table 5.1). Figures B.1 and B.2 represent the distribution of the measured peak temperatures and propagation velocities along the axis of the sample for the five experiments. It is evident how temperature and velocity drop after ignition and termination of the igniter, then increase in the middle part of the sample and decrease again as the reaction approaches the end of the sample.

The uncertainty estimated from these data for the average temperature and velocity, taken as half of the width of the confidence interval, are $\delta T = 71^{o}\mathrm{C}$ and $\delta U_S = 0.09\,\mathrm{cm/min}$, which correspond to the fractional uncertainties $\delta T/T = 7\%$ and $\delta U_S/U_S = 13\%$

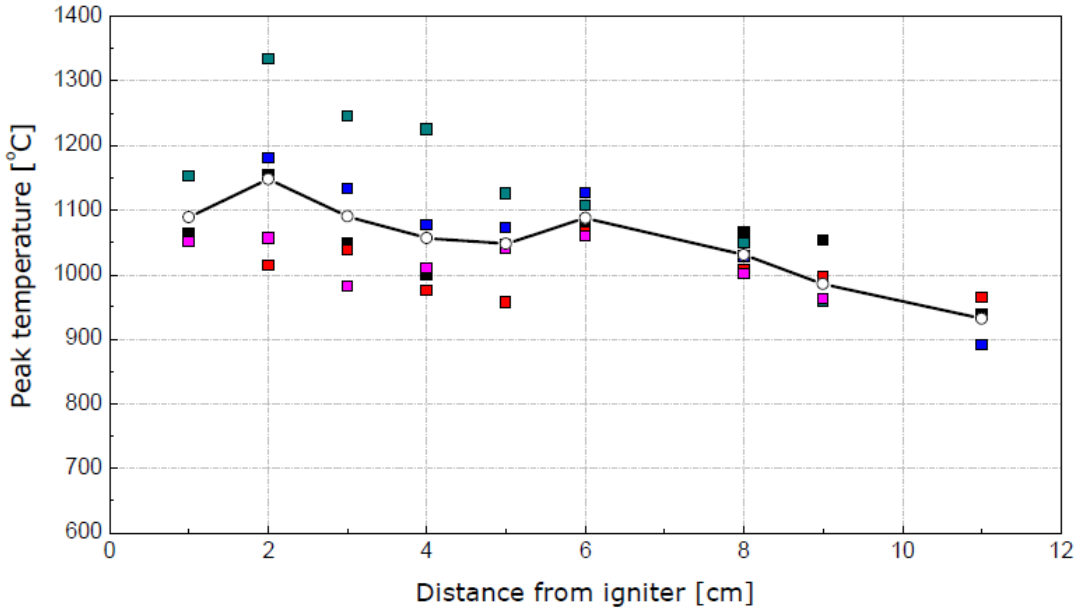

Figure B.1 Distribution of the peak temperature at various thermocouples locations for five repetitions of the base-case experiment in coal tar.

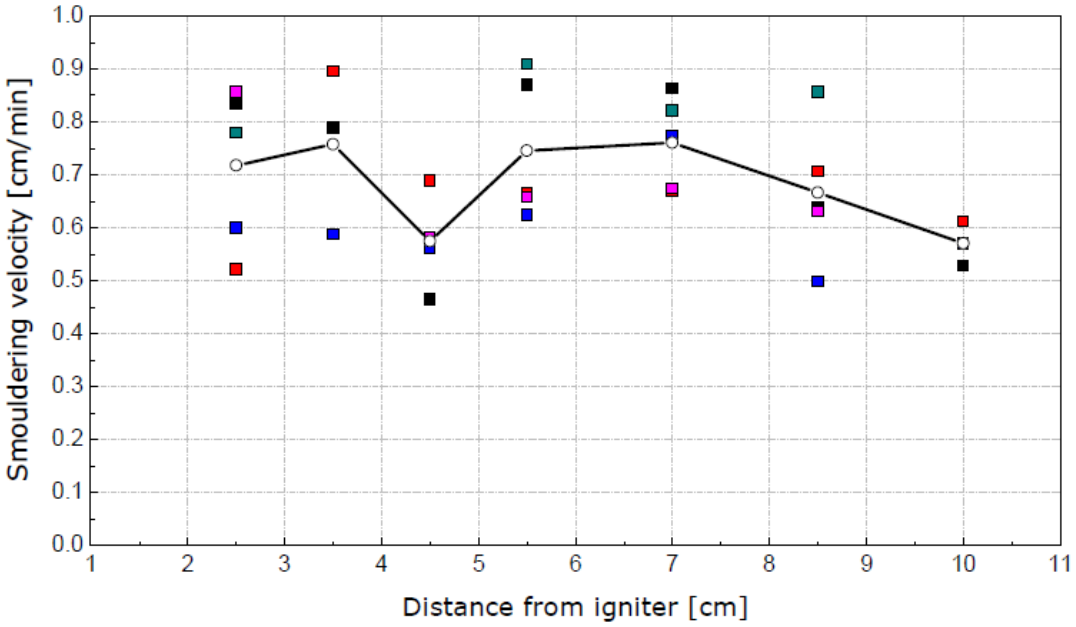

Figure B.2 Distribution of the propagation velocity at various thermocouples locations for five repetitions of the base-case experiment in coal tar.

Appendix C

NAPLs elemental analysis

The elemental composition of coal tar and crude oil has been determined by CHNS analysis using a Flash EA CHNS-O Analyzer (1112 Series, Thermo Scientific, US). The results are presented in Table C.1.

Table C.1 Results of the elemental analysis on coal tar and crude oil

Element	% Mass (coal tar)	% Mass (crude oil)
Carbon (C)	92	84.77
Hydrogen (H)	5.35	10.76
Nitrogen (N)	0.97	0.48
Sulphur (S)	0.39	2.62
Oxygen (O)	1.30	1.36

Appendix D

Fourier Transform Infrared (FTIR) gas analysis

D.1 General principles

FTIR is a technique for chemical analysis based on the principle of infrared spectroscopy. Infrared spectroscopy exploits the fact that most molecules have specific frequencies (vibrational modes) at which they can vibrate, determined by the type and strength of the chemical bonds and the masses of the atoms at either ends of them. Thus, each chemical compound can absorb electromagnetic radiation in specific frequency bands, determined by all different vibrational modes and their combinations. The frequencies of the most interest occur within the infrared range, i.e. between wavelengths of approximately 2.5 and 16 μm (Settle, 1997).

An *absorption spectrum* is a graphical representation of the absorption of infrared radiation by a gas sample as a function of the wavelength. As an example, Figure D.1 presents the absorption spectrum of carbon dioxide, with identified the vibrational modes responsible for the absorption of radiation at different wavelengths (Settle, 1997).

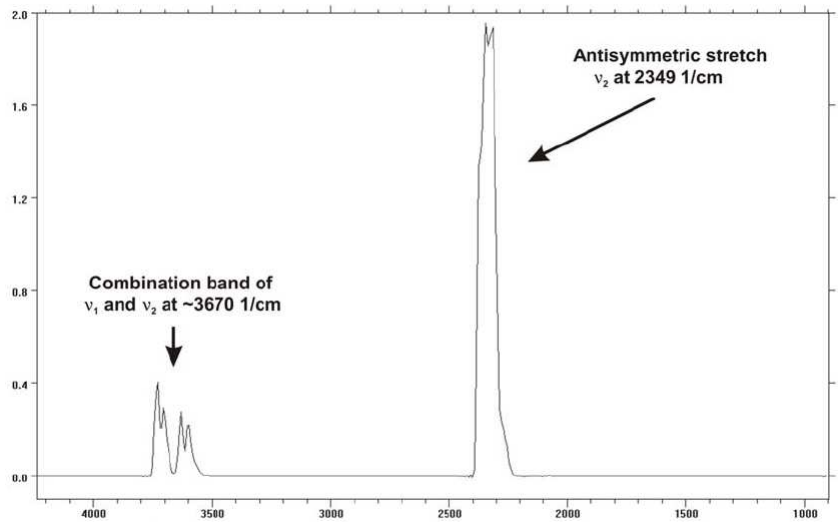

Figure D.1 Absorbance spectrum of CO_2.

FTIR is a technique for measuring absorption spectra which uses a single, wide band infrared source coupled with an optical modulator (interferometer). This allows for the simultaneous measurement of the absorbance at all the wavelengths contained in the source, in contrast with dispersive spectroscopy techniques which use a monochromatic radiation source whose wavelength is changed over time. The measurement of the absorption spectrum in an FTIR instrument works as follows: infrared radiation from the source is collected and collimated by a mirror to a beam splitter. The beam splitter ideally transmits one-half of the radiation, and reflects the other half. Both transmitted and reflected beams strike plane mirrors, one fixed and one moving, which reflect the two beams back to the beam splitter. Thus, one-half of the infrared radiation that finally goes to the sample gas has first been reflected from the beam splitter onto the moving mirror, and then back to the beam splitter. The other half of the infrared radiation going to the sample gas has first gone through the beam splitter and then reflected from the fixed mirror back onto the beam splitter. When these two beams from two optical paths are reunited, interference occurs at the

beam splitter. The strength of the interference depends on the optical path difference between the beams caused by the position of the moving mirror.

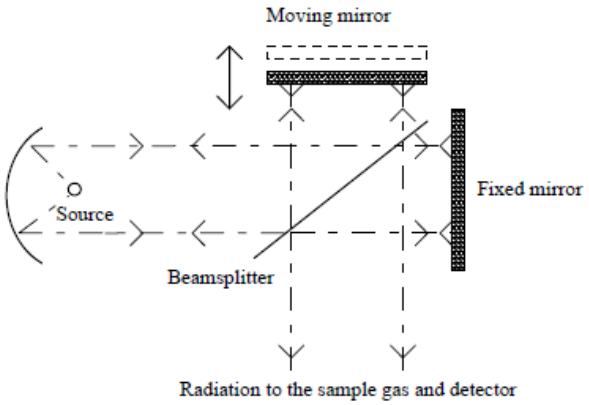

Figure D.2 Schematic representation of a Michelson type interferometer.

An *interferogram* is the interference signal measured by the detector as a function of the optical path length difference. The absorbance spectrum is computed from the digitized interferogram by performing a Fourier transform using a Fast Fourier Transform (FFT) algorithm.

D.2 Quantitative analysis

The absorbance of a chemical species at a certain wavelength is proportional to the concentration of that species (Beer-Lambert law). Thus, if the *reference spectrum* (i.e. the absorbance spectrum at a specific concentration) of a chemical species is known, the unknown concentration of a gas sample of that species can be calculated. Furthermore, the absorbance is additive, that is the total absorbance of a multi-component gas sample at each wavelength is the sum of the absorbances of the single gas components (Settle, 1997). This allows to perform quantitative multi-component gas analysis using FTIR spectra. To this end, the reference spectra of all the components present in a gas sample are linearly combined with appropriate

multipliers in order to obtain a spectrum that is as close a possible to the measured spectrum. If this process is successful the concentrations of the gas components in the sample are obtained from the reference concentrations using the multipliers that optimise the agreement between measured and model spectra (Gasmet, 2006).

Figure D.3 represents the absorbance spectrum of a gas sample of the emissions resulting from the smouldering combustion of coal tar. The experimental set-up used for the analysis is that represented in Figure 3.1 (Chapter 3), with an imposed volumetric flow rate in the extraction hood of 150 L/s. In Figure D.4 are presented the corresponding results of the quantitative analysis, performed by the software Calcmet 1.2 (Temet Instruments, Helsinki, Finland). The concentrations are calculated using the multipliers that minimise the (global) residue between the sample spectrum and the model spectrum formed as a weighted sum of the reference spectra.

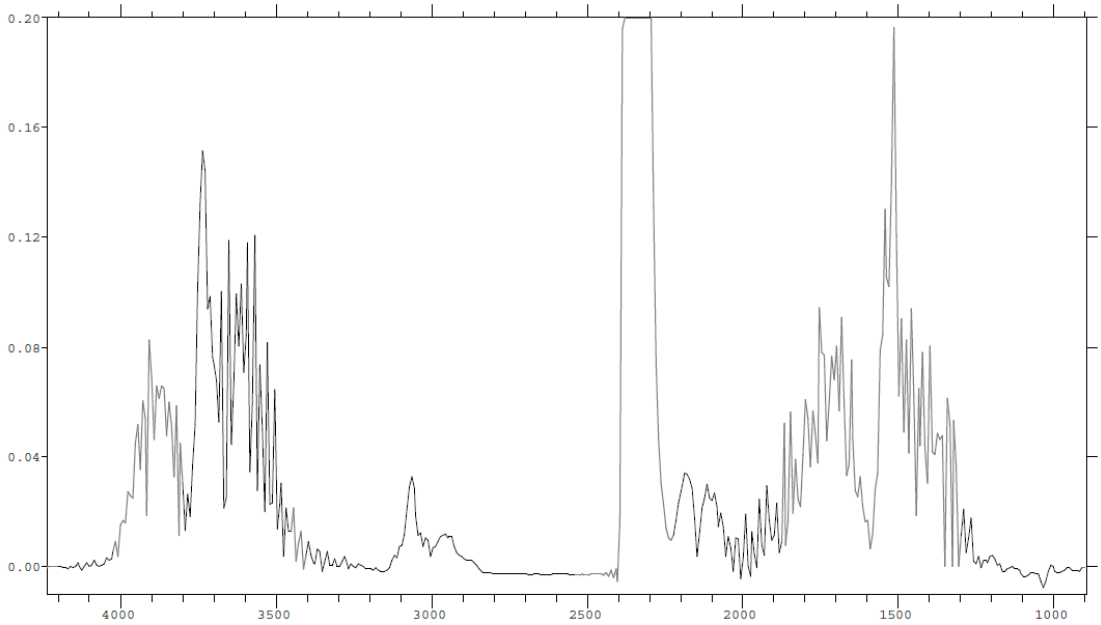

Figure D.3 Example of absorbance spectrum obtained from the analysis of coal tar smouldering gases.

2008-02-22 14:00:30 SN071242_lab_v1.LIB

Ch	Component	Concentration	Unit	Output	Compensation		Range	Resid
1	Water vapor H2O	0.57	vol-%		wet		40	0.0003
2	Carbon dioxide CO2	0.193	vol-%		wet		30	0.0074
3	Carbon monoxide CO	400	ppm		wet		2000	0.0016
4	Nitrogen monoxide NO	2.97	ppm		wet		1000	0.0008
5	Nitrogen dioxide NO2	0.00	ppm		wet		1000	0.0015
6	Nitrous oxide N2O	0.15	ppm		wet		200	0.0015
7	Sulfur dioxide SO2	3.76	ppm		wet		1000	0.0047
8	Hydrogen chloride HCl	0.00	ppm		wet		50	0.0002
9	Hydrogen fluoride HF	0.76	ppm		wet		50	0.0003
10	Ammonia NH3	0.72	ppm		wet		50	0.0043
11	Methane CH4	6.87	ppm		wet		1000	0.0010
12	Ethylene C2H4	0.00	ppm		wet		500	0.0043
13	Ethane C2H6	0.00	ppm		wet		500	0.0018
14	Propane C3H8	7.45	ppm		wet		500	0.0009
15	Hexane C6H14	3.81	ppm		wet		500	0.0009
16	Formaldehyde CHOH	0.83	ppm		wet		100	0.0001
17	Benzene C6H6	0.00	ppm		wet		500	0.0010
18	Toluene C7H8	13.94	ppm		wet		500	0.0009
19	Trichloroethylene C2HCl3	2.67	ppm		wet		500	0.0048
20	Naphtalene C10H8	56.49	ppm		wet		500	0.0009
21	o-Xylene C8H10	0.00	ppm		wet		500	0.0012
22	m-Xylene C8H10	7.29	ppm		wet		500	0.0010
23	p-Xylene C8H10	3.41	ppm		wet		500	0.0009
24	Ethylbenzene C8H10	0.00	ppm		wet		500	0.0015
220	Oxygen (O2)	21.22	vol-%		wet		25	

Figure D.4 Quantitative analysis of the absorbance spectrum presented in Figure D.3.

D.3 References

Gasmet DX-Series FTIR Gas Analyser – Instruction and operating manual. Gasmet Technology, 2006.

Settle, F.A., Handbook of instrumental techniques for analytical chemistry, Prentice Hall, 1997.

Appendix E

Mass balance on carbon

Besides the level of remediation achieved, it is important to quantify the fraction of contaminant that has actually been destroyed (converted to carbon oxides) and that that is instead removed by vaporisation and transferred into the exhausts stream. Due to the increase in vapour pressure, the rate of mass transfer from the liquid to the gas phase of most volatile and semivolatile compounds is greatly enhanced by an increase in temperature (e.g. Davis, 1997 in Chapter 1). Since the implementation of NAPL smouldering involves the injection of gas into the soil and the increase of the soil temperature, it is expected that a fraction of the mass of NAPL initially present be recovered in the gas phase without undergoing combustion. In this research, the fractions of NAPL destroyed/volatilised have been quantified as the masses of contaminant transformed in carbon oxides (CO_2 and CO) and hydrocarbons respectively, taken as the masses of carbon recovered in the emissions for the two groups of compounds.

Chemical analysis of the exhausts revealed the presence in the exit gases of volatile hydrocarbons in significant amount (Chapters 3 and 5). From the measured composition, temperature and volumetric flow rate of the exhaust gases the instantaneous mass flow rates at each measuring time are calculated:

$$\dot{m}_i(t_j) = MW_i \cdot \frac{p\dot{V}(t_j)}{RT(t_j)} \cdot \frac{ppm_i(t_j)}{10^6} \qquad (E.1)$$

where

$\dot{m}_i(t_j)$ mass flow rate of the gas species i at the time t_j

MW_i molecular weight of the gas species i

$\dot{V}(t_j)$ volumetric flow rate in the exhaust duct at the time t_j

$T(t_j)$ temperature of the exhaust gases at the time t_j

ppm_i concentration (in ppm_v) of the gas species i at the time t_j

Time integration of the mass flow rates provides the cumulative mass of carbon emitted as carbon oxides and volatile hydrocarbons (Figures E.1 and E.2). The numerical integration of the mass flow rate was carried out using the trapezoidal rule over the uniform time grid t_j. It is found that approximately 77% and 62% of the total emitted carbon is recovered as CO_2 and CO for coal tar and crude oil respectively.

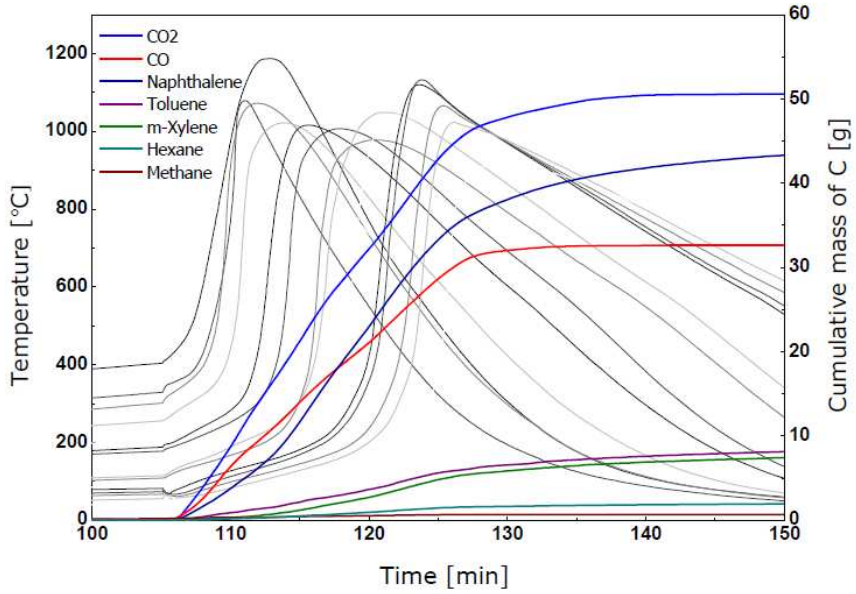

Figure E.1 Cumulative mass of C emitted as CO_x and volatile hydrocarbon for the base-case experiment on coal tar in coarse sand.

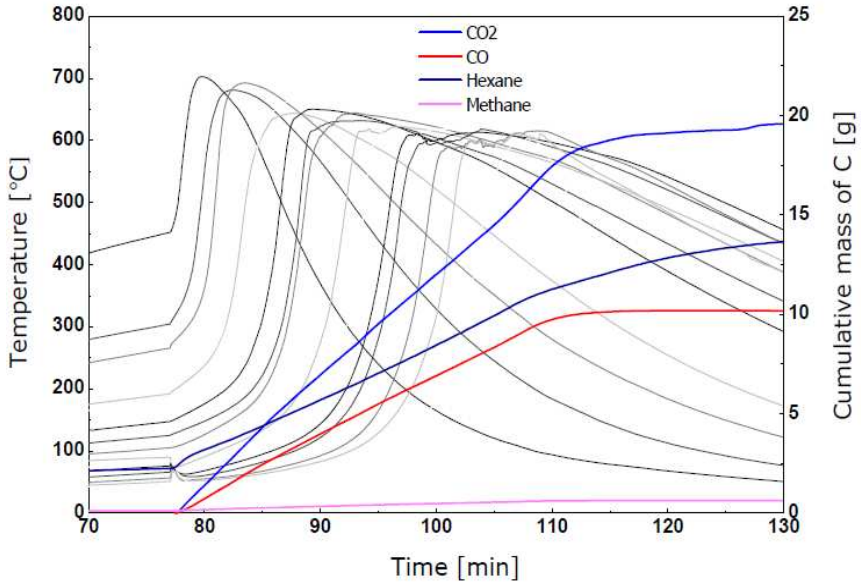

Figure E.2 Cumulative mass of C emitted as CO_x and volatile hydrocarbon for the base-case experiment on crude oil in coarse sand.

It is important to note that the total mass of carbon measured in the emissions does not account for all the mass of carbon removed from the contaminated pack, as derived from the difference between the mass of the apparatus before and after the experiment. In other words, with the present experimental apparatus and methodology it was not possible to close the mass balance of carbon. A comparison between the two measures is presented in Table E.2.

Table E.2 Comparison between mass of carbon removed and that recovered in the emissions

Quantity	Value (coal tar)	Value (crude oil)
Mass of NAPL removed (g)	171	106
Mass of C removed (g)	157	90
Mass of C in the emissions (g)	118	63
Fraction of C recovered	0.75	0.70

The discrepancy between the values in Table E.1 may be attributed to both the measurement apparatus and the methodology employed for the calculations. The maximum accuracy of the FTIR analyser is rated at 2% of the measurement range. However, to gain optimal accuracy, all the compounds contained in the gas sample should be listed in the instrument library of reference spectra (see Appendix D). If the sample gas contains a significant amount of any gas component that is not in the library the results will become inaccurate Also, the ability to correctly identify species depends on the spectral resolution of the instrument: if the emissions contain compounds with absorptions bands that cannot be discriminated by the instrument in use, computed concentrations may be incorrectly assigned. Finally, species quantification may be affected by nonlinearity errors if the concentrations in the sample are far from the reference concentrations. For example, Jaakkola et al. (1996) report a 10% error in the measurement of the concentration of CO in a gas mixture of known composition, attributing it to inadequate nonlinearity correction.

Other sources of error may be related to the experimental methodology and the assumptions used in the calculations. For example, partial condensation of the higher boiling hydrocarbons in the exhausts duct and/or in the tubing from the probe to the analyser may affect the effective composition of the mixture reaching the analyser's cell. Further, the assumption that the carbon content of the residual contaminant is the same as in the original contaminant (assumption implicit in the calculation presented in Table E.2) may be not correct. Indeed it is plausible that the residual contaminant has undergone at least a partial devolatilisation, and therefore its carbon content is higher than that of the fresh contaminant (because it would contain a

higher fraction of high molecular mass compounds). This would lead to an overestimate of the mass of carbon removed.

References

Jaakkola, P.T. et al., On-line analysis of stack composition by a low resolution FT-IR gas analyzer, Water, air and soil pollution, (1998) 101 79-92.